



UNIVERSIDADE ESTADUAL DE CAMPINAS
FACULDADE DE ENGENHARIA MECÂNICA
E INSTITUTO DE GEOCIÊNCIAS

JULIANA MAIA CARVALHO DOS SANTOS

**SEMI-QUANTITATIVE 4D SEISMIC
INTERPRETATION INTEGRATED WITH
RESERVOIR SIMULATION: APPLICATION TO THE
NORNE FIELD**

**INTERPRETAÇÃO SEMI-QUANTITATIVA DE
SÍSMICA 4D INTEGRADA À SIMULAÇÃO DE
RESERVATÓRIOS: APLICAÇÃO AO CAMPO DE
NORNE**

CAMPINAS

2017

JULIANA MAIA CARVALHO DOS SANTOS

**SEMI-QUANTITATIVE 4D SEISMIC INTERPRETATION
INTEGRATED WITH RESERVOIR SIMULATION:
APPLICATION TO THE NORNE FIELD**

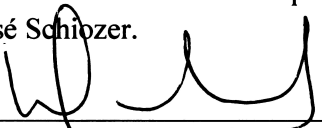
**INTERPRETAÇÃO SEMI-QUANTITATIVA DE SÍSMICA 4D
INTEGRADA À SIMULAÇÃO DE RESERVATÓRIOS:
APLICAÇÃO AO CAMPO DE NORNE**

Dissertation presented to the Mechanical Engineering Faculty and Geosciences Institute of the University of Campinas in partial fulfillment of the requirements for the degree of Master in Petroleum Sciences and Engineering in the area of Reservoirs and Management.

Dissertação apresentada à Faculdade de Engenharia Mecânica e Instituto de Geociências da Universidade Estadual de Campinas como parte dos requisitos exigidos para a obtenção do título de Mestra em Ciências e Engenharia de Petróleo na área de Reservatórios e Gestão.

Orientador: Prof. Dr. Denis José Schiozer

Este exemplar corresponde à versão final da Dissertação defendida pelo aluno Juliana Maia Carvalho dos Santos e orientada pelo Prof. Dr. Denis José Schiozer.


Assinatura do Orientador

CAMPINAS

2017

Agência(s) de fomento e nº(s) de processo(s): Não se aplica.

Ficha catalográfica
Universidade Estadual de Campinas
Biblioteca da Área de Engenharia e Arquitetura
Luciana Pietrosanto Milla - CRB 8/8129

Santos, Juliana Maia Carvalho dos, 1985-
Sa59s Semi-quantitative 4D seismic interpretation integrated with reservoir
simulation : application to the Norne field / Juliana Maia Carvalho dos Santos. –
Campinas, SP : [s.n.], 2017.

Orientador: Denis José Schiozer.
Dissertação (mestrado) – Universidade Estadual de Campinas, Faculdade
de Engenharia Mecânica.

1. Engenharia de petróleo - Métodos de simulação. 2. Reservatórios
(Simulação). 3. Prospecção sísmica. 4. Integração. I. Schiozer, Denis
José, 1963-. II. Universidade Estadual de Campinas. Faculdade de Engenharia
Mecânica. III. Título.

Informações para Biblioteca Digital

Título em outro idioma: Interpretação semi-quantitativa de sísmica 4D integrada à
simulação de reservatórios : aplicação ao campo de Norne

Palavras-chave em inglês:

Petroleum engineering - Simulation methods

Reservoirs (Simulation)

Seismic prospecting

Integration

Área de concentração: Reservatórios e Gestão

Titulação: Mestra em Ciências e Engenharia de Petróleo

Banca examinadora:

Denis José Schiozer [Orientador]

Emilson Pereira Leite

Marcos Hexsel Grochau

Data de defesa: 17-02-2017

Programa de Pós-Graduação: Ciências e Engenharia de Petróleo

UNIVERSIDADE ESTADUAL DE CAMPINAS
FACULDADE DE ENGENHARIA MECÂNICA
E INSTITUTO DE GEOCIÊNCIAS

DISSERTAÇÃO DE MESTRADO ACADÊMICO

**SEMI-QUANTITATIVE 4D SEISMIC
INTERPRETATION INTEGRATED WITH
RESERVOIR SIMULATION: APPLICATION TO
THE NORNE FIELD**

Autor: Juliana Maia Carvalho dos Santos
Orientador: Prof. Dr. Denis José Schiozer

A Banca Examinadora composta pelos membros abaixo aprovou esta Dissertação:

Prof. Dr. Denis José Schiozer, Presidente
DEP / FEM / UNICAMP

Prof. Dr. Emilson Pereira Leite
DGRN / IG / UNICAMP

Dr. Marcos Hexsel Grochau
PETROBRAS

A Ata da defesa com as respectivas assinaturas dos membros encontra-se no processo de vida acadêmica do aluno.

Campinas, 17 de fevereiro de 2017.

DEDICATION

To my beloved parents, Inês and Pedro.

ACKNOWLEDGEMENTS

To my advisor, Denis Schiozer, for the opportunity to be part of the research group, for the guidance and support throughout my studies.

To my co-advisor, Alessandra Davolio, for her immense attention, discussions and corrections.

To Colin MacBeth and the ETLP group, who made me feel so welcome during my visit in Edinburgh. Thank you for the excellent training on 4D seismic interpretation and for the valuable contribution to my work.

To BG, for sponsoring the project and my studies.

To Statoil (operator of the Norne field), ENI and Petoro for the release of the Norne data and the Centre for Integrated Operations at NTNU for cooperation and coordination of the Norne Case. The views expressed in this dissertation are the views of the author and do not necessarily reflect the views of Statoil and the Norne license partners.

To Schlumberger and CGG for providing software licenses.

To Guilherme Tonin for his help with all the administration issues.

To my colleagues from DEP for the technical discussions and leisure times.

And finally, agradeço à minha família, especialmente aos meus pais, Janda e Mã, por estarem sempre ao meu lado (mesmo longe), torcendo e rezando por mim, e ao Lino, pelas alegrias que nos trouxe. Aos meus amigos, especialmente à Jéssica, pelos incentivos desde sempre, e à Fernanda, pela companhia e risadas. Por último, agradeço ao Guilherme por sua paciência e carinho.

ABSTRACT

4D seismic attributes are extensively used as input to history matching workflows as the spatial information provided by such data can be very important for reservoir characterization and management. However, this integration can potentially bring problems if not done properly. Some of the uncertainties regarding seismic acquisition, processing and interpretation can be incorrectly incorporated into the reservoir simulation model yielding an erroneous production forecast. Very often, the information provided by 4D seismic can be noisy or ambiguous. For this reason, it is necessary to estimate the level of confidence on the data prior to its incorporation to the simulation model updating process. The methodology presented in this dissertation aims to diagnose which information from 4D seismic we are confident enough to incorporate in the model. Two passes of seismic interpretation are proposed in order to assess the data quality and to compare the simulation-to-seismic synthetic response to the observed seismic signal. The methodology is applied to the Norne field benchmark case, with several examples of inconsistencies between the two responses. It is then evaluated whether these inconsistencies are caused by a simulation model inaccuracy or by uncertainties in the actual observed seismic. After a careful qualitative and semi-quantitative analysis, the confidence level on the interpretation is evaluated before suggesting simulation model updates. The main contribution of this work is to introduce a diagnostic step that classifies the seismic interpretation reliability considering the uncertainties inherent to this data. The results show that medium to high confidence interpretation can be achieved even for poorly repeated data, but there is a general agreement between poor repeatability and lower confidence.

Key Words: Reservoir simulation, Reservoir Monitoring, 4D Seismic

RESUMO

Atributos sísmicos são frequentemente utilizados como dados de entrada no processo de ajuste de histórico, pois a informação espacial fornecida por estes dados podem ser muito importantes para a caracterização e gerenciamento de reservatórios. No entanto, esta integração pode, potencialmente, introduzir problemas se não for feita de modo apropriado. Algumas das incertezas advindas da aquisição, processamento e interpretação sísmica podem ser incorretamente incorporadas ao modelo de simulação, resultando em uma previsão do comportamento do reservatório errônea. Muito frequentemente, a informação dada pela sísmica 4D pode ser ruidosa ou ambígua. Por este motivo, é necessário estimar o nível de confiança nos dados antes de incorporá-los ao processo de atualização do modelo de simulação. A metodologia apresentada nesta dissertação tem como objetivo fazer um diagnóstico sobre qual informação da sísmica 4D deve ser incorporada com confiança ao simulador. Duas passadas de interpretação sísmica são propostas para avaliar a qualidade deste dado e para compará-lo à resposta sísmica sintética obtida pelo simulador. A metodologia é aplicada ao caso benchmark do campo de Norne, com diversos exemplos de inconsistências entre as duas respostas. Em seguida é avaliado se estas inconsistências são causadas por uma imprecisão no modelo de simulação ou pelas próprias incertezas na sísmica observada. Após uma análise semi-quantitativa meticulosa, o nível de confiança na interpretação é avaliado antes de sugerir atualizações no modelo de simulação. A contribuição principal deste trabalho é a introdução de um passo diagnóstico que classifica a confiança na interpretação sísmica considerando as incertezas inerentes aos dados. Os resultados mostram que um grau de confiança médio a alto pode ser obtido até mesmo para dados com repetibilidade inferior, porém, no geral, há uma concordância entre grau de repetibilidade e confiança na interpretação sísmica.

Palavras Chave: Simulação de reservatórios, Monitoramento de reservatórios, Sísmica 4D

LIST OF FIGURES

Figure 1.1: (a) Water saturation of old simulation model. Red is high water saturation. (b) 4D acoustic impedance difference. Red is increase in impedance from 2001 to 2003, indicating water replacing oil. (c) Water saturation of new simulation model, updated using information from 4D seismic. Red is high water saturation (extracted from Osdal et al., 2010).....	18
Figure 2.1: Pre-production baseline seismic survey (left) and monitor survey (right), recorded after waterflood production. The monitor detects the changes in amplitudes and time-shifts (extracted from Johnston, 2013).	22
Figure 3.1: Different levels of 4D seismic data interpretation (extracted from Amini, 2014).	28
Figure 4.1: A typical seismic interpretation sequence (in black) and the addition of confidence check steps (in blue).	30
Figure 5.1: (a) Location of the Norne field and (b) Geological setting around the Norne field (modified from NPD, 2016)	35
Figure 5.2: Stratigraphic column of the Norne field (extracted from Huang et al., 2013).	37
Figure 5.3: 3D view of the Norne simulation model, with segment and well locations (oil and gas producers in green, water injectors in blue and water and gas injectors in red).	40
Figure 6.1: PEP (left) and delay (right) plots from the selected trace location and well location	42
Figure 6.2: Statistical wavelet extracted from the best PEP location, in a window of 2100-2492ms.....	43
Figure 6.3: Log data for well 10-4 (a) caliper (green) and gamma-ray (black) logs; (b) density (red), porosity (blue); (c) computed acoustic impedance; (d) trace at well borehole path; (e) seismic traces from the best match location; (f) synthetic traces generated with data from best match location; and (g) synthetic seismic traces from well location.	44
Figure 6.4: Cross correlation function before (blue curve) and after bulk time-shift (red curve) application.....	44
Figure 6.5: Log data for well 10-4 (a) caliper (green) and gamma-ray (black) logs; (b) density (red), porosity (blue); (c) computed acoustic impedance; (d) trace at well borehole path; (e) seismic traces from the best match location; (f) synthetic traces generated with data from best match location; and (g) synthetic seismic traces from well location, after bulk shift was applied.....	45

Figure 6.6: Original horizon picks (blue line on the left) and edited horizon (right) QC'ed and plotted in the baseline (2001) 3D vertical section	46
Figure 6.7: Example 4D difference line (2004 minus 2001) showing non-repeated edge effects and a portion inside the reservoir (between black lines) where the magnitude of the signal may be the same as the noise. The arrows in the colour bar show the amplitude difference intervals for unchanged amplitude (U), noise (N) and signal (S). Note that N and S may overlap.	47
Figure 6.8: Example 4D difference line (2004 minus 2001). The rectangle shows diffractions in the sea bed and their multiples propagating all the way down. Care should be taken when interpreting the reservoir zone underneath these areas as they can affect the reservoir zone. .	48
Figure 6.9: NRMS values for 2003 versus 2001 comparison with segments location (a), 2004 versus 2001 comparison (b) and 2006 versus 2001 comparison (c).....	48
Figure 6.10: NRMS map of 2004 vs. 2001 comparison with a black line passing through the undershooting zone (left) and 4D difference vertical intersection from the black line (right). The arrows show differences in reflectivity in the undershoot zone, which also affects the deeper areas. The black horizons are the top and base of the reservoir.....	49
Figure 6.11: Norne FPSO and templates (left) and 4D acquisition area indicating the location of the obstruction (right) (extracted from Osdal et al., 2008).....	50
Figure 6.12: NRMS map of 2003 versus 2006 comparison.	50
Figure 6.13: RMS values of the 3D Baseline survey (2001). Note the brighter zones are located in G and E segments and may be related to hydrocarbons from Not 2 Formation.	52
Figure 6.14: RMS differences in the top reservoir + 15ms horizon. (a) RMS 2003 minus 2001; (b) RMS 2004 minus 2001; and (c) RMS 2006 minus 2001. Solid black circles are the producer well locations and non-solid arrowed circles are the injectors. Red colours are related to a decrease in impedance (softening) and blue, to an increase (hardening).	52
Figure 6.15: Crossplot time-shift versus correlation coefficient 2006 versus 2001 comparison. The red dashed lines indicate the threshold ranges selected for cross-correlation and time-shifts estimates.	54
Figure 6.16: Example vertical section showing (a) amplitude differences within and below reservoir (red and black horizons); (b) calculated time-variant time-shifts; (c) correlation coefficients; and (d) time-shifts after conditioning, for 2006 versus 2001 comparison.	54
Figure 6.17: Amplitude difference before time-shift correction (a); calculated time-shifts after conditioning step (b); and amplitude differences after time-shift correction (c) for a vertical section along two water injectors. The negative (orange) time-shift is a delay caused by velocity decrease from pore pressure increase. The small advance time-shift above (blue) is caused by upward OWC movement.	55

Figure 6.18: Stress sensitivity curves from equation 6.3 for the whole Ek range in MacBeth (2004).....	57
Figure 6.19: Extracted wavelet and its frequency spectra. Note the Nyquist frequency is 125 Hz (4ms sample rate) and peak frequency is 19Hz.	58
Figure 6.20: (a) Baseline (2001) 3D observed seismic; (b) 2001 3D sim2seis; and (c) P-wave impedance from the petroelastic model.	59
Figure 6.21: E-4AH well activity (a) gas-oil ratio (red) and oil production rate (green); and (b) BHP (grey) and water-cut (blue). Circles are the historical and solid lines are the simulated rates. The dashed lines are the approximate seismic acquisition dates.	60
Figure 6.22: F-4H well activity (a) water injection (blue) and BHP (grey). Circles are the historical and solid lines are the simulated rates. The dashed lines are the approximate seismic acquisition dates.....	60
Figure 6.23: (a to c) Observed RMS amplitude differences and (d to f) sim2seis RMS amplitude differences for 2003, 2004 and 2006 minus 2001 comparisons, extracted from a 15ms window below top reservoir.....	62
Figure 6.24: (a to c) Simulated water saturation differences, (d to f) Simulated oil saturation differences, (g to i) Simulated gas saturation differences (in decimal), (k to l) Simulated pore pressure differences (in bar) for 2003, 2004 and 2006 minus 2001 comparisons.	63
Figure 6.25: Vertical section location (left) and vertical permeability across this section (right).	64
Figure 6.26: (a) 2001 observed seismic, (b) 2003 observed seismic, (c) 2003-2001 observed seismic and (d) RMS 2003 – RMS 2001.	64
Figure 6.27: (a) Location of the interpreted seismic section (blue line); and (b) gas (red) and water (blue) injection rates. The solid lines are the rates from the simulator and the circles are the historical data for well C4-AH.....	66
Figure 6.28: (a) Observed seismic, (b) simulated water saturation, (c) simulated pore pressure (bar), (d) Sim2seis, (e) simulated gas saturation (e) and (f) simulated oil saturation 2006-2001 differences for well C4-AH.	66
Figure 6.29: (a) Well and analysed vertical seismic section locations; (b) gas (red) and water (blue) injection rates; and (c) BHP from simulation for well C1-H. Circles are the historical and solid lines are the simulated rates.	68
Figure 6.30: (a) Observed seismic, (b) simulated water saturation, (c) simulated pore pressure (bar), (d) Sim2seis, (e) simulated gas saturation (e) and (f) simulated oil saturation 2006-2001 differences for well C1-H.	68

Figure 6.31: 3D view of the location of wells C-2H, D-1CH, D-1H and D-1BH and the analysed seismic section in blue (plotted at Ile 1.3 layer).	70
Figure 6.32: (a) water injection rates (blue) and simulated BHP (black) for C-2H; (b) water cut (blue) and BHP (black); and (c) gas-oil ratio (red) and oil production rate (green) for D1-CH. Circles are the historical and solid lines are the simulated rates.....	70
Figure 6.33: (a) Observed seismic, (b) simulated water saturation, (c) simulated pore pressure (bar), (d) Sim2seis, (e) simulated gas saturation (e) and (f) simulated oil saturation 2006-2001 differences. The blue lines in (a) and (b) represent the rise in OWC from 2001 to 2006.	71
Figure 6.34: Time-shift for 2003, 2004 and 2006 vs. 2001 (a, b and c respectively). Negative values correspond to a delay in timing from baseline to monitor.....	71
Figure 6.35: B-1H, E-1H and analysed vertical seismic section locations.....	73
Figure 6.36: (a) and (c) water cut (blue) and BHP (black); (b) and (d) gas-oil ratio (red) and oil production rate (green) for B-1H and E-1H wells respectively. Circles are the historical and solid lines are the simulated rates.	73
Figure 6.37: (a) Observed seismic, (b) simulated water saturation, (c) simulated pore pressure (bar), (d) Sim2seis, (e) simulated gas saturation (e) and (f) simulated oil saturation 2006-2001 differences. The blue lines in (a) and (b) represent the rise in OWC from 2001 to 2006 for E-1H and B1-H.	74
Figure 6.38: (a) Horizontal permeability from simulation model. The blue arrow highlights a high permeability zone. (b) Time-shifts estimated in the same vertical section.	74
Figure 6.39: (a) Well and analysed vertical seismic section locations; (b) gas-oil ratio (red) and oil production rate (green); and (c) BHP (black) and water-cut (blue) for D2-TH2. Circles are the historical and solid lines are the simulated rates.....	75
Figure 6.40: Observed seismic (a), Sim2seis (b), water saturation (c), gas saturation (d), pore pressure (bar) (e) and oil saturation (f) 2006-2001 differences. The blue lines in (a) and (b) represent the OWC movement between 2001 and 2006 for D2-TH2.	76
Figure 6.41: Time-shifts between 2001 and 2004 (a) and 2006 (b). Negative values represent timing delay from baseline to monitor.....	76
Figure 6.42: (a) Location of the interpreted seismic section (blue line) and (b) gas-oil ratio (red) and water cut (blue). The solid lines are the simulation results and the circles are the historical data for B1-BH.....	78
Figure 6.43: Observed seismic (a), Sim2seis (b), water saturation (c), gas saturation (d), pore pressure (bar) (e) and oil saturation (f) 2006-2001 differences near wells B1-BH and B4-H.	78

Figure 6.44: (a) Well and analysed vertical seismic section locations; (b) gas-oil ratio (red) and oil production rate (green); and (c) BHP (black) and water-cut (blue) for B2-H. Circles are the historical and solid lines are the simulated rates.....	79
Figure 6.45: Observed seismic (a), Sim2seis (b), water saturation (c), gas saturation (d), pore pressure (bar) (e) and oil saturation (f) 2006-2001 differences. The blue lines in (a), (b) and (c) represent the interpreted OWC movement between 2001 and 2006 near B2-H.....	80
Figure 6.46: (a) Well and analysed vertical seismic section locations; and (b) gas (red) and water (blue) injection rates and simulated BHP (black line) for C3-H. Circles are the historical and solid lines are the simulated rates.	81
Figure 6.47: Observed seismic (a), Sim2seis (b), water saturation (c), gas saturation (d), pore pressure (bar) (e) and oil saturation (f) 2006-2001 differences. The blue lines in (a), (b) and (c) represent the interpreted OWC movement between 2001 and 2006 near C3-H and C2-H.	81
Figure 6.48: Time-shifts between 2001 and 2003 (a), 2004 (b) and 2006 (c). Negative values represent timing delay from baseline to monitor near C3-H and C2-H.	82
Figure 6.49: 3D view of D3-AH and D3-BY1HT2 wells and analysed vertical seismic section across them.	83
Figure 6.50: (a) and (c) gas-oil ratio (red) and oil production rate (green); (b) and (d) BHP (black) and water-cut (blue) for D3-AH and D3-BY1HT2 wells. Circles are the historical and solid lines are the simulated rates.	84
Figure 6.51: Observed seismic (a), Sim2seis (b), water saturation (c), gas saturation (d), pore pressure (bar) (e) and oil saturation (f) 2006-2001 differences. The blue lines in (a), (b) and (c) represent the interpreted OWC movement between 2001 and 2006.....	85
Figure 6.52: (a) Time-shifts between 2001 and 2004 and (b) Time-shifts between 2001 and 2006 near D3-AH and D3-BY1HT2 wells	85
Figure 6.53: (a) Well and analysed vertical seismic section location.....	87
Figure 6.54: (a) Simulated BHP (black) and water injection rate (blue) for F-2H; (b) gas-oil ratio (red) and oil production rate (green); and (c) BHP (black) and water-cut (blue) for D4-AHT2. Circles are the historical and solid lines are the simulated rates.	87
Figure 6.55: Observed seismic (a), sim2seis (b), water saturation (c), gas saturation (d), pore pressure (bar) (e) and oil saturation (f) 2006-2001 differences. The blue lines in (a), (b) and (c) represent the interpreted OWC movement between 2001 and 2006.....	88
Figure 6.56: (a) Location of the interpreted seismic section (blue line); (b) oil production rate (green) and gas-oil ratio (red); (c) bottom-hole pressure; and (d) water production rate. The solid lines are the simulation results and the circles are the historical data for the well.	89

Figure 6.57: Observed seismic (a), water saturation (b), pore pressure (bar) (c), sim2seis (d), gas saturation (e) and oil saturation (f) 2006-2001 differences. 89

Figure 6.58: Time-shifts for 2004 vs. 2006 comparison near well E3-CHT2. 90

Figure 6.59: (a) Location of the wells and interpreted seismic section (blue line); (b) water injection rate (blue) and BHP (black) for F-1H; and (c) water injection rate (blue) and BHP (black) for F-3H. The solid lines are the simulation results and the circles are the historical data for the well. 91

Figure 6.60: Observed seismic (a), water saturation (b), pore pressure (bar) (c), sim2seis (d), gas saturation (e) and oil saturation (f) 2006-2001 differences. The blue lines in (a), (b) and (c) represent the interpreted OWC movement between 2001 and 2006. 91

Figure 6.61: (a) Map view of well completion trajectories between segments D and E and (b) 3D seismic across D and E-segments (blue line in (a)) and the major fault in blue between them. 93

Figure 6.62: (a to c) Observed RMS amplitude differences from top reservoir to 15ms below; (d to f) sim2seis RMS amplitude differences; and (g to i) gas saturation differences for 2003, 2004 and 2006 minus 2001 comparisons, extracted from a 15ms window below top reservoir. 94

Figure 6.63: Location of the interpreted seismic sections throughout the field. The lines in green present high seismic interpretation confidence, yellow are medium confidence and red, low confidence. No 4D signal was detected in the dashed areas. 95

Figure 6.64: Interpretation confidence maps for each survey comparison: (a) 2003, (b) 2004 and (c) 2006 versus 2001. The black polygons represent the high NRMS areas defined in Figures (d), (e) and (f). The black arrows show examples where seismic confidence is medium to high in spite of a poorer repeatability. 96

Figure 6.65: OWC Interpretation confidence maps for each survey comparison: (a) 2003 and (b) 2006 versus 2001. 97

CONTENTS

1. INTRODUCTION	17
1.1. Motivation.....	19
1.2. Objectives.....	19
1.3. Text description.....	20
2. THEORETHICAL BACKGROUND	21
2.1. Saturation changes	22
2.2. Reservoir pressure changes	23
2.3. 4D seismic undesired differences	24
3. LITERATURE REVIEW	26
3.1. 4D Seismic interpretation.....	26
3.1.1. Qualitative interpretation	26
3.1.2. Quantitative interpretation	27
3.1.3. Model-based interpretation.....	27
3.2. 4D seismic interpretation and the link with dynamic reservoir models.....	28
3.3. 4D seismic and simulation model updating of the Norne field	29
4. METHODOLOGY	30
4.1. The seismic domain	31
4.1.1. First pass of seismic interpretation.....	31
4.2. The engineering domain.....	32
4.2.1. Predicted saturation and pressure differences.....	32
4.2.2. Sim2seis modelling.....	32
4.3. The seismic and the engineering domain integration	33
5. APPLICATION	35
5.1. Description of the Norne field	35

5.1.1. Location and tectonic setting	35
5.1.2. Stratigraphy.....	36
5.1.3. Production in the Norne field	37
5.1.4. Dataset available	39
6. RESULTS AND DISCUSSION	41
6.1. The seismic domain – data preparation.....	41
6.1.1. Seismic data polarity.....	41
6.1.2. Seismic-well tie	41
6.1.3. Pick top and base of the reservoir using the 3D baseline seismic cube.....	45
6.1.4. Quality control of the seismic data available.....	46
6.1.5. Understanding the 4D seismic response	51
6.1.6. Time-variant time-shift estimation and correction	52
6.2. The engineering domain: simulation-to-seismic (sim2seis) modelling	55
6.3. The integration domain – seismic and sim2seis comparison.....	59
6.3.1. G-segment.....	59
6.3.2. C-Segment	64
6.3.3. D-Segment	82
6.3.4. E-Segment.....	88
6.4. Field analysis.....	94
7. CONCLUSIONS	98
7.1. Suggestions for future work.....	99
8. REFERENCES	100

1. INTRODUCTION

4D seismic has proven to be an important reservoir management technique over the last few decades. The information provided by 4D data, when properly combined with engineering, geology and petrophysics disciplines, can be a valuable contribution to field development.

Examples of 4D seismic applications range from purely qualitative analysis (such as locating amplitude anomalies due to saturation and pressure variations, identifying fluid paths and reservoir compartmentalization), to quantitative use (such as actual estimates of the variations detected in the qualitative analysis).

One important use of 4D seismic in particular is at the reservoir simulation model updating process. Simulation models are traditionally built at first using static information provided by 3D seismic data, well logs and other information available. Dynamic information from wells production data and 4D seismic are used subsequently to validate and update these models. Calibrated models (e.g. data from simulator matching with well production/historical data and observed 4D seismic) should provide better production forecast. The process of perturbing the simulation model properties to match production and 4D seismic data is called seismic history matching. Figure 1.1 shows one example where 4D seismic was successfully used to map the oil-water contact movement and to confirm a carbonate cemented zone was not sealing as previously assumed. The originally planned well path (black line) was in the water zone. To avoid early water production, the well location was moved upward and away from the water front (yellow line). The well was drilled successfully in the oil zone, and the first year after start up, it produced with a rate of approximately 4000 sm³/d without water (Osdal et al. 2010).

Several papers outline different techniques for combining 4D seismic and simulation modelling. For example, in the Marlim field (offshore Brazil), Oliveira et al. (2007) and Brito et al. (2011) discuss how this combination resulted in a better geological characterization. A number of fields in the North and Norwegian Sea, such as the Gullfaks, have many cases where the integration resulted in new targets identification (e.g. Byerley et al., 2016). Open sources estimate the added value of North Sea 4D to be more than US\$ 4 billion, with the added value at Gullfaks alone calculated to be close to US\$ 1 billion.

Furthermore, 4D is estimated to have reduced drilling costs by more than 6%, and contributed to additional reserves averaging 5% per field (Amundsen and Landrø, 2007). Other examples from Gannet field in the North Sea (Kloosterman et al., 2002 and Staples et al., 2005) and Girassol field (Roggero et al., 2007 and Jourdan et al., 2006) offshore Angola also demonstrate the value of the technique.

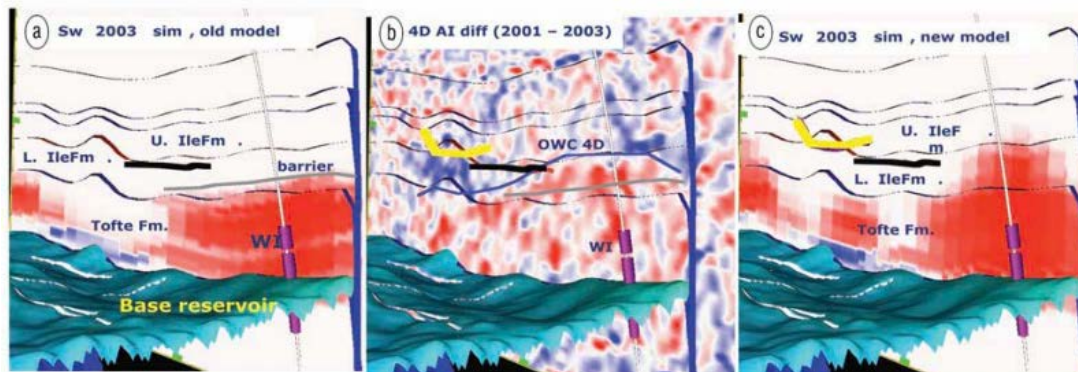


Figure 1.1: (a) Water saturation of old simulation model. Red is high water saturation. (b) 4D acoustic impedance difference. Red is increase in impedance from 2001 to 2003, indicating water replacing oil. (c) Water saturation of new simulation model, updated using information from 4D seismic. Red is high water saturation (extracted from Osdal et al., 2010).

Although most applications of 4D seismic data to reservoir model updates are qualitative and manual, a significant amount of research is being applied to the development of more quantitative and automatic workflows for history matching (Johnston, 2013). Quantitative and automated workflows might successfully speed-up and address non-unique solutions issues of history matching. However, automatic procedures might inadvertently rely on seismic derived attributes (such as amplitude, impedance, saturations changes or time-shifts) that might be obtained from unreliable low-quality portions of seismic data. In this case, it is important to identify which information from 4D seismic is ambiguous, noisy or poorly repeated prior to the history matching procedure, to effectively flag when the magnitude of the noise or the side-lobes is similar to the amplitude level of the signal.

Therefore, the interpretation process must reflect a good understanding of the character of the seismic prior to its integration in the simulation model. For this reason, the focus of this dissertation is on a seismic interpretation methodology that aims to diagnose which information from 4D seismic we are confident to incorporate in the model.

The Norne field benchmark case proposes to use real field data for research (Rwechungura, 2010). The database was made available by Statoil and their license partners and it is managed by the Norwegian University of Science and Technology.

There are many examples where qualitative use of 4D seismic significantly improved Norne reservoir behaviour understanding (e.g. Boutte, 2007; Cheng and Osdal, 2008; Huang et al., 2013; Osdal et al., 2006 and Aschjem, 2013). Several researches about the quantitative incorporation to history matching procedure are available (e.g. Fahimuddin, 2010 and Suman, 2013) but limited detailed information is available regarding the character of the seismic from the field and its reliability before the incorporation in the history matching process. For this reason, the importance of this work is to raise this discussion to serve as a base for history matching studies.

1.1. Motivation

4D seismic data has limitations due to acquisition and processing problems that can affect the repeatability of the traces. Non-repeated/random noise content or imperfect processing can obscure the real 4D signal that represents the actual changes in the reservoir. Plus, there is the subjectivity inherent to the interpretation (for example, when the signal is ambiguous) and situations when 4D signal is weak. Tools that integrate 4D seismic and simulation modelling are likely to embed these uncertainties into the process, and therefore one of the motivations of this dissertation is to evaluate and discuss 4D seismic data reliability prior to this integration.

Besides, although the literature about the Norne benchmark case contains valuable examples on how 4D seismic has assisted in improving the reservoir comprehension, they are local examples on few regions of the field. The second motivation of this work is to achieve a comprehensive interpretation of all the areas that, together with the seismic reliability knowledge, can result in a more appropriate input data for history matching process.

1.2. Objectives

The objective of this dissertation is to propose a 4D seismic interpretation workflow to (1) identify areas where the 4D seismic interpretation is reliable, (2) flag the areas where

the simulation model properties should be adjusted and (3) use this information to suggest simulation model updates or to incorporate their uncertainty into the simulator.

1.3. Text description

This dissertation is structured in seven chapters. The first chapter is an introduction about 4D seismic interpretation, the motivations of this work and its objectives.

The second chapter gives a theoretical background to understand the key concepts for understanding 4D seismic data, linking the reservoir's physical effects such as pressure and saturation changes to the 4D signal changes.

The third chapter is a literature review on the many 4D seismic interpretation approaches, with detail to the model-based technique for validating and optimizing simulation models. Previous research approaches on integrating 4D seismic and history matching at the Norne field are also discussed.

Chapter four describes the methodology which we followed to achieve the project's objectives. The integration between engineering, seismic and a mutual domain is discussed.

The fifth chapter presents the application of the above workflow to the Norne field. This section contains a description of the field's location, geological setting, stratigraphy, deposition environment, production and injection in the reservoir, and how they relate to the seismic interpretation.

The sixth chapter focuses on the outcome of the integrated interpretation. The confidence level of each interpretation region is also presented.

Chapter seven presents the conclusions of this work and future work suggestions.

2. THEORETICAL BACKGROUND

4D seismic (or time-lapse) monitoring consists in acquiring and comparing 3D (or 2D) seismic data in different production time along the field life. The basic principle is to compare a baseline seismic survey, ideally pre-production, to one or more monitor surveys to identify changes in the seismic response, which are the result of reservoir properties changes caused by hydrocarbon production or recovery processes such as water, gas and polymer injection.

Seismic response changes can be seen by careful comparison of the position and character of reflections and associated seismic attributes between the baseline and monitor surveys (Herron, 2011). One can also use differences in refractions and diffractions for 4D studies, however they are not discussed in this work. Changes in the character of reflections are referred in this dissertation, for stacked data, as “hardening”, when the acoustic impedance (AI) increases from baseline to monitor and “softening”, when the AI decreases. Reflection position differences are the changes in traveltimes caused by velocity variations, called time-shifts. Time-shifts are normally computed and compensated for, in order to compare only the differences in reflectivity (and not misalignments) between the surveys. Figure 2.1 illustrates the amplitude change due to an increase in impedance caused by water replacing oil in a producing zone of the reservoir. The P-wave velocity and density change from baseline (Figure 2.1a) to monitor survey (Figure 2.1b) in the swept zone. As a consequence, the reflection coefficients and amplitudes at the top and bottom of reservoir also change. As the energy travels faster in the reservoir, the deeper reflection arrives earlier, causing the time-shift. The complexity increases in a real field though, where combinations of other effects (such as injection and pressure changes) may overlay or act destructively against each other. The next sections summarize the relation between 4D seismic response and each physical change that occurs in the reservoir.

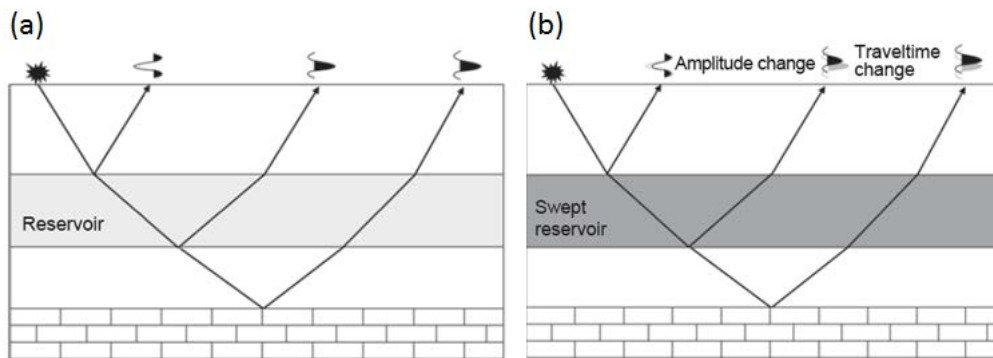


Figure 2.1: Pre-production baseline seismic survey (left) and monitor survey (right), recorded after waterflood production. The monitor detects the changes in amplitudes and time-shifts (extracted from Johnston, 2013).

2.1. Saturation changes

A key concept in interpreting seismic amplitudes is an understanding of how rock properties are affected by a change in fluid fill (Simm and Bacon, 2014). Gassmann's equation (Gassmann, 1951) is a good approximation to calculate the effect of fluid substitutions on seismic properties. Johnston (2013) presents the equation as follows:

$$\frac{K_{sat}}{K_S - K_{sat}} = \frac{K_{dry}}{K_S - K_{dry}} + \frac{K_f}{\phi(K_S - K_f)},$$

$$\mu_{sat} = \mu_{dry},$$

$$\rho_{sat} = \rho_{dry} + \phi\rho_f$$
(2.1)

where K_{sat} , μ_{sat} and ρ_{sat} are the fluid-saturated bulk and shear moduli and rock density, respectively; K_{dry} , μ_{dry} and ρ_{dry} are the dry-rock-frame bulk and shear moduli and density, respectively; K_S is the bulk modulus of the solid mineral grains that form the rock frame; K_f and ρ_f are the fluid bulk modulus and density, respectively; and ϕ is the porosity. K_{dry} , K_S , and ϕ are assumed to be constant before and after the fluid substitution. In practice, equation 2.1 is rearranged to solve for K_{dry} , given K_f for the rock at the initial saturation state. Then it is solved for K_{sat} , given K_f for the new saturation state (Johnston, 2013). The shear modulus is not affected by pore fill because shear waves do not travel through fluids (Simm and Bacon, 2014). Replacing the substituted fluid bulk modulus in equation (2.2) (and considering an isotropic medium), it is possible to determine the changes in P-wave velocity V_p after the fluid substitution.

$$V_P = \sqrt{\frac{k + \frac{4\mu}{3}}{\rho}} \quad (2.2)$$

Some assumptions are involved in the derivation and application of Gassmann's equation (Han and Batzle, 2004):

- The porous material is isotropic, elastic, monomineralic, and homogeneous.
- The pore space is well connected and in pressure equilibrium (zero-frequency limit).
- The medium is a closed system with no pore-fluid movement across boundaries.
- There is no chemical interaction between fluids and rock frame (shear modulus remains constant).

The relative motion between the fluid and the solid rock is also assumed to be negligible and the pores are assumed to be filled with a frictionless fluid.

Other models may overcome some of these assumptions (e.g. Berryman and Milton, 1991; Brown and Korringa, 1975; O'Connell, 1984; Berryman and Wang, 2000). However, in the absence of sand/shale models that are easy to use and readily parameterized, Gassmann tends to be the preferred model (Bacon et al., 2007).

In general, the following changes occur (Johnston, 2013):

- P-wave velocity and density increase for water replacing oil or gas.
- P-wave velocity and density decrease for gas replacing oil or water (gas is more compressible and K_f dominates the equation).
- S-wave velocity remains relatively constant to fluid changes.

2.2. Reservoir pressure changes

Pressure or stress variations result in K_f , ρ , K_{dry} , μ_{dry} and porosity changes in the reservoir-rock framework. If pore pressure decreases below the bubble point, it can also result in gas saturation increase. In summary the changes in 4D seismic occur as follows (Johnston, 2013):

- P- and S-wave velocities and density in the reservoir increase in response to depletion and/or compaction.
- P- and S-wave velocities decrease during injection as a result of pressure increase.

- P- and S-wave velocities change in the overburden and underburden in response to compaction.

The relation between seismic velocity and pressure can be obtained using theoretical or empirical physics models and core measures. Johnston (2013) points out most predictions of velocity sensitivity to pressure have a high degree of uncertainty: core measurements are subject to sampling biases and to damage; laboratory measurements are often made under hydrostatic conditions (and the reservoir might not be under hydrostatic stress); velocity change in the reservoir also depends on the stress path during depletion and changes in nonhydrostatic stress can induce anisotropy.

In addition to saturation and pressure effects, 4D seismic may also detect other types of changes, such as reservoir temperature differences, applied at monitoring thermal recovery processes (e.g. Byerley et al., 2009). 4D seismic is also used for monitoring CO₂ storage (e.g. Lumley, 2008; 2010). However these situations are not the focus of this work.

2.3. 4D seismic undesired differences

Undesired differences are usually present in 4D seismic data and can obscure or cancel out the actual 4D signal caused by reservoir properties changes. Ricket and Lumley (2001) discuss that time-lapse survey images may exhibit undesirable difference noise because of the inability to repeat the identical seismic survey each time or to process the seismic data in exactly the same manner. Even in best-case scenarios, surveys shot at different times can never be completely repeatable, and there is always some level of non-repeatable noise. According to Hubans (2016), from a very general point of view, 4D noise can be assigned to three classes according to its source:

- Random noise is the independent energy recorded by seismic sensors even when no seismic survey source is active. This includes environmental noise such as swell, drilling, ground roll, seabed currents, rig noise and microseismic.
- Repeatability noise is the 4D noise linked to the fact that the acquisition experiment cannot be perfectly repeated. The main source of non-repeatability in offshore streamer acquisition survey is the positioning error for source and receiver locations. Ricket and Lumley (2001) also include as examples different acquisition geometries (grid orientation, bin sizes, offset, azimuths, etc.),

different source waveforms or shooting directions, different receiver hardware or deployment methods, cable feather, different acquisition crews and equipment.

- Coherent noise is when similar noise is present in equivalent portions of both images. This noise is very often related to multiple reflections.

Other sources of 4D undesired seismic differences can be related to the data processing. Ricket and Lumley (2001) state as common reasons for this kind of “noise” different processing contractors and algorithm implementations, inaccuracies in processing navigation data and defining geometries, differences in processing flows, data-dependent processing, differences in processing parameters (e.g., velocity models, statics time picks etc.) or advances in seismic processing methods. Baseline and monitors should ideally be processed as similarly as possible and therefore some of these situations are unlikely to happen in a 4D project.

3. LITERATURE REVIEW

3.1. 4D Seismic interpretation

Data integration is crucial to increase the level of confidence in the 4D seismic interpretation. When available, well logs, cores, well injection and production data, simulation, static (3D) seismic and static geological models and all knowledge about the field should be used in order to correctly interpret 4D data. There are many interpretation approaches, and they will depend on the kind of seismic data acquired (P, S-wave, acquisition method, broad-band seismic), its quality (repeatability, noise) and certainly on the objectives of the project. In this section we discuss some of these approaches, their implementation and how they relate to history matching.

3.1.1. Qualitative interpretation

Qualitative 4D seismic interpretation is essentially the visual detection of time-lapse seismic changes (or absence of changes) and understanding how they calibrate to the reservoir behaviour. This step also consists at identifying if these changes can be related to the problems in acquisition and processing, as discussed in Chapter 2.

Qualitative interpretations of saturation changes evaluate the 4D seismic data in terms of sweep, to identify bypassed oil, baffles, flood fronts, and contact movement. Interpreted pressure changes can be used to infer connectivity, fault seal, and compartmentalization. Most 4D interpretations reported in the literature are qualitative (Johnston, 2013), being done generally in amplitude, impedance and time-shift domains.

Calvert et al. (2016) show an example where 4D seismic was qualitatively used to prove the impact of local porosity variations on the lateral sweep for the Halfdan field. The 4D also provided evidence that some faults serve as potential pathways for formation-water entry into the oil-producing layers. In addition, numerous well-intervention opportunities were identified through integrating the 4D seismic with production and geologic data.

Another successful example of qualitative 4D seismic interpretation was recently discussed in Byerley et al. (2016). The 4D hardening responses have proven to be a key attribute for identifying areas where water has replaced oil (Rose et al., 2011). Conversely, 4D softening responses now are interpreted as the response to oil migrating into previously

water-swept reservoir (i.e., oil resaturation). Since drilling the first 4D resaturation target in 2011, 22 of these targets have been drilled with an 86% success rate, delivering 15 million barrels of new oil production from the Forties Field.

3.1.2. Quantitative interpretation

Quantitative 4D seismic interpretation involves estimates of fluid distributions and their associated saturations and pressure changes quantification. These estimates can be very sensitive to noise and repeatability issues and therefore should be always proceeded after a qualitative assessment of the data. Many quantitative uses of 4D seismic are based on inversion procedures (e.g. Sarkar et al., 2003; Buland and Ouir, 2006), but there are also examples showing that saturation can be quantified using other attributes such as reflectivity changes (e.g. Alvarez et al., 2016), time-shifts (Trani et al., 2011) and well correlation attributes (e.g. Yin et al., 2016). However, these are not the focus of this study and will not be discussed in detail.

3.1.3. Model-based interpretation

The model-based interpretation approach, achieved through a process called simulation-to-seismic (sim2seis) modelling, may be used to validate and optimize geologic models and simulation models. Amini (2014) defines simulation-to-seismic modelling as a process to create the synthetic seismic response from a simulator during different stages of production.

Seismic modelling is done in two main steps. First, reservoir parameters are converted to seismic parameters, e.g., saturated P-wave velocity or density of fluid mixture by using the rock physics models. Then, synthetic seismic sections are calculated based on these seismic parameters (Fahimuddin, 2011). There are several modelling approaches, such as simple 1D convolution, ray-based and full-wavefield based, but the most commonly reported for sim2seis applications is 1D convolution (e.g. Ribeiro et al, 2007; Allo et al., 2013). More sophisticated methods include ray-tracing modelling, from which estimated point-spread functions can be used to generate PSDM (pre-stack depth migration) images without the need to generate synthetic seismograms and processing them, as presented in Drottning et al. (2009); introduced by Lecomte (2003, 2004 and 2008). Such point-spread functions can also be obtained from more advanced (and computationally

expensive) full-wavefield modelling such as finite-difference, as discussed in Lecomte et al. (2015) and, extended by a RTM (Reverse-Time Migration) image in Hill et al. (2016). Another modelling example include a matrix propagation technique developed by Stovas and Arntsen (2006), applied to a simulation based optimization study by Dadashpour et al. (2009). The approach used in this work is as described by Amini (2014): a 1D convolution with the addition of a resolution factor that improves the lateral continuity of the synthetic data.

A synthetic 4D seismic response can be compared either qualitatively or quantitatively with the actual (observed) 4D response. The results are used to update the geologic model or simulation parameters iteratively to match both the observed seismic and production data (Johnston, 2013).

3.2. 4D seismic interpretation and the link with dynamic reservoir models

All 4D seismic interpretation approaches discussed in the previous sections can be used to improve geologic and simulation models. Huang (2001) discusses this process starts with an initial static reservoir description which leads to simulator model building. The simulation model is used to generate synthetic time-lapse seismic data which in turn are compared to measured time-lapse data in a model optimization loop. Model optimization is accomplished through numerical minimization of an objective function formed from the errors between the data measured in the field and the ones predicted by the current model state. Amini (2014) discusses 4D seismic interpretation can be performed at different successive levels, as shown in Figure 3.1. By moving towards more sophisticated levels, the simulation model becomes an integral element of the analysis and more integration between engineering and seismic disciplines is required.

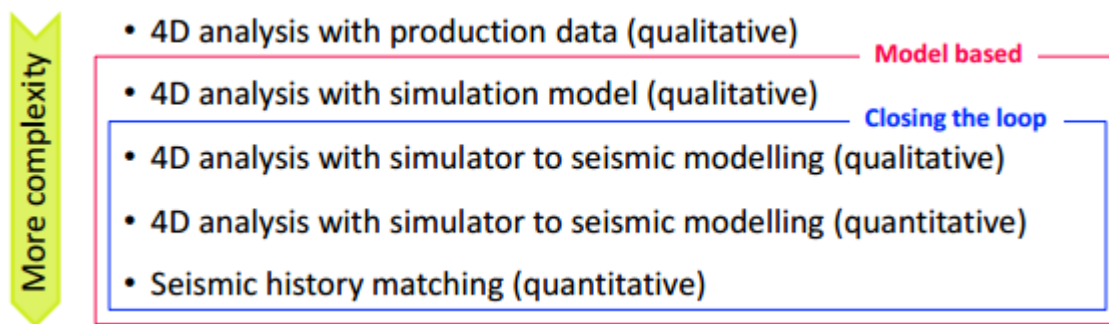


Figure 3.1: Different levels of 4D seismic data interpretation (extracted from Amini, 2014).

3.3. 4D seismic and simulation model updating of the Norne field

There are several examples proving the value of Norne 4D seismic data on history matching the reservoir model. Osdal and Alsos (2002), using sim2seis qualitative comparisons with observed fast-track 4D seismic from 1992 and 2001, identified the gas distribution in the south of the field was not as predicted by the simulation model. Lygren et al. (2005) history-matched the Norne field using acoustic impedances and downhole pressure data (RFT), improving the knowledge about vertical transmissibility and an important fault. Osdal et al. (2006) demonstrated the data both in impedance and amplitude domain was successfully applied to update fluid flow barriers in two locations, resulting in an improved match with well production data. Ouair et al. (2006) describe a computer-assisted history matching using Bayesian-inverted data and the uncertainties derived from this process in their objective function. Dadashpour et al. (2009) used synthetic zero-offset time-lapse seismic amplitudes generated with a matrix propagation technique and minimized the difference between 4D seismic and simulated data. Huang et al. (2011) describes a method that quantitatively correlates inter-well activity to 4D seismic response. They showed an example where this technique effectively detected compartmentalization, resulting in a better match between PLT data and simulation. Yan (2014) used the interpreted oil-water contact from 4D seismic to manually adjust vertical and horizontal permeability from the simulation model and achieved a better match. These work, however, show specific results from a well or an area, without a detailed discussion on how the 4D seismic interpretation was achieved, and what their associated uncertainties are. Raising these discussions for the whole field is, therefore, the focus of this dissertation.

4. METHODOLOGY

The black boxes from the flowchart presented in Figure 4.1 describe a general workflow to achieve a 4D model-based seismic data interpretation. The workflow combines the seismic and the engineering domains. The seismic domain side of the flowchart provides a detailed analysis of the static (3D) and dynamic (4D) seismic data. This includes a preliminary seismic interpretation to assess seismic data quality and to identify the location of the key producing zones, which we call first pass of seismic interpretation. On the engineering domain side, we add the simulator results converted to the seismic domain (synthetic amplitudes) through a simulation-to-seismic modelling (sim2seis) proposed by Amini (2014).

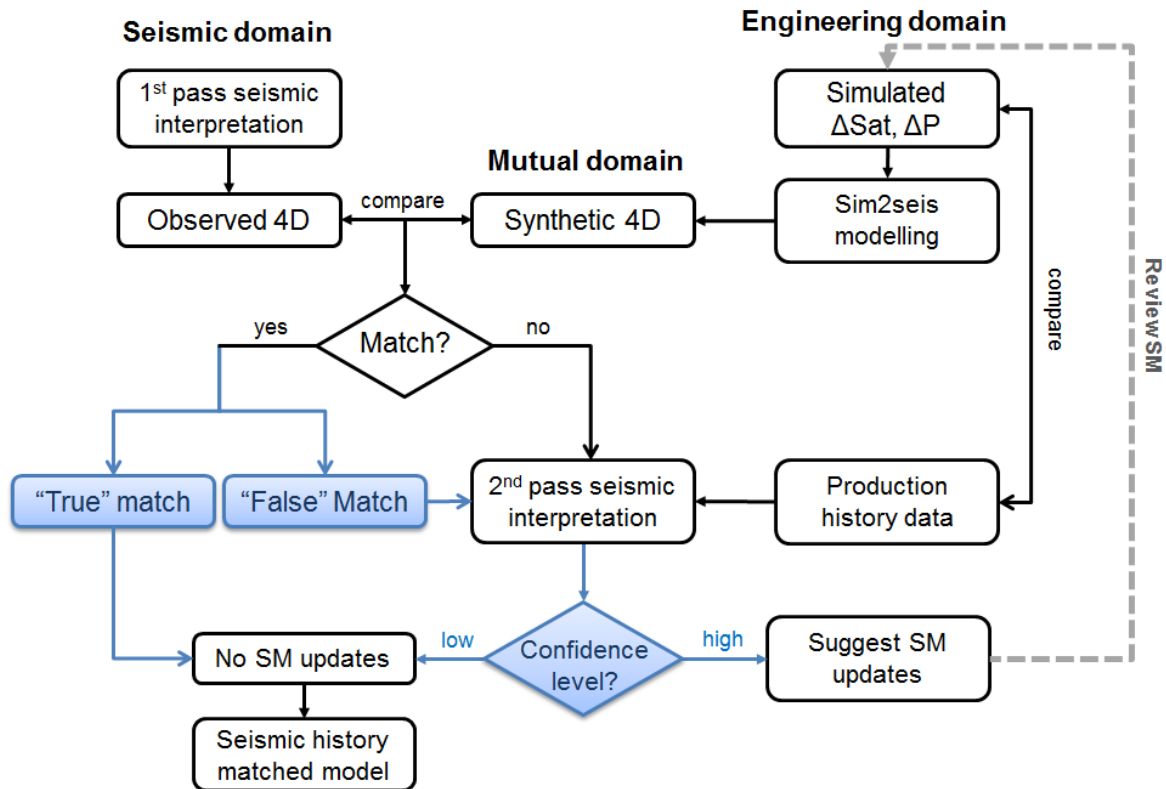


Figure 4.1: A typical seismic interpretation sequence (in black) and the addition of confidence check steps (in blue).

The next step is a comparison between the 4D observed seismic and the synthetic 4D seismic response modelled during the sim2seis step. Mismatches between the two datasets would ideally mean the simulation model has inaccuracies and should be calibrated

to the 4D seismic data. However, this is only the case for seismic data which is noiseless, perfectly acquired, processed and interpreted. The uncertainties inherent to these three stages, however, demand a more thorough knowledge regarding the reliability of the observed seismic data prior to implementing a seismic history matching procedure.

The specific contribution of this work is highlighted by the blue boxes in Figure 4.1. These steps are added to assess the uncertainties in the seismic interpretation and to rank the confidence level on them before applying simulation model updates. The next sections detail each step from the workflow.

4.1. The seismic domain

4.1.1. First pass of seismic interpretation

This step comprises the data preparation necessary to understand the character of the seismic and how they relate to the physical effects in the reservoir. The proposed sequence is as follows:

- a. Gather all necessary and available information to understand the field, including:
 - Structural geology
 - Stratigraphy
 - Reservoir thickness
 - Fluid properties such as bubble point pressure
 - Net to gross on each formation
 - Effective porosity, permeability
 - Well logs, repeated logs
 - Aquifer information
 - Internal structure of reservoir, faults and compartmentalization.
- b. Quality control of the seismic data available, such as:
 - Check “zero-phasesness” of the data
 - Remaining noise content and multiple reflection
 - Migration edge effects
- c. Check for repeatability issues, measured with NRMS difference maps for each survey comparison in a large (~1s) shallow window outside the reservoir, as defined in Stammeijer and Hatchell (2014).

- d. Perform seismic-well tie to verify if the seismic events are aligned with well log data, check for tuning effects and understand possible destructive/constructive interference.
- e. Pick top and base of the reservoir using the 3D baseline seismic cube. In some cases, 4D seismic data might assist with the horizon interpretation.
- f. Produce seismic attribute maps of the top, base and intervals within the reservoir on the separated segments.
 - Map the 3D from base and monitor volumes and 4D seismic anomalies using RMS maps. Test window sizes along the top reservoir for mapping the seismic response.
 - Other seismic attributes as required according to the dataset (e.g. average, most positive/most negative curvature and half energy).
 - Use the maps to identify the location of the main producing zones.
 - Obtain a general understanding on how the wells behaviour relates to the anomalies.
- g. Time-variant time-shift estimation and correction.
 - Generate volumes of time-shift estimations, time-shift compensated amplitude differences and time-strain.

4.2. The engineering domain

4.2.1. Predicted saturation and pressure differences

This step consists in extracting dynamic properties from simulation model corresponding to the time of seismic vintages acquisition to allow a proper comparison. A preliminary comparison between this data and the mapped anomalies from Step 4.1.1.f, combined with the production data from the wells, can also give significant insights to the overall interpretation prior to the sim2seis modelling.

4.2.2. Sim2seis modelling

The sim2seis modelling steps in this methodology are as follows:

- a. Run the simulation model and extract static/dynamic properties for the selected time-steps (same time as seismic datasets were acquired).
- b. Convert to elastic properties (V_p , V_s and density) using a petro-elastic model (PEM) and Gassmann's equations (Gassmann, 1951).

- c. Assign elastic properties to overburden/underburden.
- d. Select an appropriate wavelet.
- e. Seismic forward modelling.

4.3. The seismic and the engineering domain integration

The next step is a qualitative comparison between the observed 4D seismic and the synthetic seismic response modelled during the sim2seis step. This comparison can be done using areal maps and 3D visualization tools around the main horizons within the reservoir to give an overall understanding on the extension of the anomalies and then complemented by vertical sections, as general areal analysis might average out certain features, which can lead to suppressing ambiguities, sidelobes, noise or other issues in the data.

The comparison can be supported by time-shift estimations, time-strain, time-shift corrected sections and the static (3D) seismic volumes. A side-by-side comparison of the seismic datasets with the simulated delta saturations (oil, gas and water) and pore pressure changes is also necessary to understand the physical effects which are linked to the sim2seis anomalies.

Each region or anomaly compared is classified as good, medium or poor match. A good match does not always mean the observed and synthetic data are well calibrated. The interpreter should evaluate if it is a “false match”. An example of “false match” would be sim2seis showing a hardening effect due to depletion in the simulation model, whereas observed seismic shows a hardening effect due to water replacing oil. Proving which interpretation is assumed to be correct in that case will depend on the confidence level assigned to each data, and might be confirmed using historic data from wells, for example. A “true match” means the anomalies represent the same physical effect in the reservoir for both synthetic and real seismic data. In the areas where “true matches” occur and the observed seismic data is reliable, we assume the simulation model is a good representation of the reservoir and does not need further updating. A 4D seismic anomaly can also be a good match and its real cause not be fully comprehended. In this case, the anomaly can also be classified as “false”.

The workflow can be ran in a loop, as indicated by the grey line in Figure 4.1, until all the areas in the simulation model with mismatches caused by simulation model errors

can be given suggestions for updates (using high confidence seismic data). For this reason, while analysing the various comparisons we classify the confidence level of each area. For the poorly matched areas the aim is to first evaluate whether the inconsistency is caused by a simulation model inaccuracy or by uncertainties on the actual seismic response. Information from the mismatches is considered to be used as input for simulation model updating only in the case of a high confidence on seismic data, and having two additional steps to verify the interpretation reliability is beneficial in order to address seismic uncertainties issues.

5. APPLICATION

The methodology was applied to the Norne field, which is a real dataset benchmark case provided by Statoil and their license partners for research purposes, managed by the Norwegian University of Science and Technology. This chapter describes the Norne field and the data available for this work.

5.1. Description of the Norne field

5.1.1. Location and tectonic setting

The Norne field is located in the mid-Norwegian Sea around 200km offshore Norway (Figure 5.1a) at the transition zone between the Nordland Ridge and Dønna Terrace, in an area called Revfallet Fault Complex (Figure 5.1b). The field is a horst structure of 3km x 9km comprising license blocks 6608/10 and 6608/11, at a water depth of 380m.

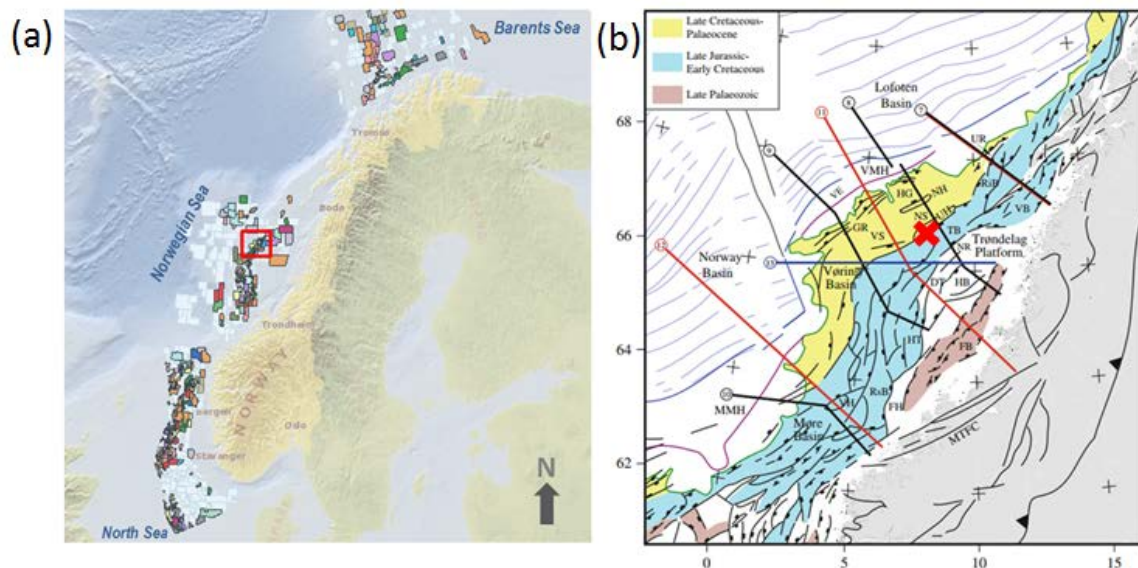


Figure 5.1: (a) Location of the Norne field and (b) Geological setting around the Norne field (modified from NPD, 2016).

The Norwegian Margin formed in response to early Cenozoic continental breakup and subsequent opening of the Norwegian-Greenland Sea. There is a well-defined margin segmentation and the various segments are characterized by distinct crustal properties, structural and magmatic styles, and post-opening history of vertical motions. The

sedimentary basins at the conjugate continental margins off Norway and Greenland and in the western Barents Sea developed as a result of a series of post-Caledonian rift episodes until early Cenozoic time, when complete continental separation took place (Faleide et al., 2008).

The Nordland area has been exposed for two periods of rifting; in Perm and Late Jurassic - Early Cretaceous. During the first rifting, faulting affected a wide part of the area. Especially normal faults, with NNE-SSW trends, are common from this period. The second rifting period can be subdivided into four phases ranged in age from Late Bathonian to Early Albian. The trend during this rifting was footwall uplift along the Nordland Ridge, and erosion of high structures. Between the two rifting periods the tectonic activity was limited, although some faulting occurred in the Mid and Late Triassic. This period was dominated by subsidence and transgression. Some unconformities are discovered, possibly related to tectonic activity. These unconformities are found between the Tofte and Tilje Formations, and within the Ile Formation. After the last rifting no major structural development affecting the Norne reservoir has taken place. The reservoir has gradually been buried deeper, allowing the oil and gas to form and to accumulate within the reservoir (Verlo and Hetland, 2008).

The field consists of two separate oil compartments, the Norne Main Structure (C, D and E-segments) and the Northeast G-Segment. The compartments are bounded by the major horst structure and compartmentalized by minor associated faults (Huang et al., 2013).

5.1.2. Stratigraphy

Figure 5.2 shows a simplified stratigraphic column for the Norne field. The reservoir rocks are of Late Triassic to middle Jurassic age and are subdivided, from top to base, into Not, Ile, Tofte and Tilje Formations. The gas filled soft sandstone from Not 2 Formation (named Garn before Fawke, 2008) and the gas-oil contact in the vicinity of the Not 1 Formation claystones were discovered in December 1991 (Statoil, 2004). 80% of the oil is located in the Ile and Tofte formations, and the free gas in the Not 1 Formation (Statoil, 2004). The reservoir thickness varies from 260m in the southern region and 120m in the northeast part to region due to the erosion trend in Ile and Tilje formations (Verlo and

Hetland, 2008). Most of the sandstones have good reservoir properties, with porosity in the range of 25–30%, and permeability between 20 and 2500mD.



	Not 3	Upper Not Shale
	Not 2 (Not Sandstone)	Not 2.3
		Not 2.2
		Not 2.1
	Not 1	Lower Not Shale
	Ile 2	Ile 2.2
		Ile 2.1
		Ile 1.3
	Ile 1	Ile 1.2
		Ile 1.1
	Tofte 2	Tofte 2.2
		Tofte 2.1
	Tofte 1	Tofte 1.2
		Tofte 1.1
	Tilje 4	
	Tilje 3	

Figure 5.2: Stratigraphic column of the Norne field (extracted from Huang et al., 2013).

The reservoir sandstones are dominated by fine-grained and well to very well sorted sub-arkosic arenites. The sandstones are buried at a deep of 2500-2700m and are affected by diagenetic processes. Mechanical compaction is the most important process which reduces reservoir quality. Still, most of the sandstones are good reservoir rocks. The source rocks are believed to be the Spekk Formation from Late Jurassic and coal bedded Åre Formation from Early Jurassic. The cap rock which seals the reservoir and keeps the oil and gas communicating between the Not 2 and Ile Formations is the Not 3 (or Melke before Fawke, 2008) Formation. The rotated faulted blocks also act as traps (Statoil, 1994). Several stratigraphic barriers are also present in the field, caused by thin carbonate cemented layers within Not 2 and Ile Formations and between Tilje 4 and Tofte 1 Formations. More details about Norne's stratigraphy can be found in Statoil (1994) and Correia and Schiozer (2016).

5.1.3. Production in the Norne field

The field is being developed with four production and two injection templates at the sea bottom connected to a floating production, storage and offloading (FPSO) vessel. Production started in November 1997 and the initial development plan called for the field to be shut down during 2014. However, due to good maintenance work of the Norne FPSO

and a recovery factor of 56.5% which is aimed to increase to 60%, the ambition is to extend the field's life to 2030 (Statoil, 2015).

The field is developed only with horizontal producers. Some of the producers were first drilled vertical, to accelerate the build-up of well potential until plateau production was reached, but these wells were side-tracked later to horizontal production wells (Statoil, 2004).

Both gas and water have been injected into the reservoir, but the gas injection was stopped in 2005. However, injection of gas from the C-wells started again in 2006 for an extended period to avoid depletion in the gas cap (NPD, 2008).

The decision of wellbore locations is based on these principles (Verlo and Hetland, 2008):

- Water injectors located at the flanks of the reservoir.
- Gas injectors located at the structural heights of the reservoir.
- Oil producers located between gas and water injectors for delaying gas and water breakthrough.
- Oil producers located at some distance from major faults to avoid gas inflow.

Table 5.1 summarizes the well completion dates, type of well and their status as of December 2006, which is the end of the production period provided in the benchmark database.

Table 5.1: Well list, with completion dates, well type and status as of end of 2006

Well	Completion	Type	Status
6608/10-B1-AHT2	03/12/2005	observation	plugged (12/2005)
6608/10-B1-BH	09/01/2006	production	open
6608/10-B1-H	05/04/1999	production	plugged (10/2005)
6608/10-B2-H	09/12/1997	production	open
6608/10-B3-H	01/07/1999	production	open
6608/10-B4-AH	12/07/2001	observation	plugged (07/2001)
6608/10-B4-BH	01/08/2001	production	plugged (09/2003)
6608/10-B4-CH	19/06/2004	observation	-
6608/10-B4-DHT2	4/07/2004	production	open
6608/10-B4-H	27/04/1998	production	plugged (05/2001)
6608/10-C1-H	20/07/1998	injection	open
6608/10-C2-H	27/11/1998	injection	plugged (05/2006)
6608/10-C3-H	20/05/1999	injection	open
6608/10-C4-AH	13/01/2004	injection	open

Well	Completion	Type	Status
6608/10-C4-H	18/08/1997	injection	plugged (11/2003)
6608/10-D1-AH	25/06/2002	observation	-
6608/10-D1-BH	05/09/2002	production	plugged (09/2002)
6608/10-D1-CH	02/11/2003	production	open
6608/10-D1-H	18/11/1996	production	plugged (09/2002)
6608/10-D2-TH2	24/12/1997	production	open
6608/10-D3-AH	30/08/2000	production	plugged (06/2005)
6608/10-D3-BY1HT2	07/10/2005	production	open
6608/10-D3-BY2H	25/09/2005	production	abandoned
6608/10-D3-H	04/08/2000	observation	-
6608/10-D4-AH	12/01/2003	production	abandoned
6608/10-D4-AHT2	04/06/2003	production	open
6608/10-D4-H	18/06/1998	production	plugged (11/2002)
6608/10-E1-H	19/06/1999	production	open
6608/10-E2-AH	15/08/2005	production	open
6608/10-E2-H	21/11/1999	production	plugged (07/2005)
6608/10-E3-AH	12/12/2000	production	plugged (12/2000)
6608/10-E3-AHT2	20/12/2000	production	plugged (01/2005)
6608/10-E3-BH	03/04/2005	observation	plugged (04/2005)
6608/10-E3-CH	07/05/2005	production	open
6608/10-E3-H	23/09/1998	production	plugged (5/2000)
6608/10-E4-AH	01/06/2000	production	abandoned
6608/10-E4-AHT2	06/2000	production	plugged (7/2005)
6608/10-E4-H	12/03/2000	production	abandoned
6608/10-F1-H	27/05/2005	injection	open
6608/10-F2-H	15/10/1999	injection	open
6608/10-F3-H	05/02/2000	injection	open
6608/10-F4-H	06/07/2001	injection	open

5.1.4. Dataset available

The following data is part of the Norne field benchmark case:

- 3D seismic cubes acquired in 2001, 2003, 2004 and 2006 (full, near, mid and far angle stacks) in SEG-Y format
- 2 checkshots
- Reservoir top/base horizons in time
- Oil-water contact horizons for 2001, 2003 and 2006 in time and depth
- Interpreted faults from seismic data

- Simulation model in Eclipse 100 format
- Well history data (Bottom-hole/well-head pressure and production rates for producers; Injection rates for injectors) from 1997 to 2006
- Well logs
- Well markers
- Interval velocity model
- Time-depth relations for the wells
- Petrophysical and seismic data processing reports

The simulation model provided in the dataset comprises the whole field with history data described above from the beginning of production until December 2006. The total number of operating wells at this time was 17 (11 oil producers, 6 injectors). Figure 5.3 shows the simulation model structure with the locations of the four segments and the producer and injector wells from the Norne field. More details on the data provided within the benchmark case can be found in Verlo and Hetland (2008).

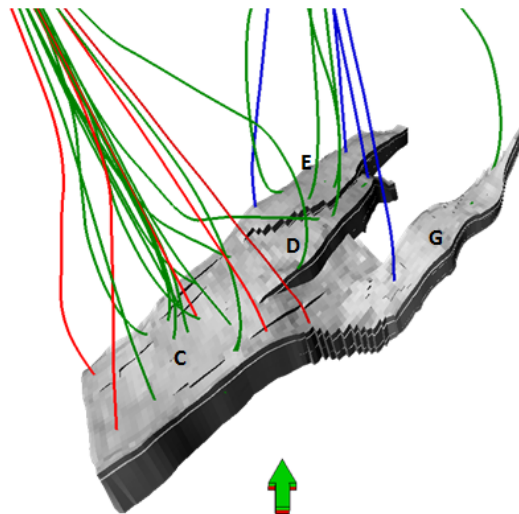


Figure 5.3: 3D view of the Norne simulation model, with segment and well locations (oil and gas producers in green, water injectors in blue and WAG injectors in red).

6. RESULTS AND DISCUSSION

6.1. The seismic domain – data preparation

The 3D seismic surveys available for this study cover 85km², and they have been acquired and 4D processed between June and August of 2001, 2003, 2004 and 2006. In this work we consider 2001 survey as baseline and the others, monitors. Undershoot (seismic acquisition technique in which sources and receivers are in opposite side of an obstruction) of Norne FPSO has been performed for all the available surveys with same undershoot geometry but with different source volumes for 2001 and 2003 surveys (Osdal and Alsos, 2010). The available seismic datasets are assumed to have been properly 4D processed (noise and multiple reflections attenuated, zero-phased and 4D matched). More details on Norne's processing can be found in WesternGeco (2006).

This section describes the character of the seismic data in the Norne field, denominated in the methodology as the first pass of seismic interpretation. Note that all vertical axes for seismic figures from this and next chapters are in milliseconds (two-way-time). All the seismic data analysis, visualization, attributes calculation and quality control was done using Petrel (2014 version), except the time-variant time-shift computation and correction which was done using Hampson-Russell (HRS-9/R2.1 version) and the well-tie, ran in RokDoc.

6.1.1. Seismic data polarity

The polarity is SEG positive, which means an increase in acoustic impedance is plotted as a peak.

6.1.2. Seismic-well tie

Exploration well 10-4 was selected for this analysis as it is the only well with checkshot data available throughout the whole reservoir interval. The workflow is described by the following steps:

- a. Conversion of well's measured depth into two-way-time

The well has been checkshot-corrected and the depth-time conversion was performed.

b. Wavelet estimation

The RokDoc well tie tool uses the approach described in White and Simm (2003), in which the wavelet is extracted from the data using a least-squares technique. A volume of data around the well (20x20 inlines and crosslines) is scanned for the best fit and the wavelet is extracted from the traces with the best proportion of trace energy predicted (PEP) by the synthetic seismogram:

$$\text{PEP} = 1 - \frac{\text{energy in the residuals}}{\text{trace energy}} \quad (6.1)$$

where the energy of a trace is the sum of the squares of a segment of a time series and the residuals are the difference between a seismic trace and its matched or filtered synthetic seismogram.

For this dataset, the smaller the time window, the more disperse the PEP map is. Therefore it was decided to use 2100-2492ms window which was the best compromise between PEP values, as they are focused in one area, and window size. The delay plot, defined by the shift in reflectivity which optimizes the PEP value, shows reasonable values for this same area. Figure 6.1 shows the PEP and shift maps for the traces at the well location (black cross) and for the trace location considered to be the best match (red “plus” in Figure 6.1).

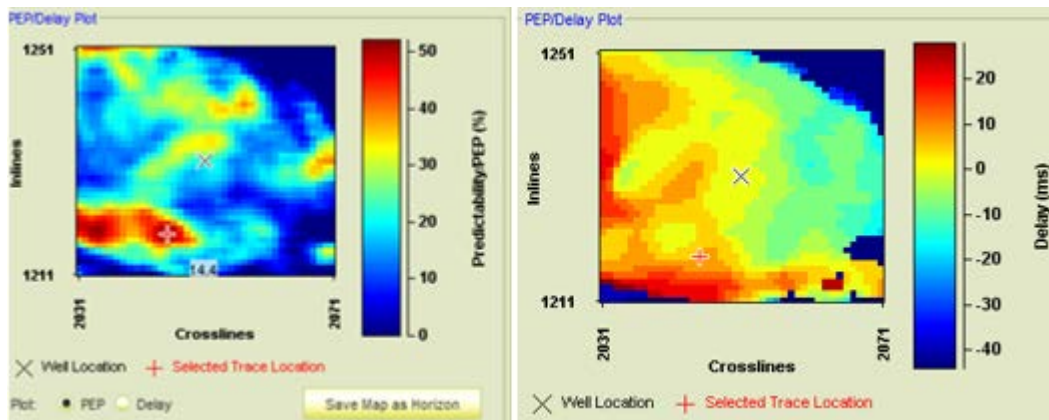


Figure 6.1: PEP (left) and delay (right) plots from the selected trace location and well location

c. Create synthetics

The extracted wavelet from best match location (Figure 6.2) was convolved with the reflection coefficients from this well, producing the synthetics shown in Figure 6.3. The generated synthetic displays and the asymmetry of the cross-correlation function of the

synthetic trace with the seismic trace indicates a bulk time-shift exists between them. This shift has been applied using the automatic tool from RokDoc (Figure 6.5) and the cross-correlation function became more symmetric, improving from 81% to 87.5%, indicating a good tie. Figure 6.4 shows the cross-correlation function before (blue curve) and after the shift (red curve), measured at the window displayed between the two horizontal black lines from Figure 6.3. No stretch and squeeze was applied.

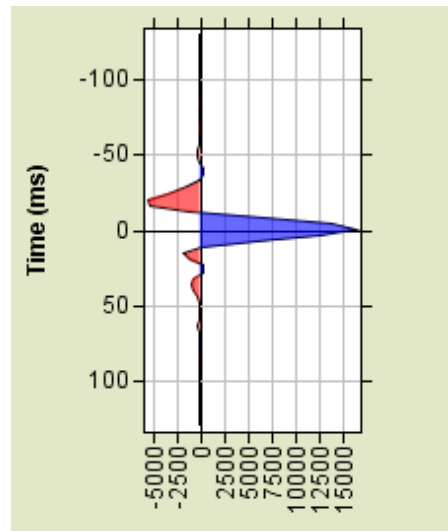


Figure 6.2: Statistical wavelet extracted from the best PEP location, in a window of 2100-2492ms.

The synthetic from Figure 6.5f indicates the top reservoir (Top of Not 2 Formation) is located at the zero-crossing. There is not a lot of acoustic impedance contrast between the claystones from Not 3 and the soft sandstones from Not 2 Formation and tuning effects between these thin layers (Not 2 package is approximately 35m thick) are present. The reservoir at the G-segment is also known to be thinning and slightly dipping towards the area of well 10-4. The caliper log (green curve in Figure 6.3a) indicates a bigger borehole diameter at this location, possibly resulting in degraded data in that interval. Therefore, it is uncertain whether the top reservoir horizon, picked at the through, is exactly the through or it is the zero-crossing below it. It was decided to rely on the top reservoir horizon picked by Statoil, as discussed in the following item, with these uncertainties in mind.

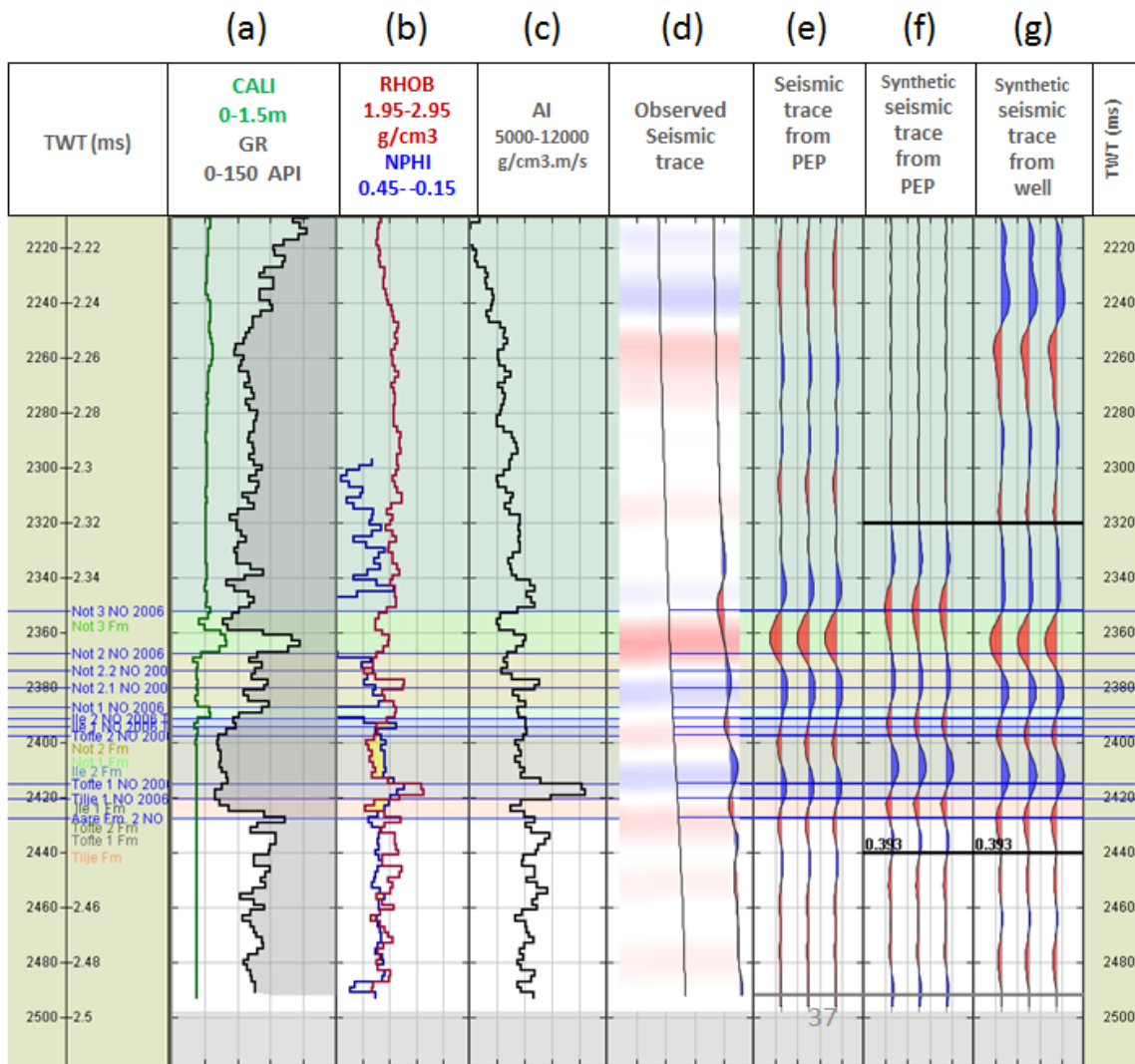


Figure 6.3: Log data for well 10-4 (a) caliper (green) and gamma-ray (black) logs; (b) density (red), porosity (blue); (c) computed acoustic impedance; (d) trace at well borehole path; (e) seismic traces from the best match location; (f) synthetic traces generated with data from best match location; and (g) synthetic seismic traces from well location.

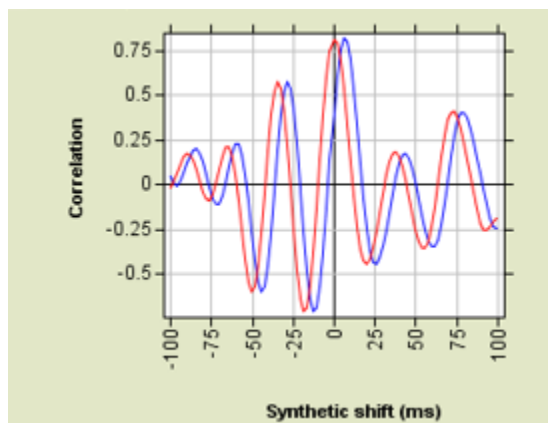


Figure 6.4: Cross correlation function before (blue curve) and after bulk time-shift (red curve) application.

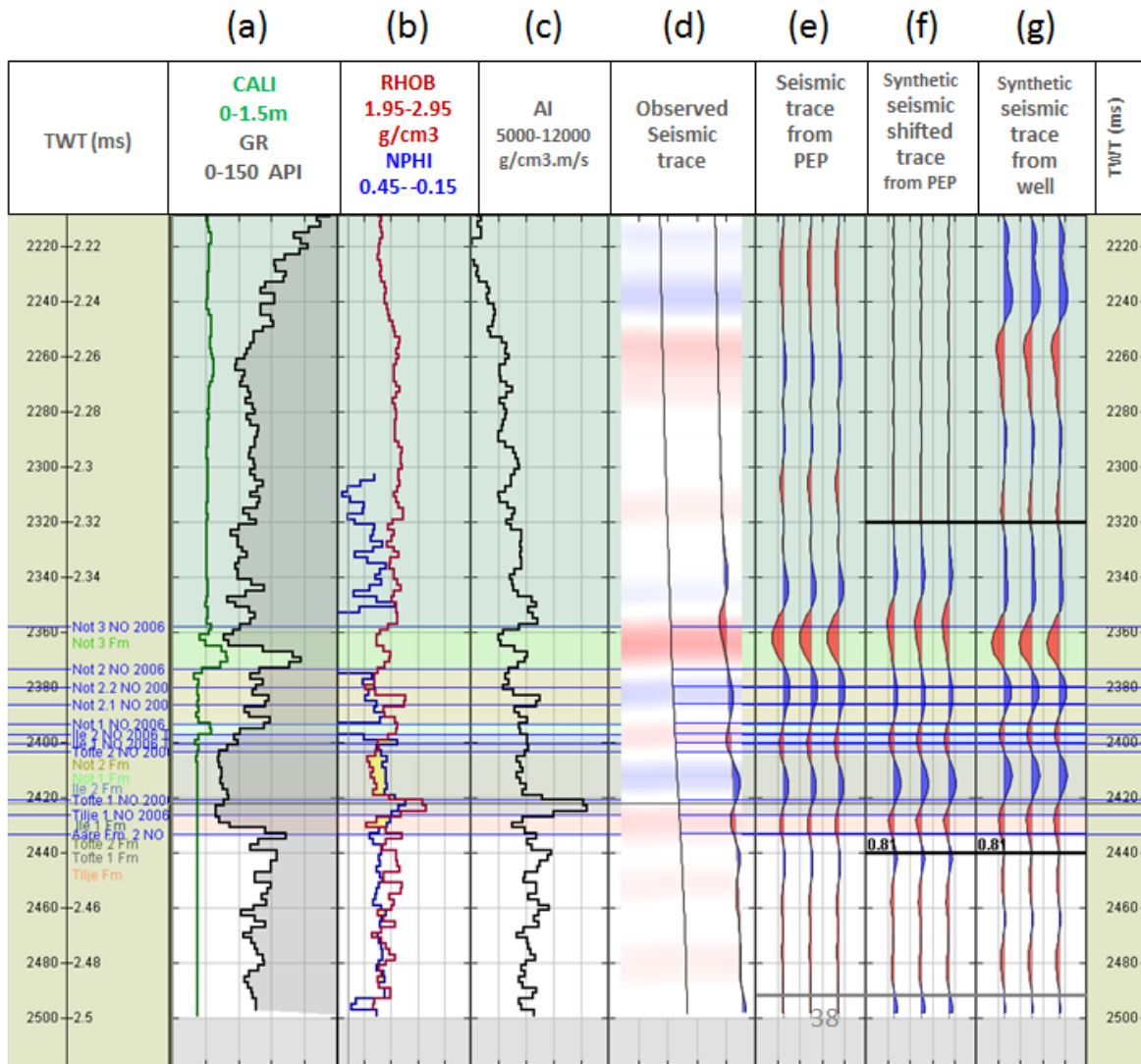


Figure 6.5: Log data for well 10-4 (a) caliper (green) and gamma-ray (black) logs; (b) density (red), porosity (blue); (c) computed acoustic impedance; (d) trace at well borehole path; (e) seismic traces from the best match location; (f) synthetic traces generated with data from best match location; and (g) synthetic seismic traces from well location, after bulk shift was applied.

6.1.3. Pick top and base of the reservoir using the 3D baseline seismic cube

Both top and base reservoir horizons were provided by Statoil. The troughs from the strong negative reflector at the reservoir zone were picked as the top, and they are assumed to represent the softening caused by the decrease in acoustic impedance at the interface between the cap rocks from Not 3 (claystones with siltite intercalation) and the reservoir at the Not 2 (soft sandstones) Formations. Given that the polarity of the data is SEG positive (increase in acoustic impedance is represented by a positive peak), and assuming the

seismic resolution is enough to detect this impedance contrast, we assume the trough is correctly considered as the top of reservoir, or top of Not 2 Formation.

The provided horizons were edited so that the picks outside the interest zone were removed. The anomalous and discontinued picks have been identified and modified in order to smoothly follow the negative reflector. Figure 6.6 shows an example of the original and the edited picks.

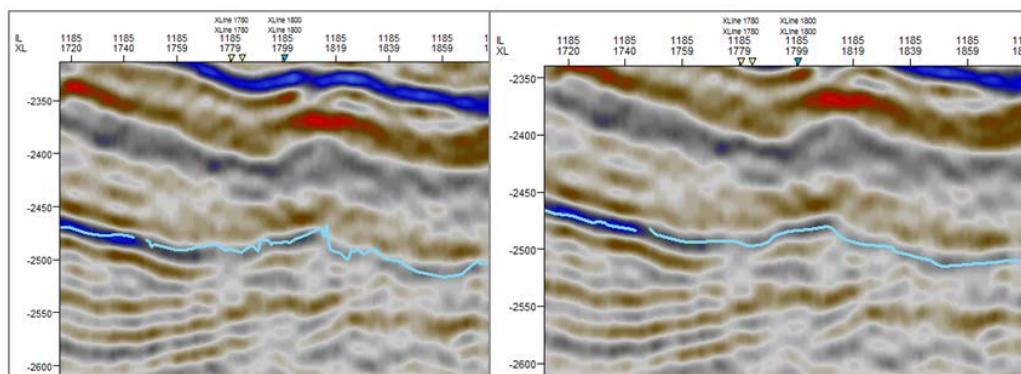


Figure 6.6: Original horizon picks (blue line on the left) and edited horizon (right) QC'ed and plotted in the baseline (2001) 3D vertical section

6.1.4. Quality control of the seismic data available

Regardless of the assumption seismic data was properly 4D processed (and noise-attenuated), the data was acquired and processed more than ten years ago, when more sophisticated algorithms and acquisition techniques were not available. This section points some examples of uncertain seismic data and measurements of its 4D quality.

- Remaining noise content

One of the main uncertainties of the available seismic is its remaining 4D noise, which in some cases may have the same magnitude as the 4D signal. Figure 6.7 shows one example where production-related changes may be similar or even smaller relative to non-repeated noise.

- Edge effects

Edge effects are present; however they do not affect the reservoir zone as displayed in Figure 6.7.

- Sea-bed diffractions

The sea-bed at the Norne field, as for several of the northern fields in Norway, is dominated by glacial depositions. A variety of ice scours of different sizes and shapes are

observed (Grude et al., 2012), causing diffractions (and diffracted multiples) that not always are collapsed during migration. Diffracted multiples are very sensitive to water column changes and therefore difficult to repeat (Osdal and Landrø, 2010). This can be a source of noise in the time-lapse data as seen in Figure 6.8.

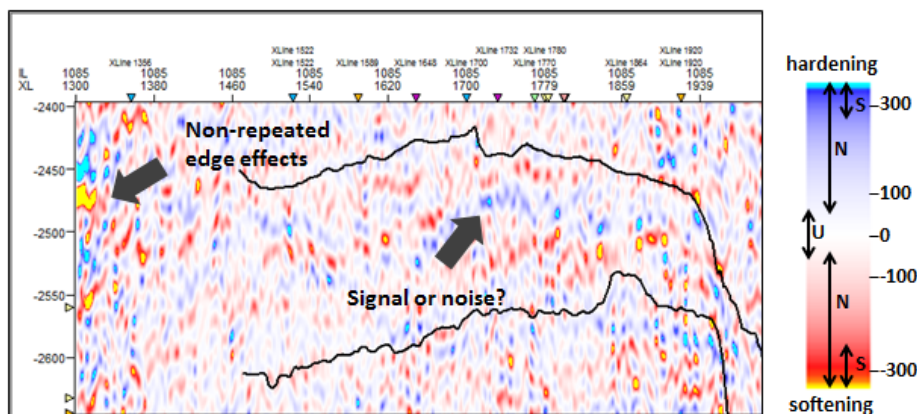


Figure 6.7: Example 4D difference line (2004 minus 2001) showing non-repeated edge effects and a portion inside the reservoir (between black lines) where the magnitude of the signal may be the same as the noise. The arrows in the colour bar show the amplitude difference intervals for unchanged amplitude (U), noise (N) and signal (S). Note that N and S may overlap.

- Repeatability issues

Repeatability can be measured using various attributes. In this item we chose to display NRMS, which is the most widely used to quantify repeatability of 4D data (and easier to find reference values in the literature). NRMS can be defined as:

$$NRMS = \frac{RMS(M - B)}{\frac{1}{2} (RMS_M + RMS_B)} \quad (6.2)$$

The NRMS is sensitive to phase and amplitude differences (distortion), time shifts, and noise. Typical “good” values of NRMS quoted in the literature range from 0.1 to 0.3 (10% to 30% non-repeatability) (Johnston, 2013).

The window chosen to calculate this attribute on Norne was from 1200 to 2200ms (just above the reservoir zone), where no production-related differences are expected and where the position is deep enough to avoid the water-bottom. Figure 6.9 shows NRMS maps for the three pairs of survey comparisons, using 2001 as a baseline. We can note 2006 versus 2001 presents lower NRMS values in general (mean of 0.26), whilst the other two comparisons present a mean of 0.27.

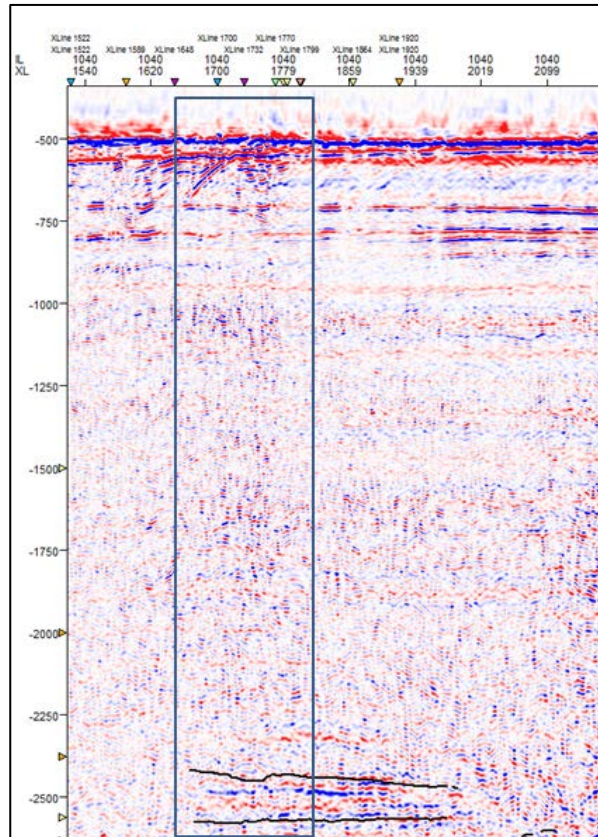


Figure 6.8: Example 4D difference line (2004 minus 2001). The rectangle shows diffractions in the sea bed and their multiples propagating all the way down. Care should be taken when interpreting the reservoir zone underneath these areas as they can affect the reservoir zone.

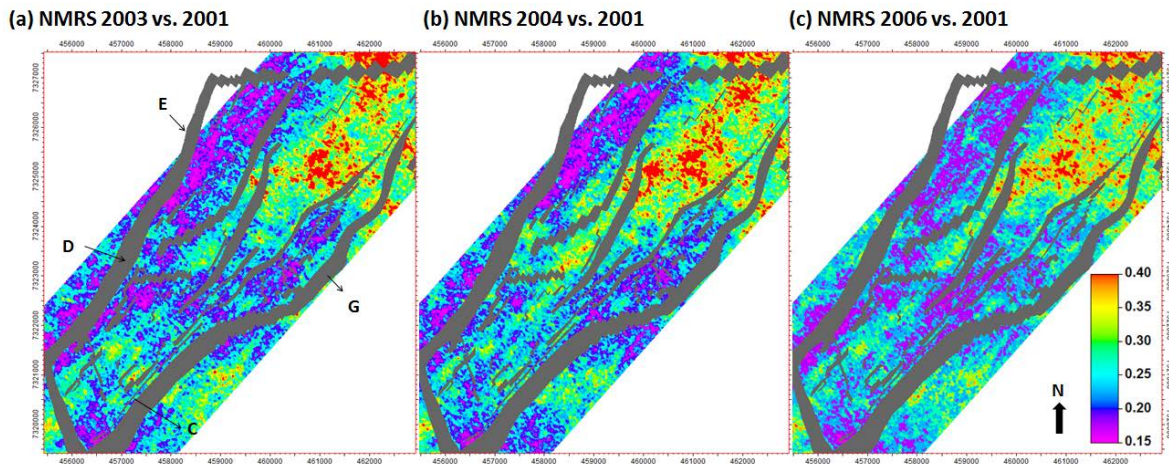


Figure 6.9: NRMS values for 2003 versus 2001 comparison with segments location (a), 2004 versus 2001 comparison (b) and 2006 versus 2001 comparison (c).

All comparisons present higher values in the northern zone between E and G segments (red area). In Figure 6.10, we observe a section through the region with higher NRMS values. These are affected by differences in reflectivity caused by undershooting.

The differences are most evident in the shallow part (pointed by the black arrows), but amplitude scaling differences also seem to be present underneath it. Chu et al. (2015) comment there are three issues regarding undershoot and prime data compatibility:

- Lack of near-offset data reduces the fold of full- and near-angle stacks.
- Lack of near offset data presents a challenge in attaining a high-quality water column statics solution.
- Geometric non-repeatability is generally higher than in prime lines, leading to inferior seismic repeatability.

Figure 6.11 shows the location of the obstruction. According to Eiken et al. (2003), a surface obstacle as the Norne FPSO would normally cause a 600m - 1000m wide and several km long hole in the good-quality data coverage. This would hinder the monitoring of almost half the Norne field. The data hole was at Norne minimized by:

- Close-passes with an extra shooting boat;
- Streamer steering allowing tow points as near as 40-50 m from the obstruction;
- Reduced streamer array width (50 m cable separation); and
- A carefully planned and run operation.

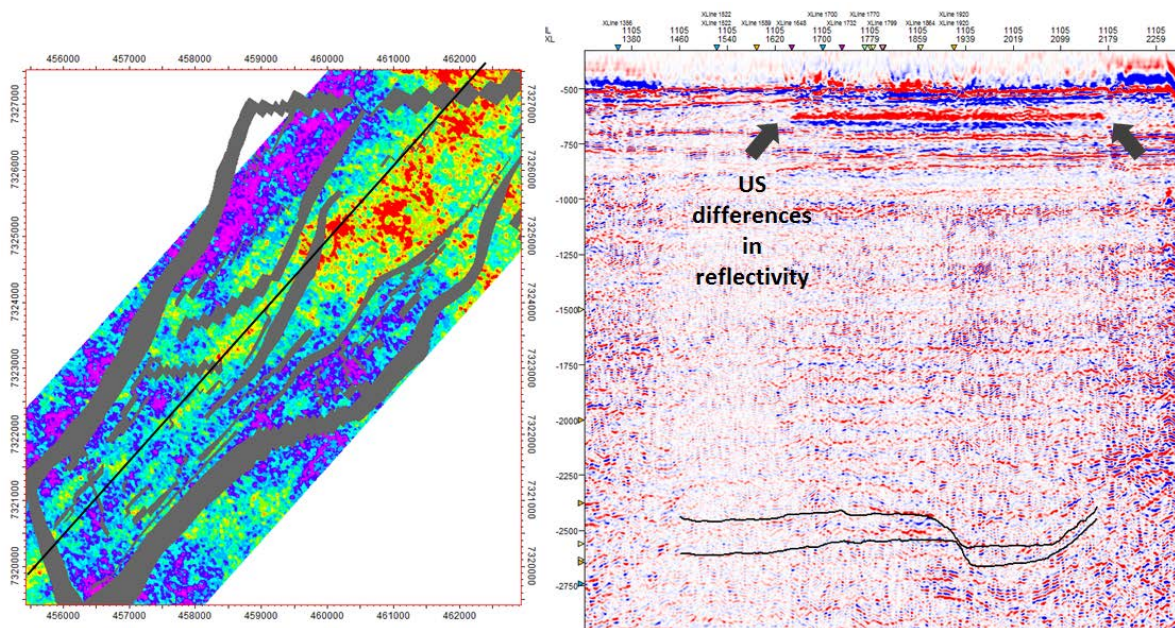


Figure 6.10: NRMS map of 2004 vs. 2001 comparison with a black line passing through the undershooting zone (left) and 4D difference vertical intersection from the black line (right). The arrows show differences in reflectivity in the undershoot zone, which also affects the deeper areas. The black horizons are the top and base of the reservoir.

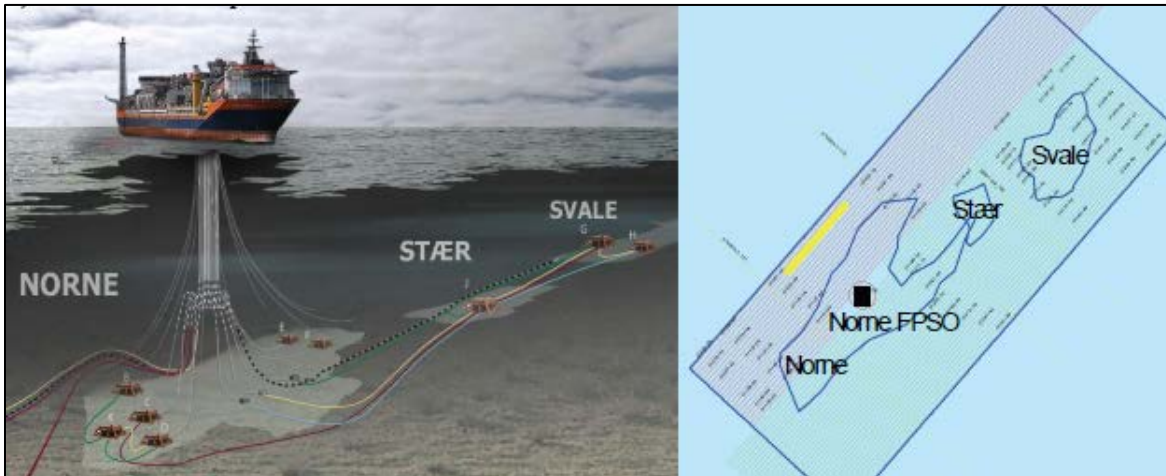


Figure 6.11: Norne FPSO and templates (left) and 4D acquisition area indicating the location of the obstruction (right) (extracted from Osdal et al., 2008).

The southern area in the C-segment presents slightly higher NRMS values for all the comparisons. Besides being in the border of the horst, in a steeply dipping zone where imaging is more challenging, this area seems to be especially problematic for 2001 survey, as when we compare the other surveys e.g. 2003 versus 2006, the NRMS map does not present the same effect in this area (Figure 6.12). This will be analysed and discussed in detail in Section 6.3.

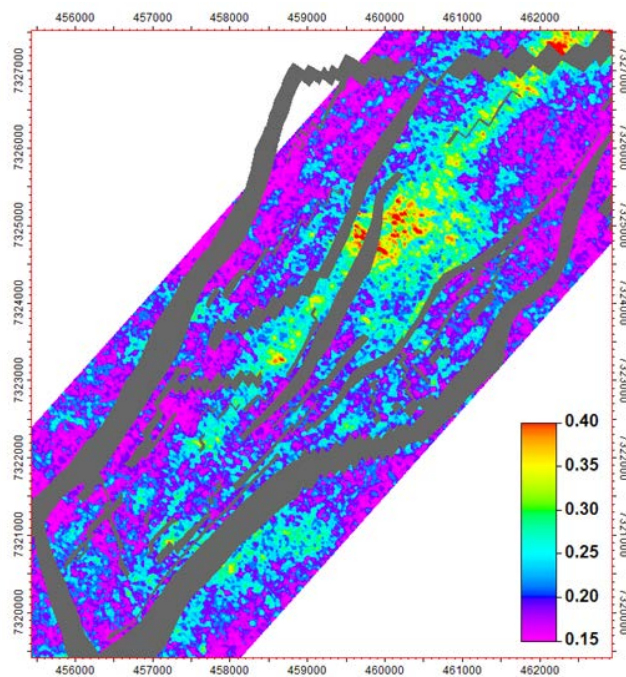


Figure 6.12: NRMS map of 2003 versus 2006 comparison.

As discussed by Kragh and Christie (2002), NRMS is sensitive to any change in the data whereas predictability is sensitive to reflectivity changes and to noise. However, predictability measures did not seem to give additional information at this point and further investigations on other attributes were not performed.

6.1.5. Understanding the 4D seismic response

RMS amplitude of the top reservoir was extracted from each 3D seismic cube. Several windows around the top reservoir horizon previously obtained were tested to compute this attribute, and we found the best compromise between resolution and noise content was 15ms below this horizon. From these maps we could identify brighter zones mainly associated with presence of gas in the E and G-segments (Figure 6.13).

To evaluate the differences in RMS we used Stammeijer and Hatchell's (2014) recommendation ($RMS_M - RMS_B$ instead of $RMS_{(M-B)}$) to preserve the polarity of the 4D anomalies. These maps are shown in Figure 6.14a to c, from which we could identify the 4D response at the top reservoir is present mainly in G and part of D and E segments. The changes in C and part of E segments occur deeper, and it is challenging to capture all of them into other windows, since they do not have the same position and the 4D signal is contaminated with side lobes. The maps were used to obtain a general understanding on how the wells' behaviour relate to the anomalies. For example, the softening response (red colour) is related to pressure increase in the G-segment and to presence of gas in D and E segments. These responses will be analysed and discussed in more detail in Section 6.3 as well as other 4D signal present on the data which include the OWC movement and anomalies around the wells.

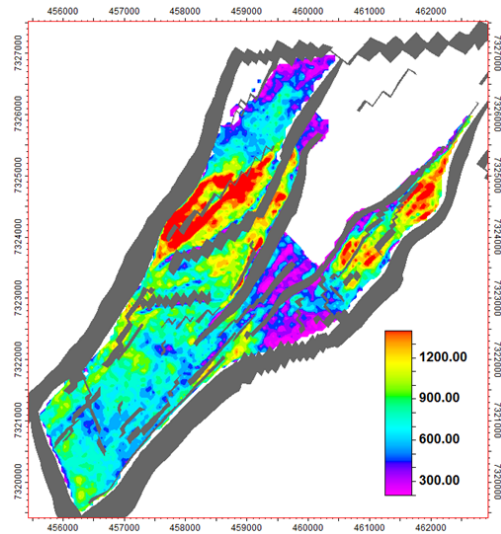


Figure 6.13: RMS values of the 3D Baseline survey (2001). Note the brighter zones are located in G and E segments and may be related to hydrocarbons from Not 2 Formation.

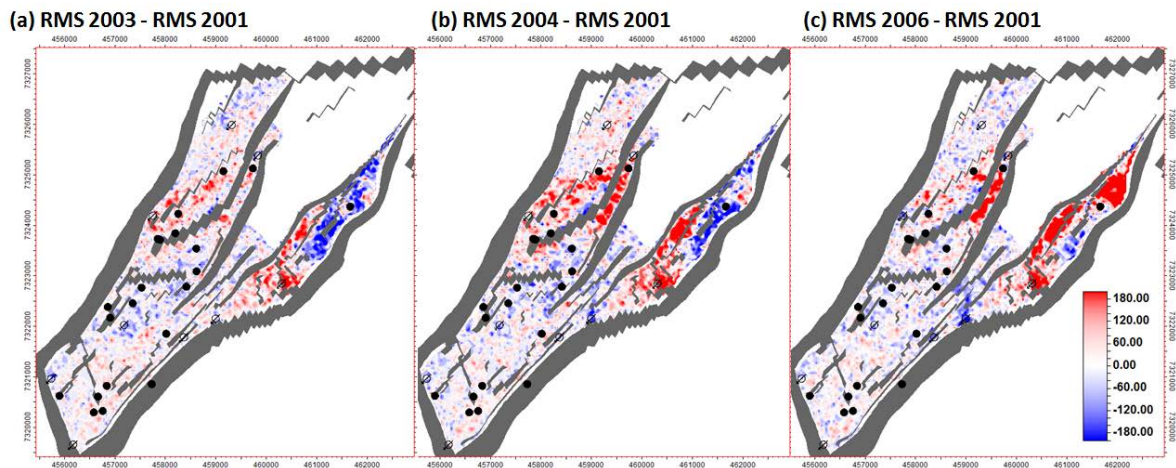


Figure 6.14: RMS differences in the top reservoir + 15ms horizon. (a) RMS 2003 minus 2001; (b) RMS 2004 minus 2001; and (c) RMS 2006 minus 2001. Solid black circles are the producer well locations and non-solid arrowed circles are the injectors. Red colours are related to a decrease in impedance (softening) and blue, to an increase (hardening).

6.1.6. Time-variant time-shift estimation and correction

Time-variant time adjustments were applied in order to compensate for changes in velocity, so that differences compare only the differences in reflectivity between the two surveys and not misalignments in structure. To get a better understanding of where in the reservoir the velocity is changing, time-shifts were estimated. Also, the surveys were time aligned creating new difference volumes. Hampson-Russell's method is described in CGG (2009) and consists in the following steps:

1. Generate time-shift and correlation coefficient volumes for each pair of survey. They were computed for all survey combinations (using 2001 and also 2003 vs. 2004, 2003 vs. 2006 and 2004 vs. 2006), since we make several cross-survey combination comparisons in the next phase of the project.
2. Cross-plot correlation coefficients and time-shifts. Typically, bad time shifts occur when correlation coefficients are poor. This is often due to poor reflectivity. Low correlations also relate to production effects. The cross-plot is also used to identify spurious time-shifts that should not be corrected for. Figure 6.15 shows one example of cross-plot for 2001 and 2006 surveys comparison.
3. Pre-condition and application. The differences we want to keep in the data are the ones related to production/injection effects. These correspond to the areas where most of the time-shifts are, and above a correlation threshold observed in step 2. This means only the time shifts within this range and above the corresponding cross-correlation threshold will be applied in the process.

Figure 6.16 shows the result of a vertical seismic section before (Figure 6.16b) and after conditioning the time-shifts (Figure 6.16d), in addition to the corresponding original amplitude differences (Figure 6.16a) and correlation coefficients (Figure 6.16c). Note that the calculations are very sensitive to window correlation in this case, which was tested and defined as 80ms. The “patchy” pattern follows the limits of the correlation windows. Figure 6.17 shows a vertical section along two water injectors before and after time-shift correction. Note that after correction, only amplitudes differences are visible.

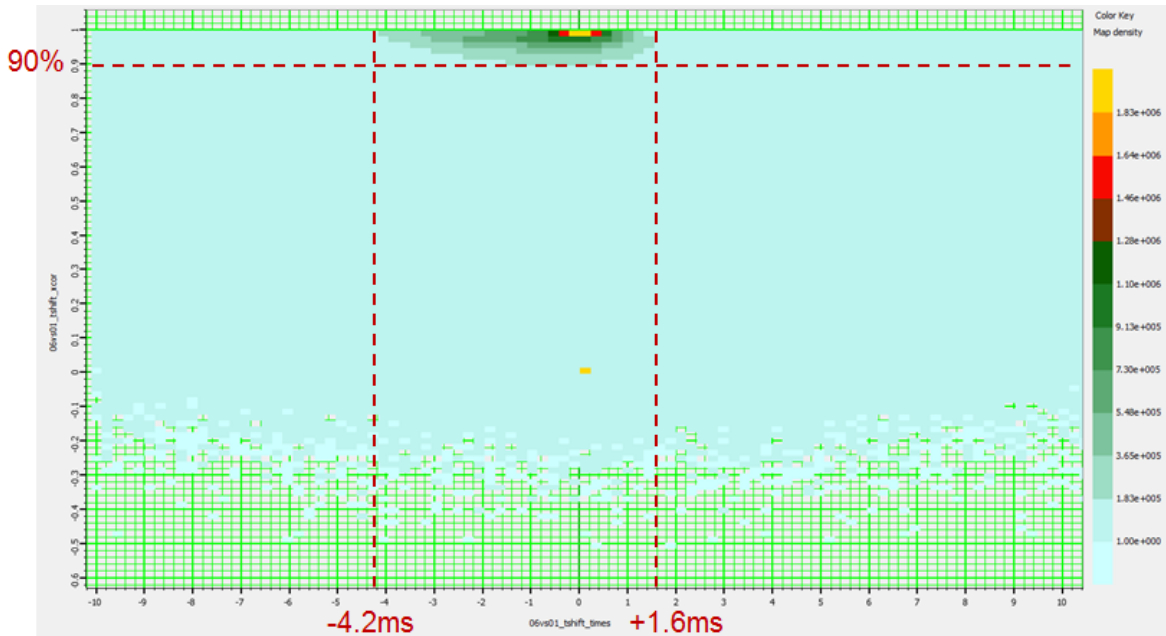


Figure 6.15: Crossplot time-shift versus correlation coefficient 2006 versus 2001 comparison. The red dashed lines indicate the threshold ranges selected for cross-correlation and time-shifts estimates.

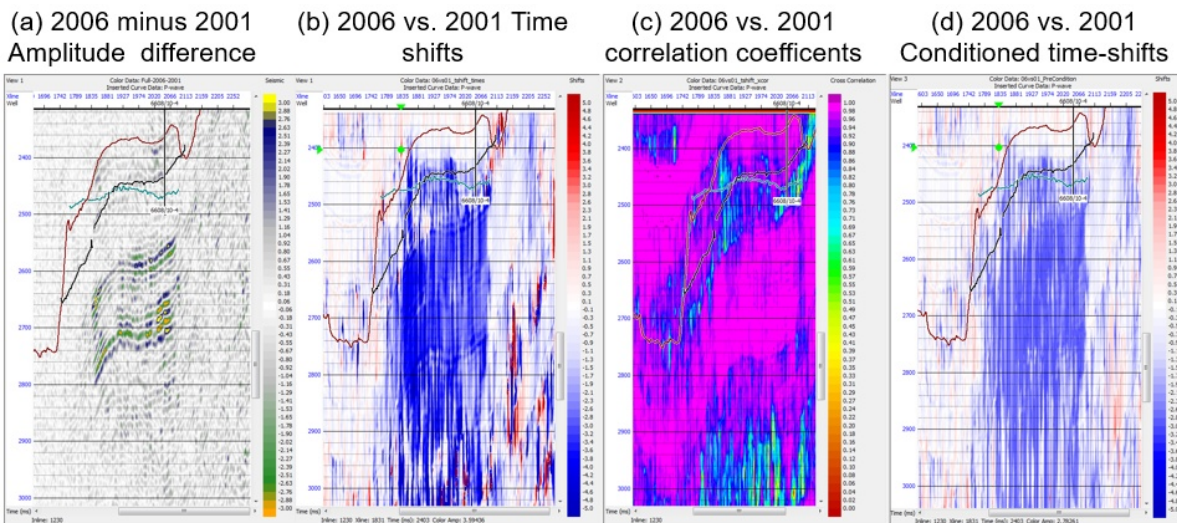


Figure 6.16: Example vertical section showing (a) amplitude differences within and below reservoir (red and black horizons); (b) calculated time-variant time-shifts; (c) correlation coefficients; and (d) time-shifts after conditioning, for 2006 versus 2001 comparison.

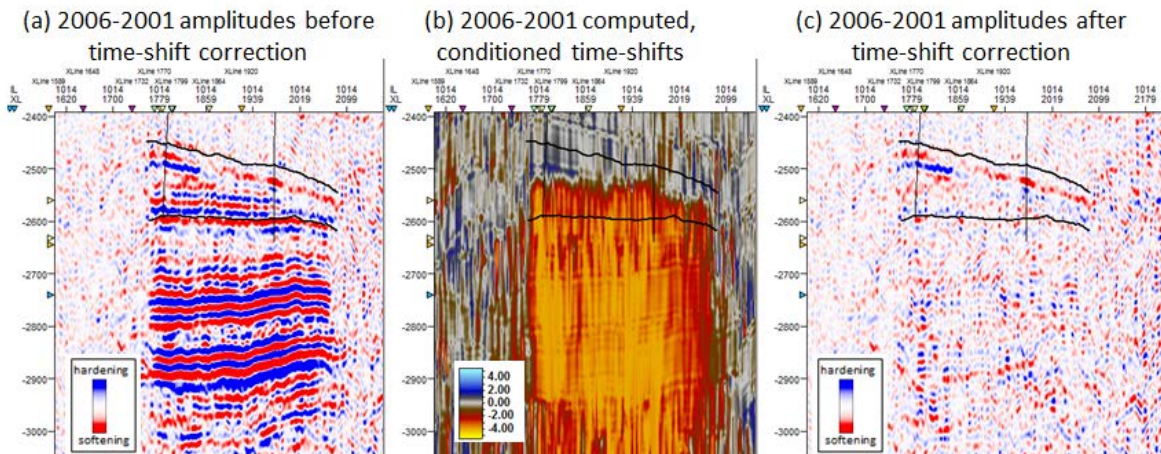


Figure 6.17: Amplitude difference before time-shift correction (a); calculated time-shifts after conditioning step (b); and amplitude differences after time-shift correction (c) for a vertical section along two water injectors. The negative (orange) time-shift is a delay caused by velocity decrease from pore pressure increase. The small advance time-shift above (blue) is caused by upward OWC movement.

6.2. The engineering domain: simulation-to-seismic (sim2seis) modelling

This section discusses each step for running sim2seis and the main parameters used for the Norne data. The code was developed and described by Amini (2014) in the following six steps. The project's specific parameters are discussed below each step explanation:

1. Run the simulation model and extract the static (ϕ , V_{shale} , lithofacies index etc.) and the dynamic properties (pore pressure and saturation for different fluid phases, solution gas-oil-ratio, oil formation volume factor, etc.) from the simulation model at the selected time-steps.

The simulation model provided was run using a black-oil commercial simulator (Eclipse 100). The time-steps were selected as close as possible to the seismic acquisition dates.

2. Convert the static and dynamic properties into elastic properties (V_P , V_S and density) using a petro-elastic model (PEM). The underlying equations and parameters in PEM should be calibrated according to the specific field of study. This calibration ensures realistic values for changes in in-situ elastic parameters due to changes in saturation and pressure.

Table 6.1 summarizes the main parameters for deriving a suitable PEM for Norne. The sand and clay properties were calibrated using F-1H well logs by Briceno (2015).

Other specific parameters such as water salinity, gas gravity, API were taken from Suman (2013). The equations proposed by MacBeth (2004) were used to derive stress sensitivity, with the modifications as proposed by Briceno et al. (2016):

$$k_{dry}^{(dyn)} = k_{dry}^{(st)} \frac{1 + E_k e^{-P_{eff\ initial}/P_k}}{1 + E_k e^{-P_{eff\ mon}/P_k}} \quad (6.3)$$

and

$$\mu_{dry}^{(dyn)} = \mu_{dry}^{(st)} \frac{1 + E_\mu e^{-P_{eff\ initial}/P_\mu}}{1 + E_\mu e^{-P_{eff\ mon}/P_\mu}} \quad (6.4)$$

where E_k , P_k , E_μ and P_μ are the rock stress sensitivity constants estimated in MacBeth (2004). $P_{eff\ initial}$ is the reservoir pre-production effective pressure and $P_{eff\ mon}$ is the effective pressure at the monitor survey time. The whole E_k and E_μ range from MacBeth (2004) was tested. The graph from Figure 6.18 shows the highest E_k value is able to detect more changes in the bulk modulus (most stress-sensitive). The same was observed for E_μ . This analysis was done to calibrate the pressure effect observed in G-segment, where no changes in 4D signal were visible after a large (>200 bar) increase in pore pressure.

Table 6.1: Main PEM parameters

Sand properties	Bulk modulus (k)	28 GPa
	Density (ρ)	2647 kg m ⁻³
	Shear modulus (G)	19 GPa
Clay properties	Bulk modulus (k)	21 GPa
	Density (ρ)	2663 kg m ⁻³
	Shear modulus (G)	11 GPa
Stress sensitivity parameters	Frame bulk modulus (k_{inf})	10.23 GPa
	P_k	5.62 MPa
	E_k	3
	μ_{inf}	4.88 GPa
	P_μ	7.97 MPa
	E_μ	2

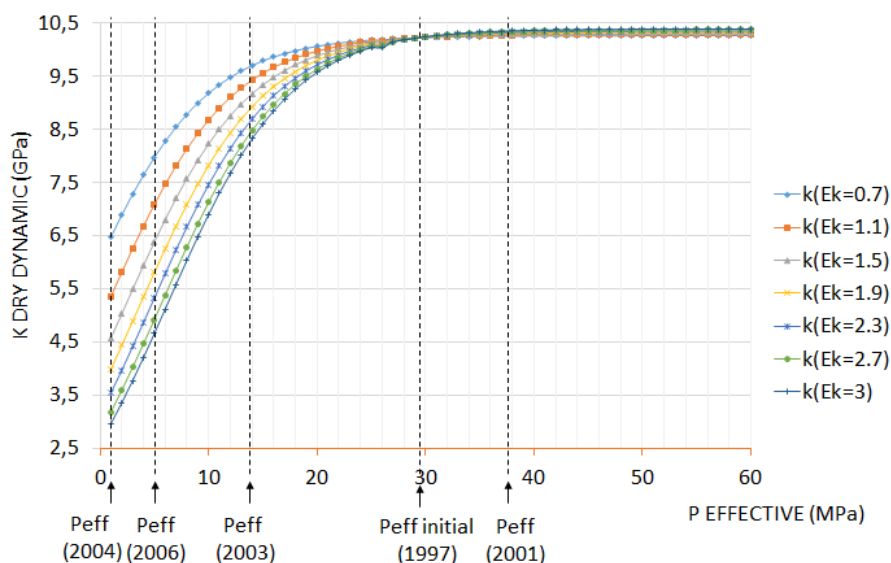


Figure 6.18: Stress sensitivity curves from equation 6.3 for the whole E_k range in MacBeth (2004).

- To be able to calculate the synthetic seismic response, elastic properties should also be assigned to the overburden and underburden.

The values for overburden and underburden were assigned using the average of the available well logs, as described in Table 6.2.

Table 6.2: Parameters for over and underburden

Overburden	V_p	2900 m/s
	Density (ρ)	2400 kg m ⁻³
	V_s	1500 m/s
Underburden	V_p	3000 m/s
	Density (ρ)	2400 kg m ⁻³
	V_s	1550 m/s

- Choose a seismic modelling approach and an appropriate wavelet to generate the pre/post stack synthetic seismic.

The wavelet was statically extracted from the baseline (3D) full-stack in a window around the reservoir, using the RokDoc software. Figure 6.19a and b show the wavelet and its amplitude spectra respectively. We can note the dominant frequency is 19Hz. For an average interval velocity of 2700 m/s (observed in the well sonic logs), the wavelength λ can be approximated as:

$$\lambda = \frac{V_{int}}{f} = \frac{2700 \text{ m/s}}{19 \text{ Hz}} = 142 \text{ m} \quad (6.5)$$

and the seismic resolution as $\lambda/4$, which equals to 35.5 m.

This wavelet was convolved with reflection coefficients generated from the elastic parameters from steps 2 and 3.

Figure 6.20a and b show that the static (3D) observed seismic and sim2seis are adequately calibrated, as the observed and synthetic seismic events have the same polarity and are aligned. The P-wave impedances generated by the petroelastic modelling are shown in Figure 6.20c.

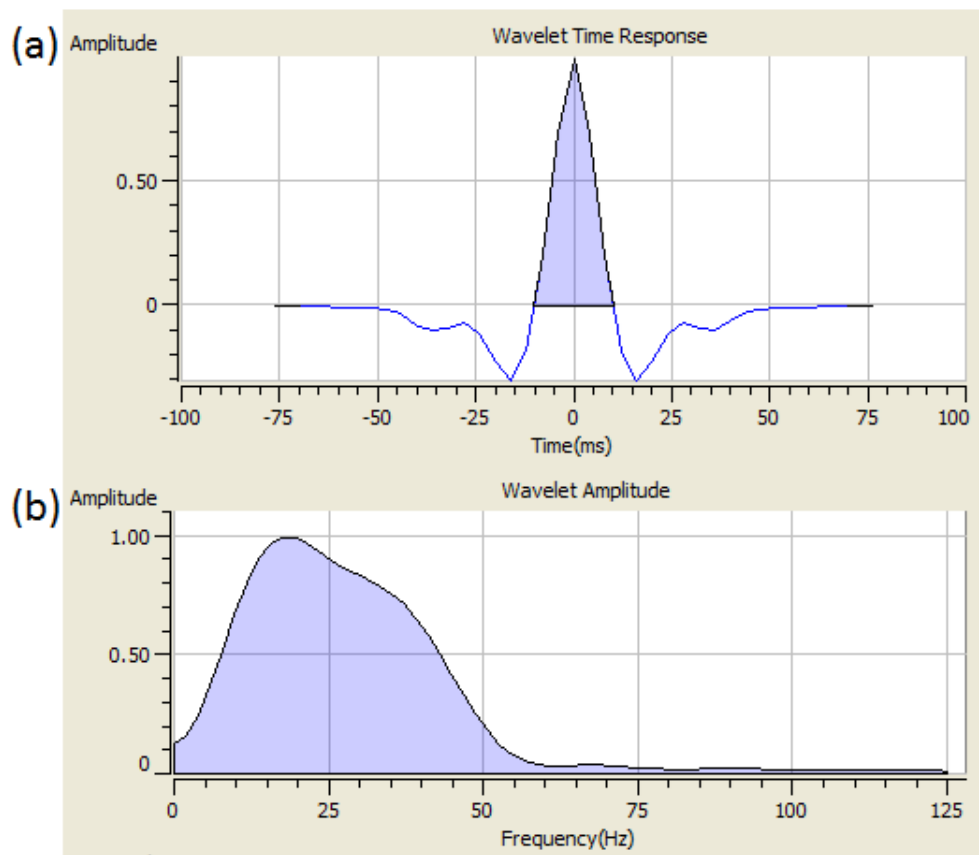


Figure 6.19: Extracted wavelet and its frequency spectra. Note the Nyquist frequency is 125 Hz (4ms sample rate) and peak frequency is 19Hz.

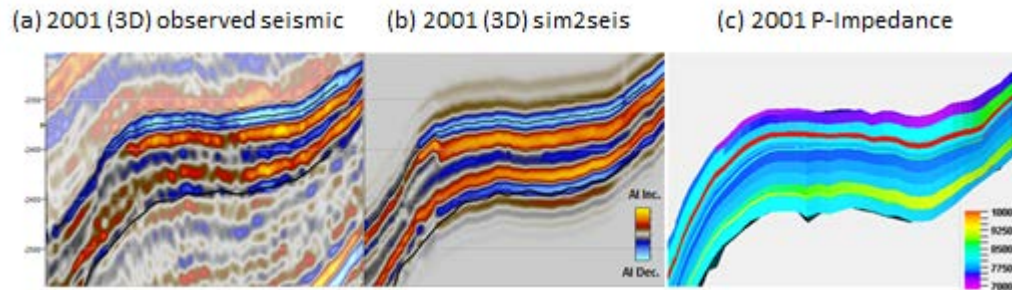


Figure 6.20: (a) Baseline (2001) 3D observed seismic; (b) 2001 3D sim2seis; and (c) P-wave impedance from the petroelastic model.

5. Assessment of the 4D signal in the presence of non-repeatable noise might also be required in some applications.

No noise was added in this work.

6. Interpret the 4D signals by generating attributes that can be tied to the production data.

The results from this step are presented in the next section.

6.3. The integration domain – seismic and sim2seis comparison

This section presents the sim2seis and observed seismic data comparison for each well (or group of wells, in case their area of influence is considered to be the same). For each analysis area, we discuss the confidence level on the seismic interpretation, considering:

- Spatial continuity of the seismic anomaly
- Geological consistency
- Production and injection rates agreement
- Uncertainties from observed seismic - noise level and repeatability issues
- Uncertainties from sim2seis

6.3.1. G-segment

Wells F-4H and E-4AH

The well E-4AH started production in June 2000 in the Not 2 Formation, with a stop between June 2001 and August 2002 due to lack of pressure. The water injector F-4H was completed in the water leg south of the G-segment in September 2001 to provide pressure

support to the producer. The graphs from Figure 6.21 and Figure 6.22 show the activity for E-4AH and F-4H wells respectively.

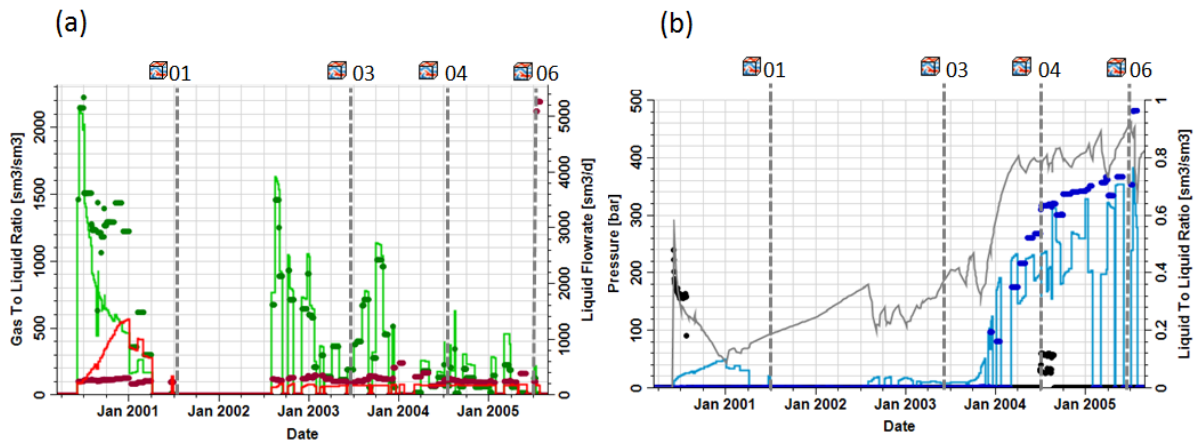


Figure 6.21: E-4AH well activity (a) gas-oil ratio (red) and oil production rate (green); and (b) BHP (grey) and water-cut (blue). Circles are the historical and solid lines are the simulated rates. The dashed lines are the approximate seismic acquisition dates.

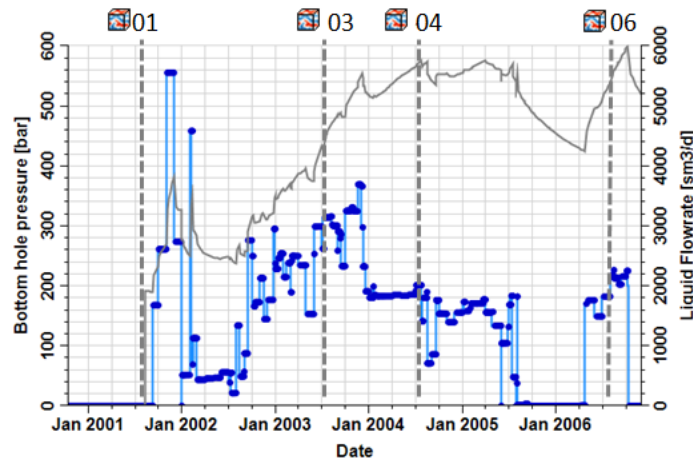


Figure 6.22: F-4H well activity (a) water injection (blue) and BHP (grey). Circles are the historical and solid lines are the simulated rates. The dashed lines are the approximate seismic acquisition dates.

The reservoir in this zone was under saturated until June 2000, when production started and pressure depleted below the bubble point. Figure 6.23a to f show a comparison between the RMS amplitude of the observed and sim2seis differences on a 15ms window below the top reservoir. The hardening effect (blue anomaly from Figure 6.23a to b) was previously interpreted by Osdal et al. (2006) as both gas going back into solution and water saturation increase. As the water had not reached the producer well in 2003, and as the gas-oil ratio was constant during this period (Figure 6.21a and b), the interpretations of this anomaly are uncertain. The red anomaly is related to the pore pressure increase due to

water injection. Figure 6.24a to l show the pore pressure and water, oil and gas saturation differences at the top reservoir, extracted from the simulation model at the time the monitor and baseline seismic surveys were acquired.

2003 minus 2001 comparison between sim2seis and observed seismic (Figure 6.23a and d), previously discussed in Santos et al. (2015), shows an inconsistency on the west side of Fault 1. We note that the modelled pore pressure built up between 2001 and 2003 took longer than the observed, and that water is reaching this area faster than the simulation is indicating. The red/blue division along Fault 1 is not detected in sim2seis, which might be an indication we should review the transmissibility of this fault and the horizontal permeability in this zone. Figure 6.24a to l prove the connectivity along this fault in the simulation model is not enough to contain the fluid movement. For this example, we conclude that the observed 4D response might offer a reasonable degree of confidence for a model update. However, mapping the boundaries of each response without uncertainty is very difficult in this case because of the presence of the ambiguous/dubious hardening response and the opposite softening effect from the pore pressure increase.

Figure 6.23e shows the increase in pore pressure has dominated the 4D seismic response in sim2seis between 2004 and 2001. The observed 4D difference from Figure 6.23b, however, still shows the fluid effect in blue on the east side of Fault 1. This is an indication the pore pressure from simulation model might be overestimated. The same effect is seen in 2006 minus 2001 comparison, with an increase in simulated pore pressure of more than 300 bar, extended throughout northeast of the producer. The vertical permeability from simulation model is lower than 5mD, as seen in the vertical section throughout the segment in Figure 6.25, which leads to a large pressure variation in the simulation model, as for the same volume it is harder to push the fluids in (and changes in pore volume lead to a large pressure fluctuation).

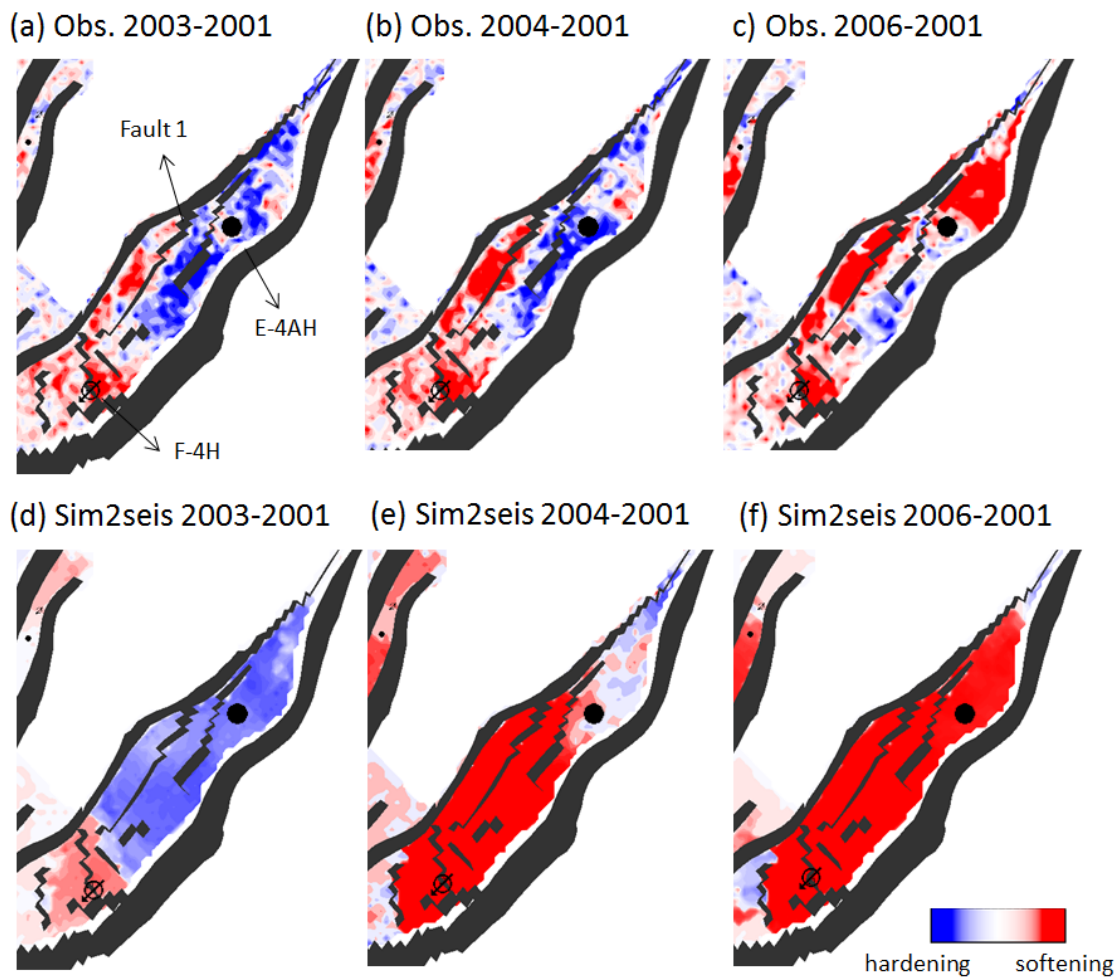


Figure 6.23: (a to c) Observed RMS amplitude differences and (d to f) sim2seis RMS amplitude differences for 2003, 2004 and 2006 minus 2001 comparisons, extracted from a 15ms window below top reservoir.

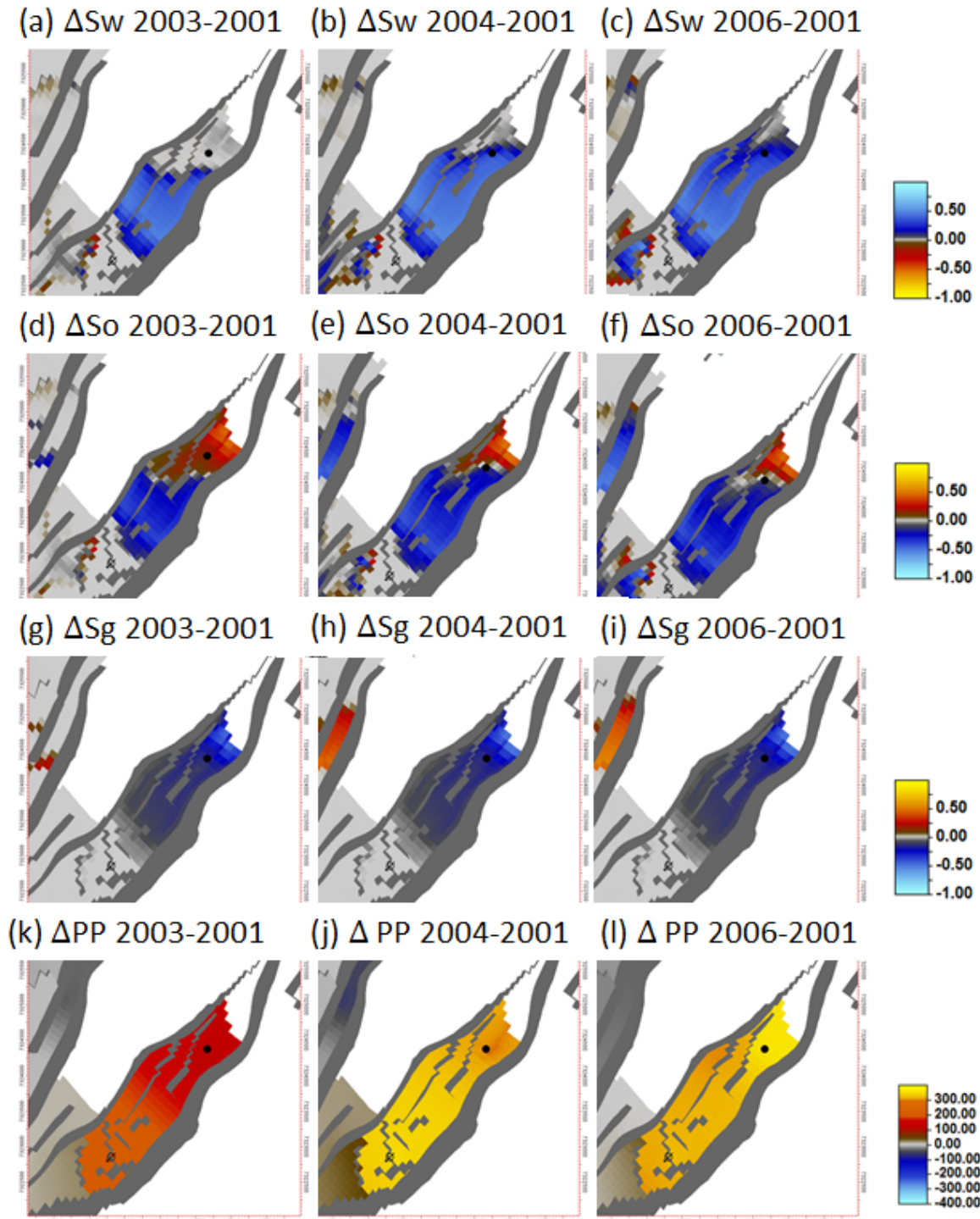


Figure 6.24: (a to c) Simulated water saturation differences, (d to f) Simulated oil saturation differences, (g to i) Simulated gas saturation differences (in decimal), (k to l) Simulated pore pressure differences (in bar) for 2003, 2004 and 2006 minus 2001 comparisons.

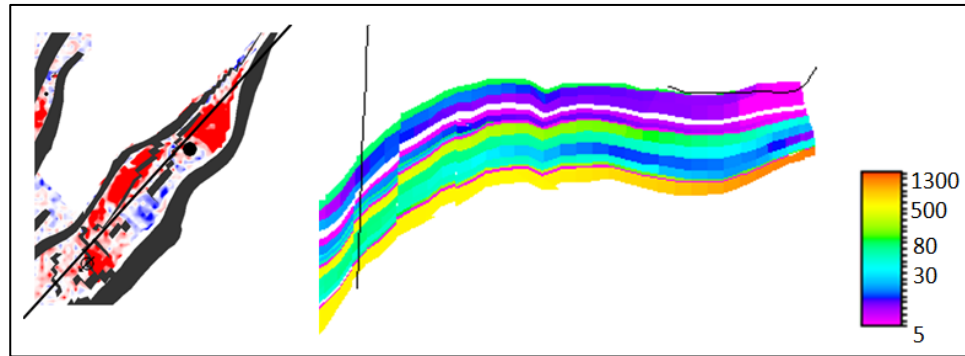


Figure 6.25: Vertical section location (left) and vertical permeability across this section (right).

6.3.2. C-Segment

A considerable part of this segment is located within the undershooting/poorer repeatability area as discussed in Section 6.1.4. The 4D signal is present deeper in the reservoir, particularly focused in the well areas and without much spatial variation (Figure 6.26d). Most of 4D anomalies are caused by water and gas injection in the borders of the horst structure. This area also contains more noise both on 3D and 4D seismic. Figure 6.26a and b show the intra-reservoir events definition and continuity from 3D seismic are poorer and Figure 6.26c shows the background noise in the 4D seismic in this same area.

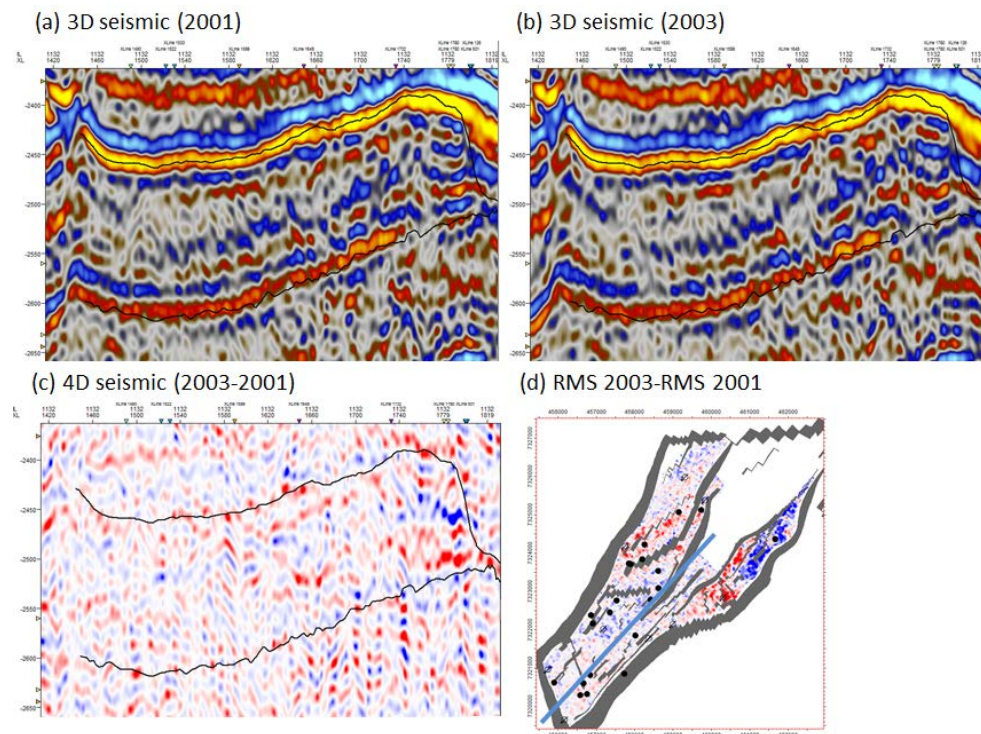


Figure 6.26: (a) 2001 observed seismic, (b) 2003 observed seismic, (c) 2003-2001 observed seismic and (d) RMS 2003 - RMS 2001.

Well C4-AH

The C-4AH well has been injecting water and gas since January 2004 to provide pressure support and to enhance the oil sweep in the Ile Formation. Figure 6.27a shows the location of the well and Figure 6.27b shows its injection rates. Figure 6.28a to f show the 4D differences for a vertical section through the well (blue line in Figure 6.27a). The anomalies circled in green from sim2seis (Figure 6.28d) and observed seismic (Figure 6.28a) difference are well matched. The blue 4D anomaly at the top reservoir was interpreted as water replacing oil in Not 2 Formation. This water comes from F4-H water injector northeast of C4-AH. The red anomaly below this was interpreted as softening response from gas saturation increase. These effects are in agreement with the simulation model differences (Figure 6.28b, c, e and f).

The softening sim2seis 4D anomaly northeast of the well (black circle in Figure 6.28c) is interpreted to be oil replacing water as shown in the simulated differences (Figure 6.28b and f). However, this effect is absent in the observed 4D seismic. Although the area is at the edge of the major faults that separate segment G, which may lead to poorer imaging, the confidence level in the observed seismic data in this area is classified as medium, as there are no wells near this area that could cause 4D changes. This is an indication that the simulation can potentially mislead interpretation to conclude that there is undrained oil in this part of the field.

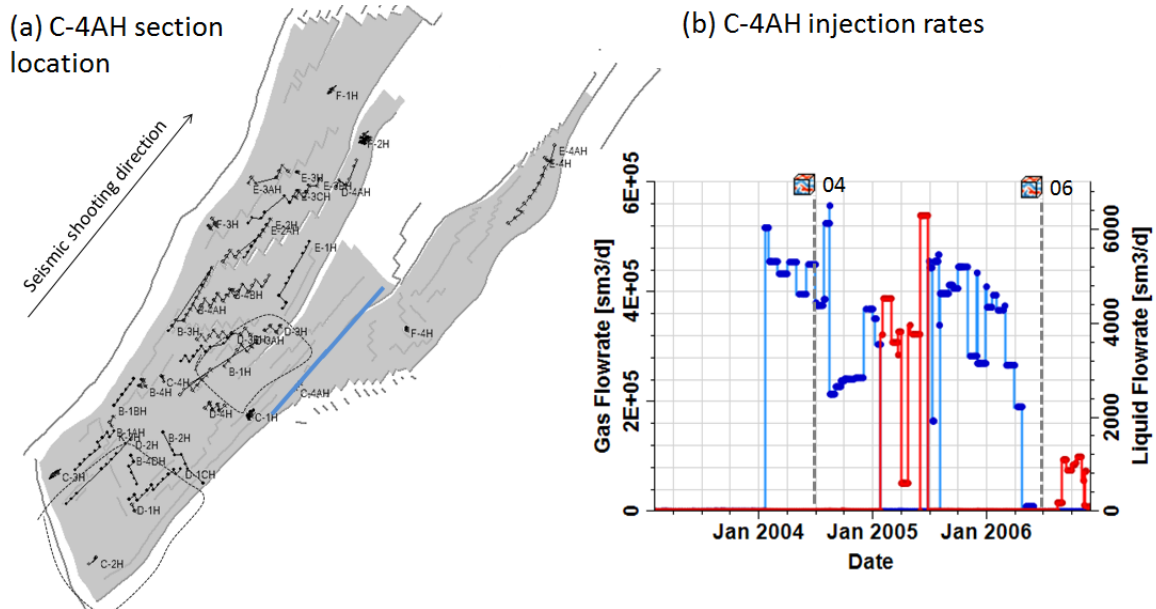


Figure 6.27: (a) Location of the interpreted seismic section (blue line); and (b) gas (red) and water (blue) injection rates. The solid lines are the rates from the simulator and the circles are the historical data for well C4-AH.

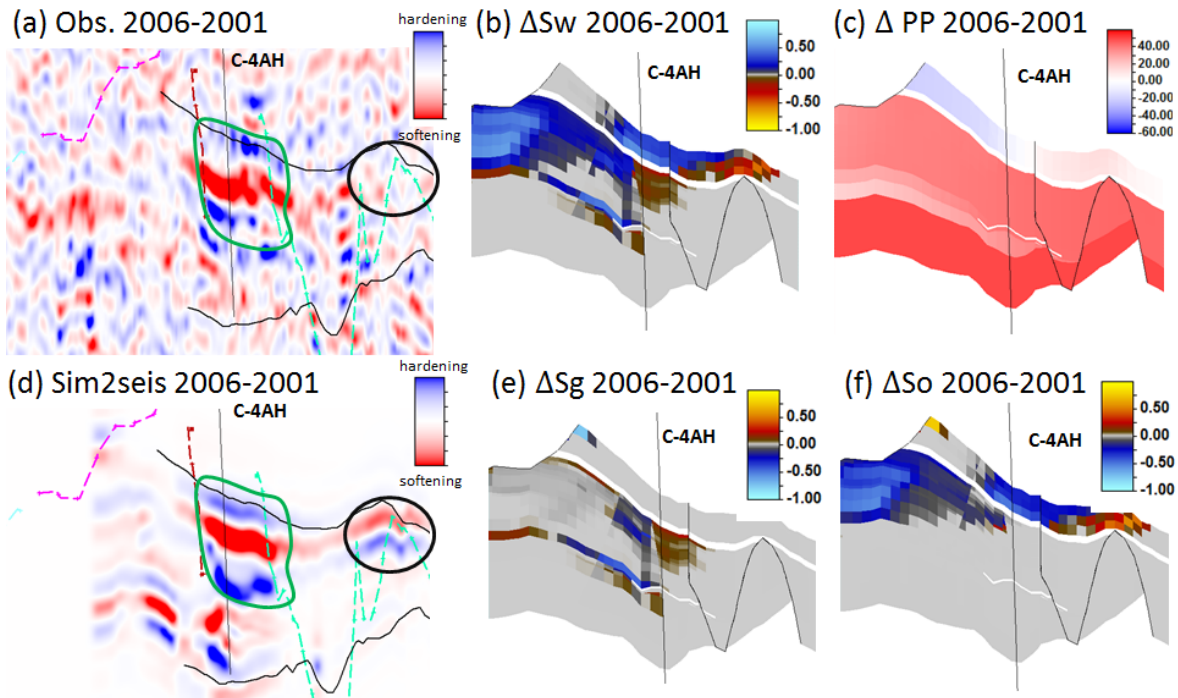


Figure 6.28: (a) Observed seismic, (b) simulated water saturation, (c) simulated pore pressure (bar), (d) Sim2seis, (e) simulated gas saturation (e) and (f) simulated oil saturation 2006-2001 differences for well C4-AH.

Well C1-H

C1-H was the first injector well in the field, open in July 1998 to give pressure support and to enhance the oil sweep in the Ile Formation. Figure 6.29a shows the well and the seismic vertical section locations and Figure 6.29b and c show the simulated and historical injection rates and bottom-hole pressure for this well. The interpreted oil-water contact (blue line along hardening effect from Figure 6.30a) does not match with sim2seis (blue line in Figure 6.30b). Indeed, the OWC from the simulation models seems to be much higher (Figure 6.30b). However, as the hardening effect from observed data does not look very continuous and there is no other information about the water level near this area, this anomaly is classified as low certainty and no updates are suggested based on that.

The second mismatch is related to the strong hardening effect inside the blue circle from Figure 6.30d, which is not seen at the observed seismic difference. This effect is caused by a pore pressure “spike” from simulation (Figure 6.30c), which is recommended to be reviewed.

The softening indicated by the arrows in Figure 6.30a and d, related to the gas saturation increase due to injection, although not presenting the same extension, are reasonably matched.

The response at top reservoir (orange circle from Figure 6.30a and d), related to gas saturation decrease, also does not present same extension as in the observed seismic; however the observed seismic cannot offer high certainty in this area for a model update.

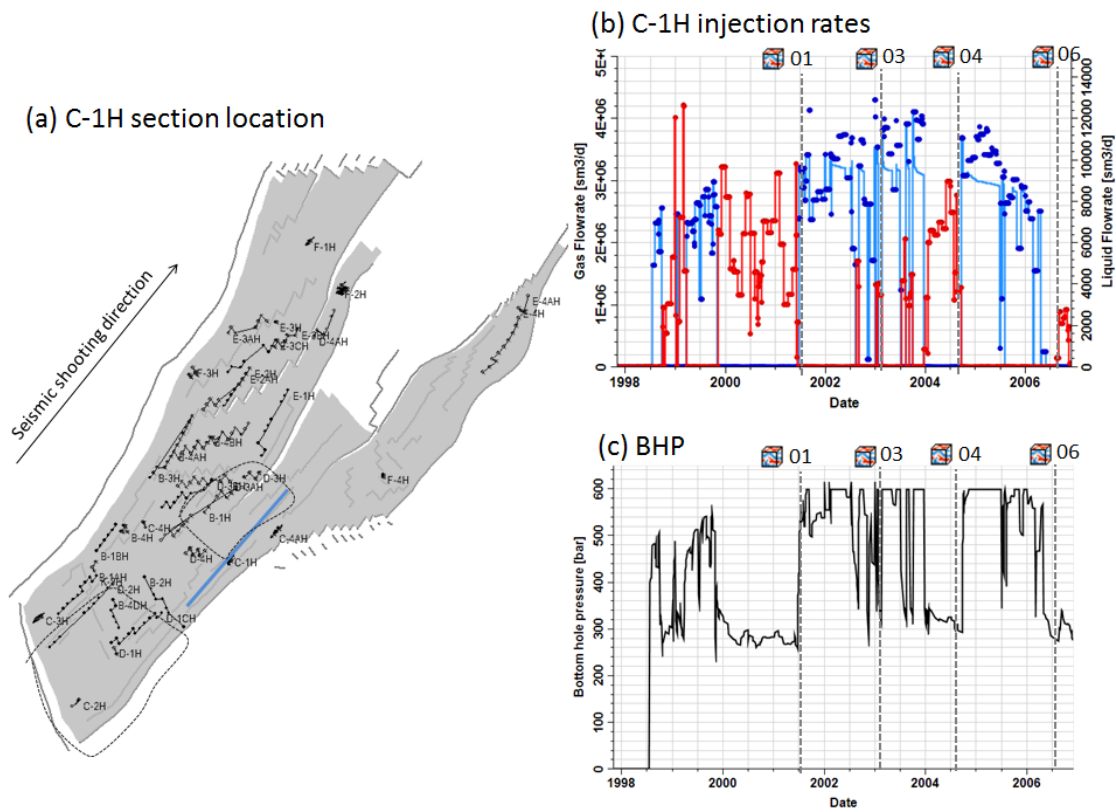


Figure 6.29: (a) Well and analysed vertical seismic section locations; (b) gas (red) and water (blue) injection rates; and (c) BHP from simulation for well C1-H. Circles are the historical and solid lines are the simulated rates.

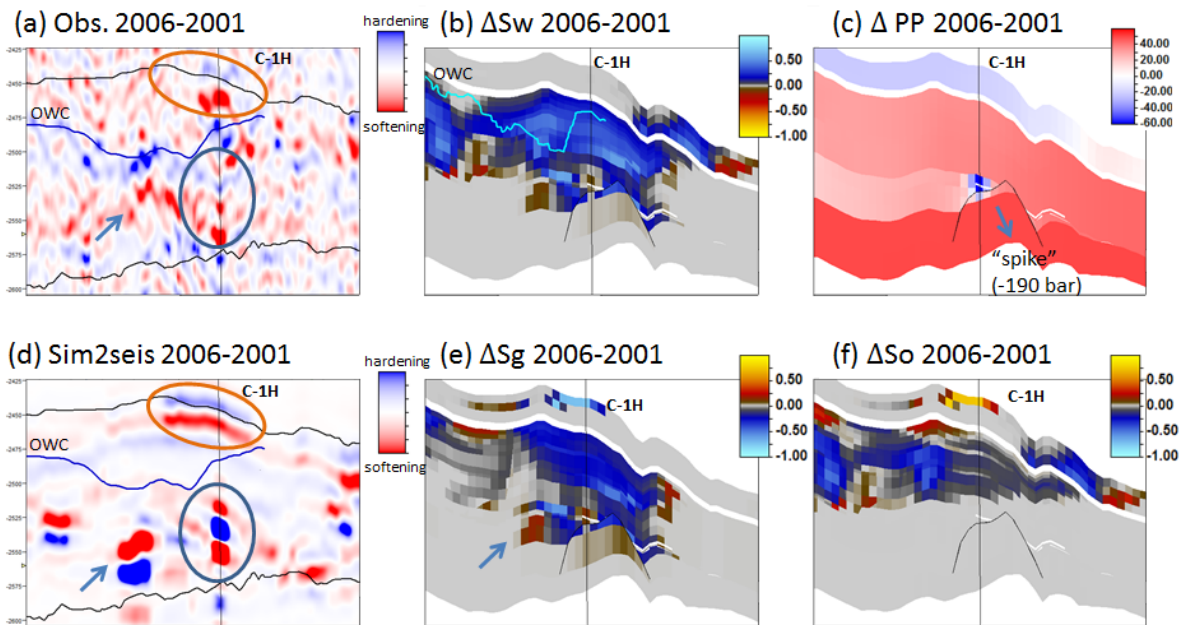


Figure 6.30: (a) Observed seismic, (b) simulated water saturation, (c) simulated pore pressure (bar), (d) Sim2seis, (e) simulated gas saturation (e) and (f) simulated oil saturation 2006-2001 differences for well C1-H.

Wells C2-H, D-1CH, D-1H and D-1BH

C-2H was the second injector to be drilled, whose injection started in January 1999. Wells D-1H stopped production before first seismic and D-1BH was side-tracked to D1-CH in 2003, when it started producing oil. Figure 6.31 shows the location of the four wells and Figure 6.32a to c show production and injection rates for C-2H and D1-CH.

Figure 6.33a does not show a clear signal around well C-2H. We know the reservoir is softening in this area due to the delayed time-shifts relative to 2001 (Figure 6.34a to c), which is caused by pore pressure increase. This area presents higher NRMS, indicating poorer repeatability, and is in the border of the major horst structure, where imaging can also be poorer. Potentially, competing hardening effect might be acting at the same against the softening from pore pressure increase. No 4D signal is present on sim2seis in this region either, and therefore no updates in the simulation are suggested.

The OWC movement plotted as blue lines in Figure 6.33a, follows a continuous hardening signal and is confirmed by the water breakthrough history data in wells D-1H, D-1CH and further northeast in well D-4H (which was shut in 2002 due to water breakthrough). This anomaly interpretation is therefore classified as high confidence. Sim2seis shows a weak hardening response near D-1CH and D1-BH, but above the OWC horizon (Figure 6.33d). The simulated water saturation difference is also above this horizon (Figure 6.33b) and the well data from Figure 6.32b shows the simulated water breakthrough occurs faster than observed. It is suggested, therefore, to delay the water rise in the simulator for this area.

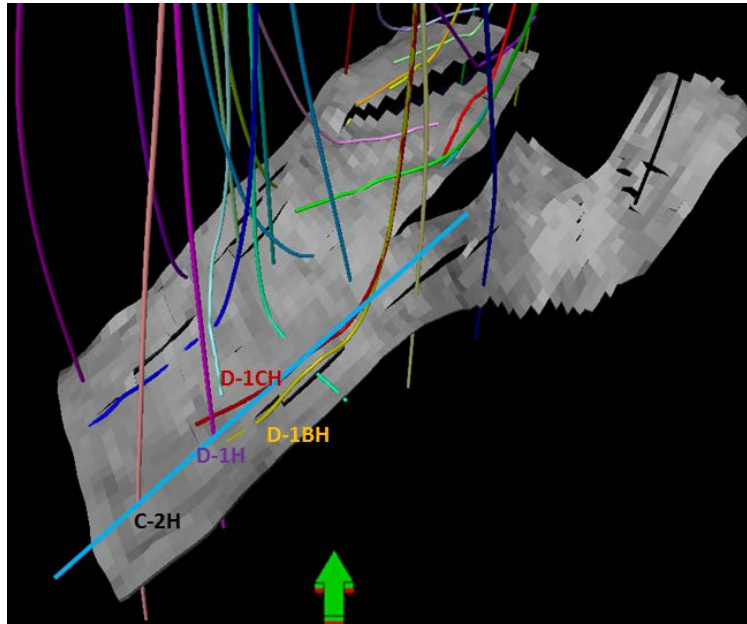


Figure 6.31: 3D view of the location of wells C-2H, D-1CH, D-1H and D-1BH and the analysed seismic section in blue (plotted at Ile 1.3 layer).

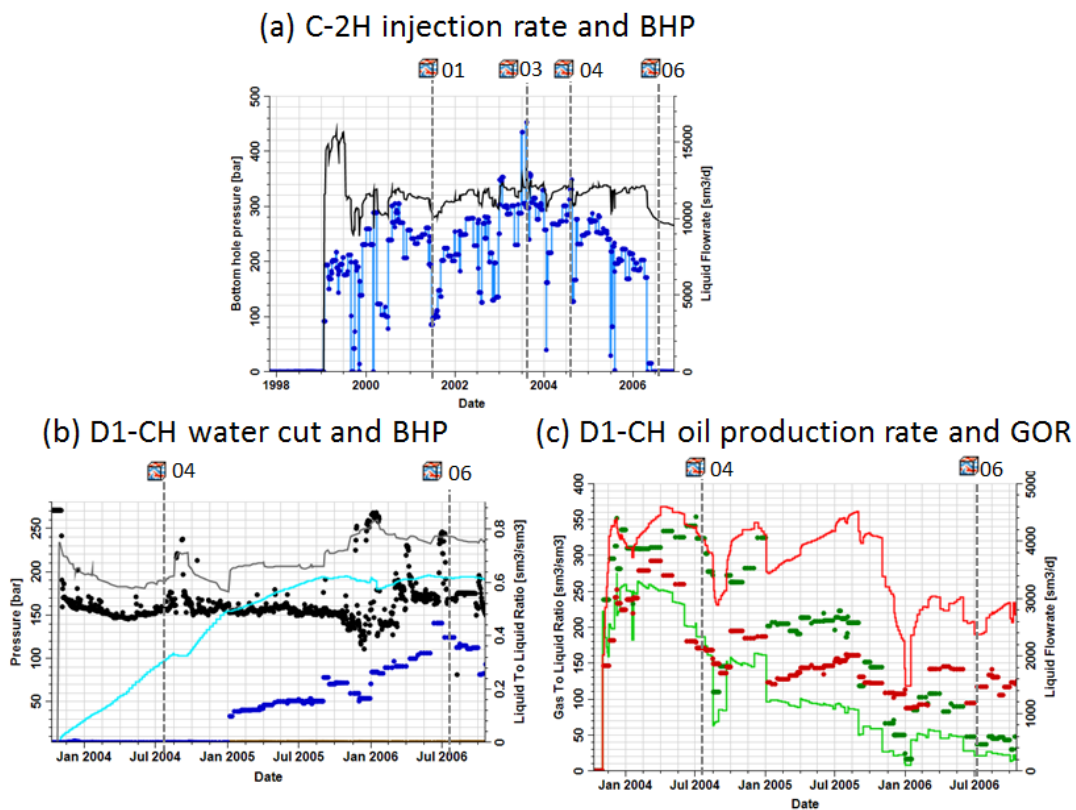


Figure 6.32: (a) water injection rates (blue) and simulated BHP (black) for C-2H; (b) water cut (blue) and BHP (black); and (c) gas-oil ratio (red) and oil production rate (green) for D1-CH. Circles are the historical and solid lines are the simulated rates.

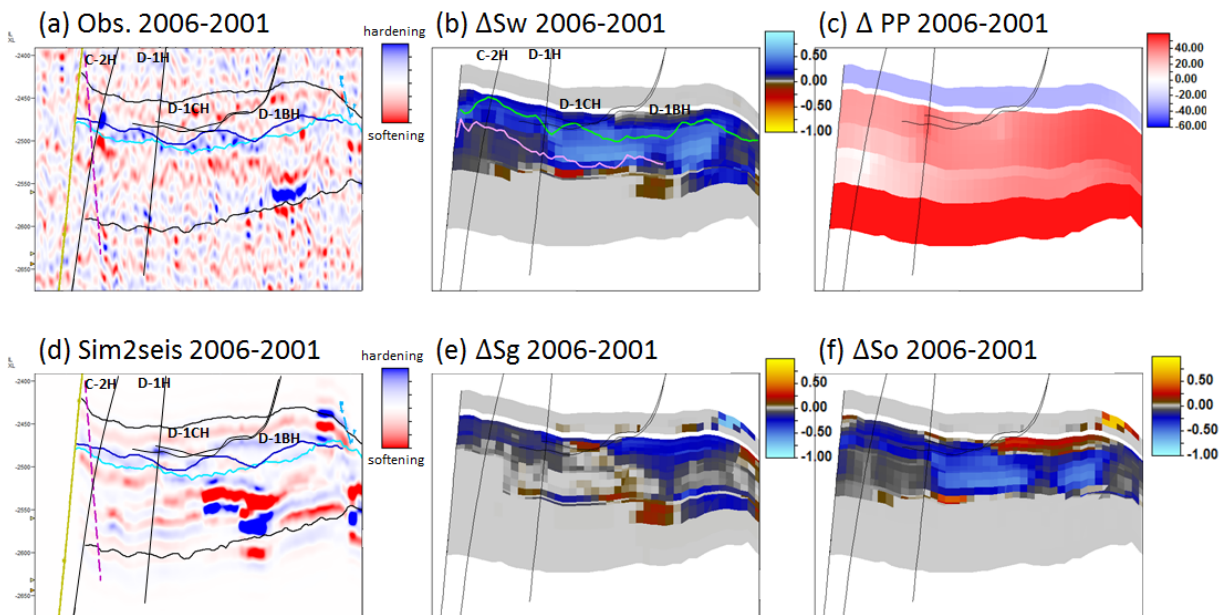


Figure 6.33: (a) Observed seismic, (b) simulated water saturation, (c) simulated pore pressure (bar), (d) Sim2seis, (e) simulated gas saturation (e) and (f) simulated oil saturation 2006-2001 differences. The blue lines in (a) and (b) represent the rise in OWC from 2001 to 2006.

(a) time-shift 2003 vs. 2001 (b) time-shift 2004 vs. 2001 (c) time-shift 2006 vs. 2001

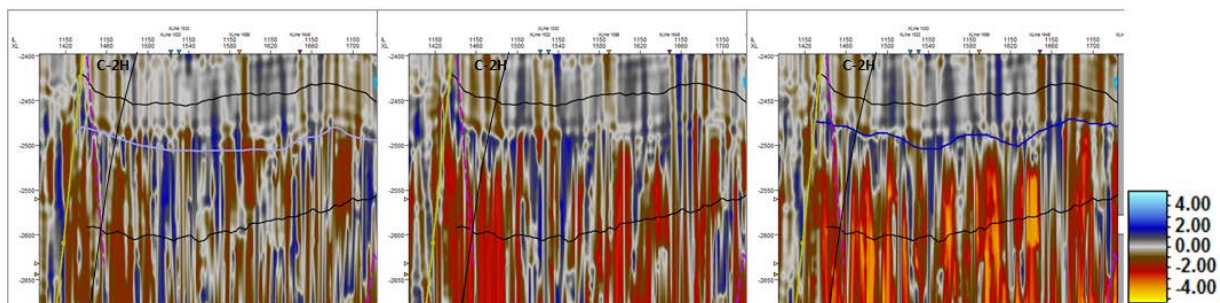


Figure 6.34: Time-shift for 2003, 2004 and 2006 vs. 2001 (a, b and c respectively). Negative values correspond to a delay in timing from baseline to monitor.

Wells B-1H and E-1H

Wells B-1H and E-1H both started production in 1999. Figure 6.35 shows the location of both wells and the analysed vertical seismic section.

The anomaly in the red circle from Figure 6.37d is interpreted as a gas saturation increase effect from the simulation model (Figure 6.37e). As the gas was not present in this area pre-production and as the gas does not go out of solution so deep in the reservoir, it is concluded that this gas comes from the gas injectors from the C-segment. This effect is not visible in the observed seismic, and the possible causes for this mismatch are:

- A high permeability layer in the simulation model (2300mD in average), shown in Figure 6.38a, might cause an unexpected gas flow in this layer. This is an indication the permeability might be overestimated in the simulation model. This corresponds to a medium to coarse grained sandstone from Tofte 1.1 Formation with permeability logs of 500mD in average, confirming a mismatch with the simulation model.
- Gas saturation increase is not visible in observed seismic because it occurs in a layer thinner than seismic resolution or observed seismic noise obscuring this effect (less probable hypotheses as gas saturation changes are usually very detectable by seismic data).

The blue lines from Figure 6.37a represent the OWC movement between 2001 and 2006. The expected 4D hardening signal occurs near well E-1H, confirmed by actual water-cut from this well (Figure 6.36c). Simulation is showing more water was produced than actual fact between mid-2003 and 2006, however sim2seis shows a very weak hardening effect near this well (Figure 6.37d). This is because the opposite softening effect from a pore pressure increase of above 70bar from simulation (Figure 6.37c) seems to be competing against it. This pore pressure increase is not seen on observed data; in fact, time-shifts present in this area (Figure 6.38b) are not as strong as it is in the other pressurized areas throughout the field and therefore suggesting that the pore pressure increase might be overestimated in the simulator (or the matrix bulk modulus may be stiffer). The BHP data from this well is roughly matched with the simulation (Figure 6.36c), which does not agree with this interpretation of pressure overestimate, with a slight mismatch between gas-oil ratio and oil production rates from simulation and well history data. These contradictions lead to a low confidence in seismic interpretation in this area. It is also important to consider that this area is in the edge of the horst block and therefore it can be affected by a poorer imaging, which can make the observed seismic data less reliable.

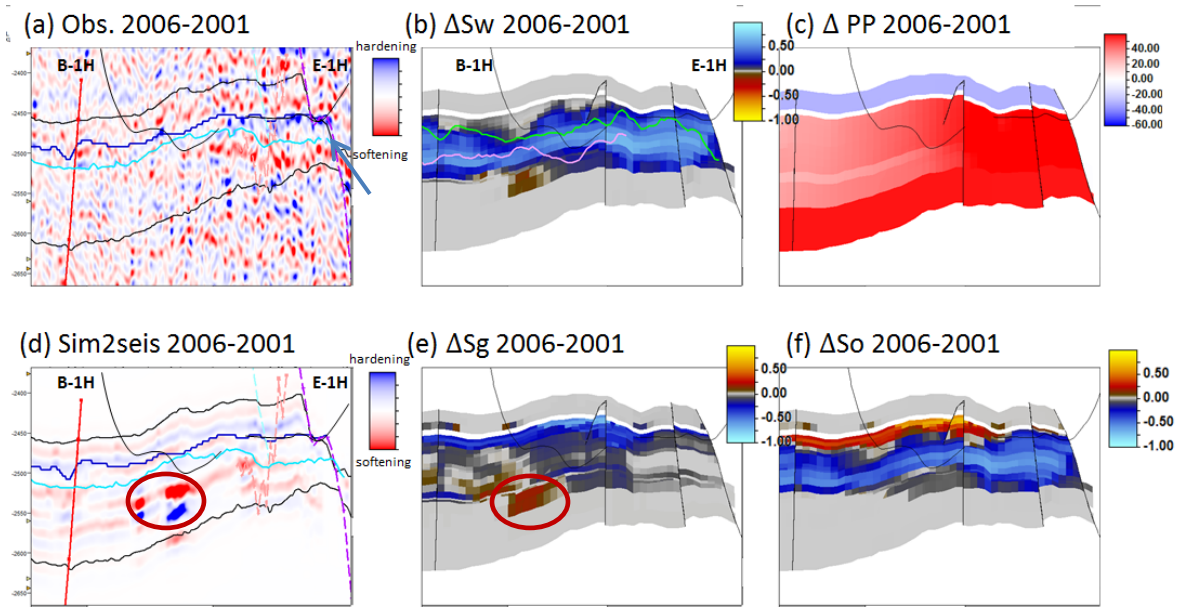


Figure 6.37: (a) Observed seismic, (b) simulated water saturation, (c) simulated pore pressure (bar), (d) Sim2seis, (e) simulated gas saturation (e) and (f) simulated oil saturation 2006-2001 differences. The blue lines in (a) and (b) represent the rise in OWC from 2001 to 2006 for E-1H and B1-H.

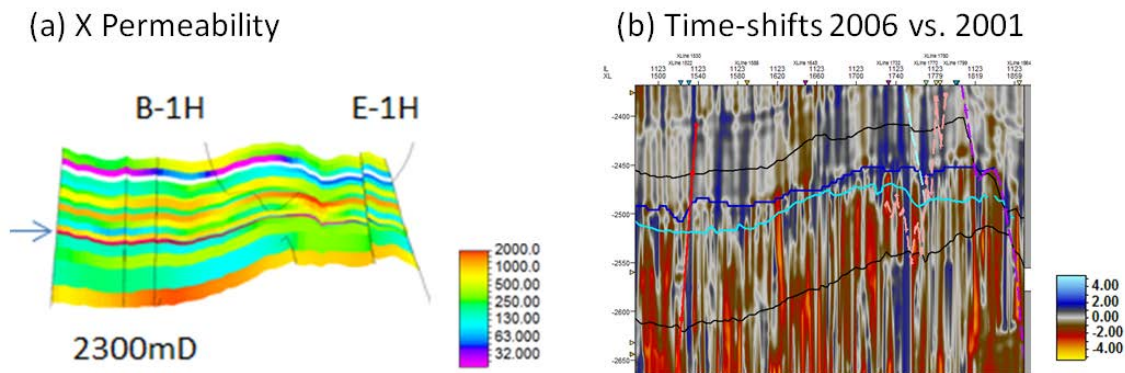


Figure 6.38: (a) Horizontal permeability from simulation model. The blue arrow highlights a high permeability zone. (b) Time-shifts estimated in the same vertical section.

Well D2-TH2

This well started production in December 1997 targeting Ile 2 and 3 formations. Figure 6.39a shows the location of the well and the analysed vertical section.

No clear 4D signal can be seen around well D2-TH2 (Figure 6.40a). The interpreted OWC contact movement (blue lines in Figure 6.40a) do not seem to follow consistent amplitude differences and therefore were classified as uncertain. In addition, the area presents poorer repeatability and more noise, as discussed in previous section. We do know the reservoir below well D2-TH2 area is softening from 2001 to 2004 and 2006 because of

the timing delays of up to 4ms, interpreted as caused by pore pressure increase and gas injection from the neighbour C-3H injector, as shown in Figure 6.41a and b. As a result, the interpretation of this area is classified as uncertain and no simulation model updates are suggested.

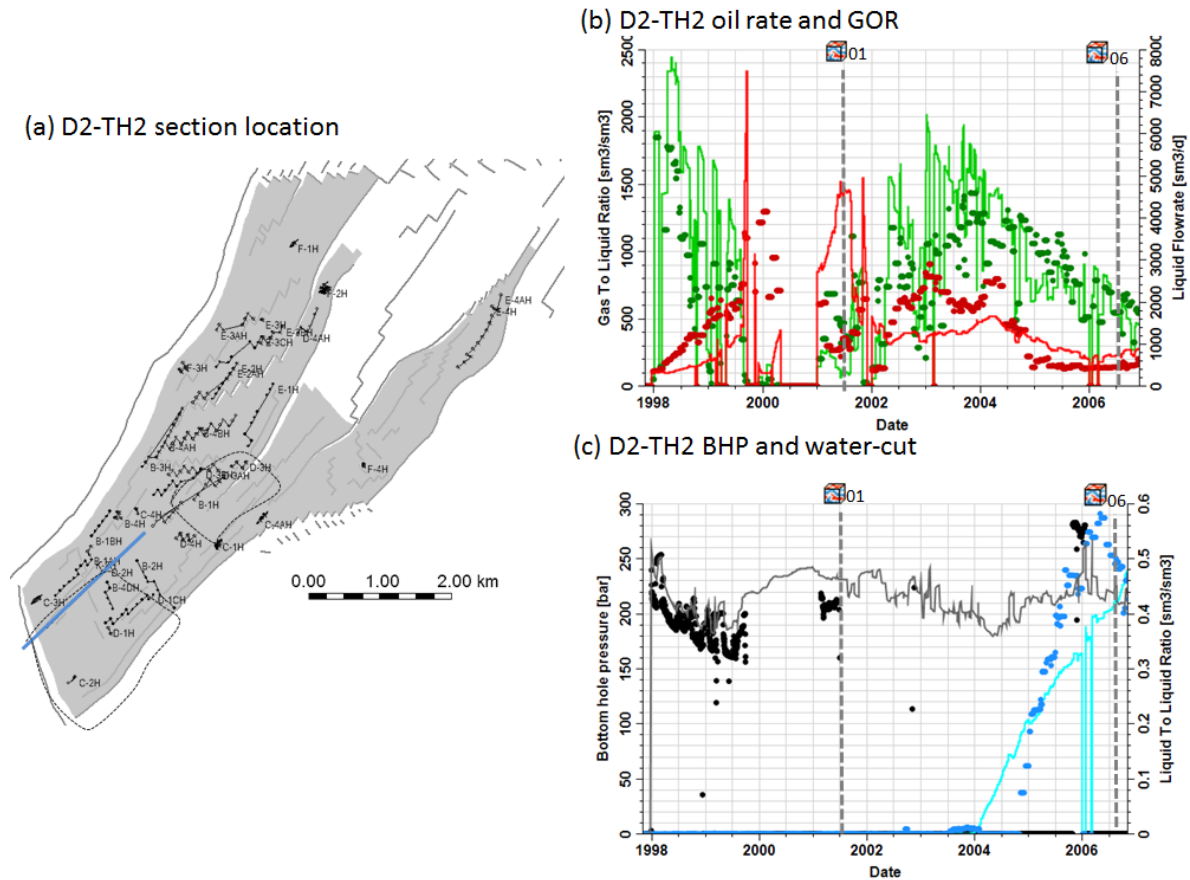


Figure 6.39: (a) Well and analysed vertical seismic section locations; (b) gas-oil ratio (red) and oil production rate (green); and (c) BHP (black) and water-cut (blue) for D2-TH2. Circles are the historical and solid lines are the simulated rates.

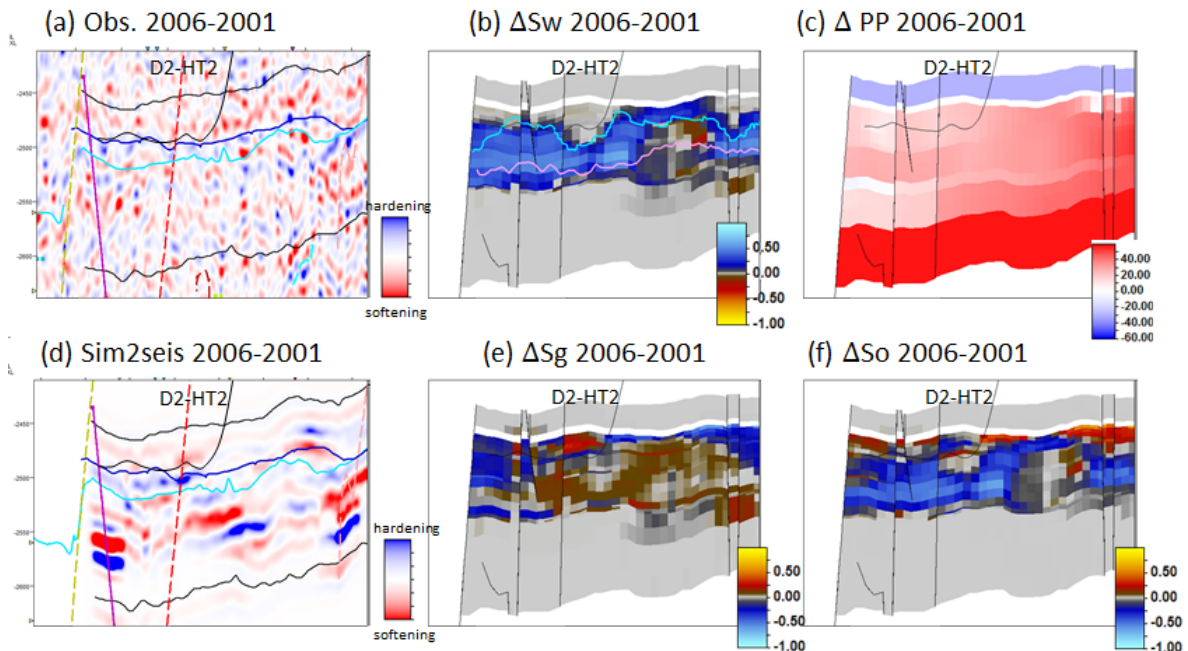


Figure 6.40: Observed seismic (a), Sim2seis (b), water saturation (c), gas saturation (d), pore pressure (bar) (e) and oil saturation (f) 2006-2001 differences. The blue lines in (a) and (b) represent the OWC movement between 2001 and 2006 for D2-HT2.

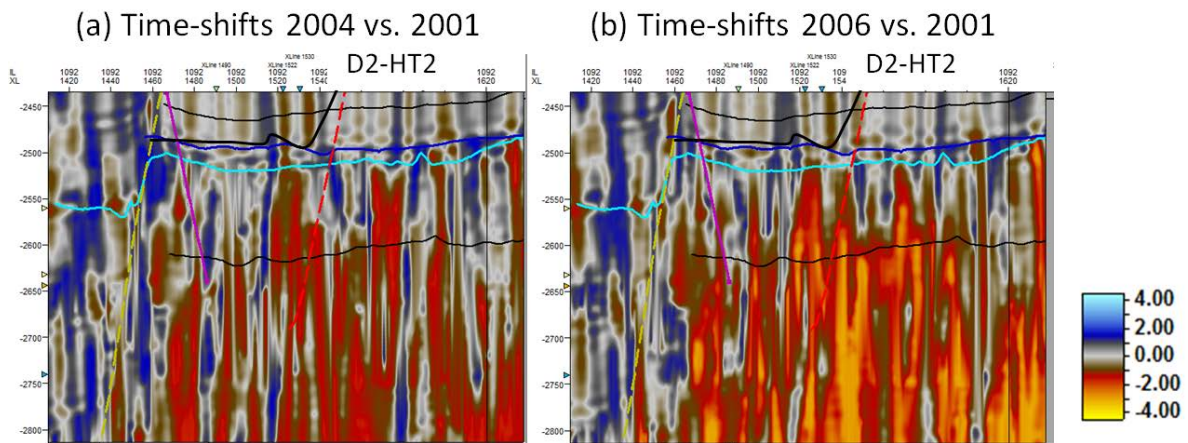


Figure 6.41: Time-shifts between 2001 and 2004 (a) and 2006 (b). Negative values represent timing delay from baseline to monitor.

Well B1-BH

A pilot well, B1-AH, was drilled to confirm the location of the oil-water contact (OWC) as interpreted from the 2004 4D seismic data. This was done to optimize the placement of the production well B1-BH, which started production January 2006 (Statoil, 2005). A neighbouring well B-4H produced between 1998 and May 2001, before the first

seismic available was shot. Figure 6.42a shows the location of the interpreted section for these wells.

Figure 6.43a to f show the differences between 2006 and 2001 in a cross section view passing through these wells. The blue anomaly inside the black circle was interpreted as water replacing oil, which is in agreement with production data, that confirmed water reached the well at the beginning of 2006 (Figure 6.42b). Sim2seis 4D differences do not show the same effect (black circle from Figure 6.43d). This is because the OWC must increase around B1-BH (black circle from Figure 6.43b) which is also confirmed by the water production curve (Figure 6.42b) that shows the simulation model presents an incorrect water breakthrough and a lower water rate. As the seismic interpretation confidence level is high in this area, it is recommended that the simulation model is updated to replicate this effect.

Further to the northeast of this well, the blue anomaly on sim2seis (black arrow in Figure 6.43b) is an ambiguous result of both gas going back into solution and water saturation increase from the simulation model (pointed by the black arrow in Figure 6.43c, d and f). The observed seismic data (Figure 6.43a) also shows a hardening effect, interpreted as a rise in the OWC. This anomaly appears to be lower than in sim2seis, which may be related to the uncertainty of sim2seis time-depth conversion. The observed anomaly is also laterally contained by the fault plotted in blue on the left. Although the fault transmissibility is low in the simulation model, and the sim2seis anomaly is laterally contained by the fault, the water saturation increase shown in Figure 6.43b seems to occur throughout this barrier. It is recommended therefore to review the connectivity of this fault in the simulation model. An opposite red anomaly above the hardening effect also does not match with the sim2seis result. This anomaly was not continuous further to the northeast, and there were no well production data or time-shift information near this area to help us understand whether it is a real softening effect or not. In this case, we cannot make suggestions for updates to the simulation model based on this mismatch, as the confidence level on the seismic is low.

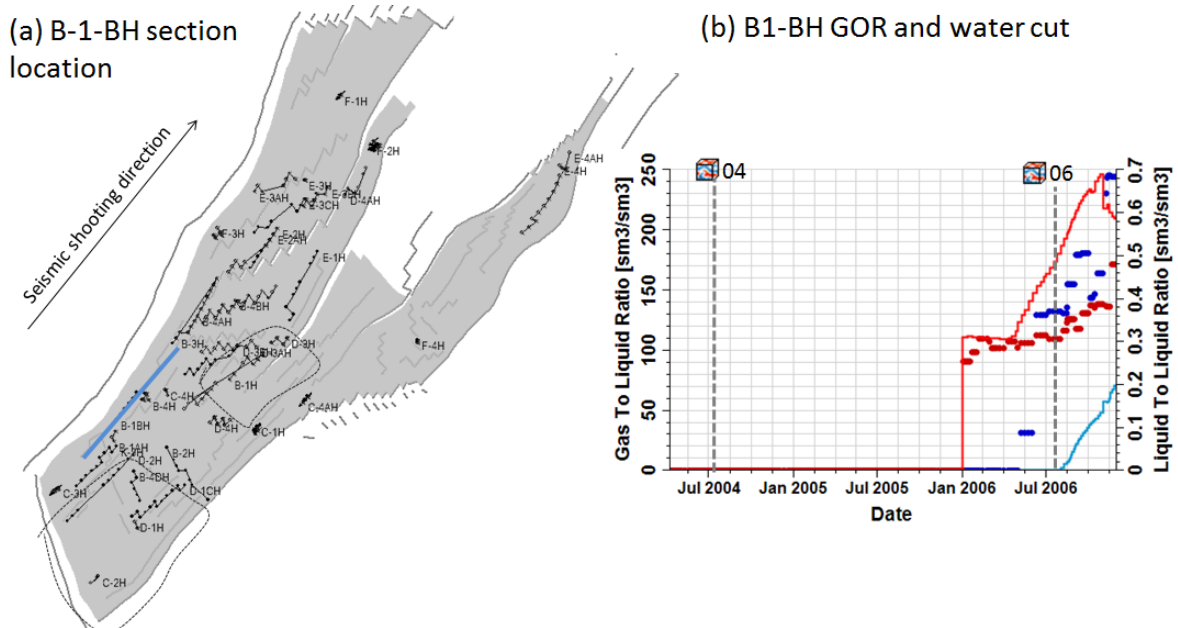


Figure 6.42: (a) Location of the interpreted seismic section (blue line) and (b) gas-oil ratio (red) and water cut (blue). The solid lines are the simulation results and the circles are the historical data for B1-BH.

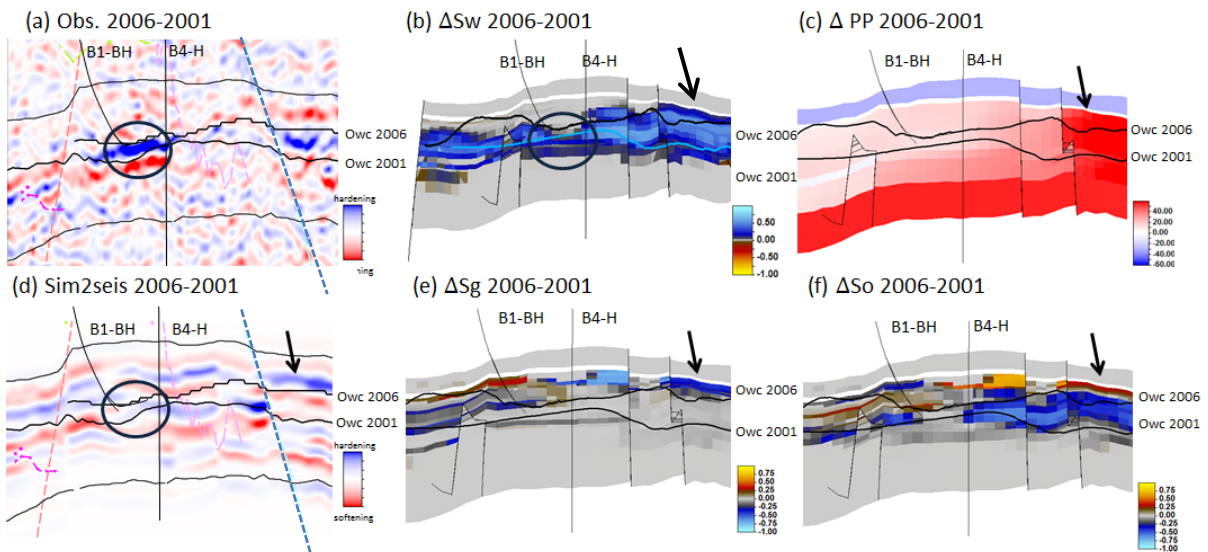


Figure 6.43: Observed seismic (a), Sim2seis (b), water saturation (c), gas saturation (d), pore pressure (bar) (e) and oil saturation (f) 2006-2001 differences near wells B1-BH and B4-H.

Well B2-H

This well started producing in December 1997 in the top of Ile Formation. The location and production rates are presented in Figure 6.44a to c.

This area presents the same effect as discussed near well B1-H due to the gas saturation increase in a thin high permeability layer (black arrows from Figure 6.45d and e). This is also mismatched with the observed seismic, which although is noisy in this area, can

have its interpretation confidence classified as medium due to the confirmation from the petrophysical logs that this layer presents a permeability of around 500mD, as opposed to more than 2000mD indicated by the simulation model.

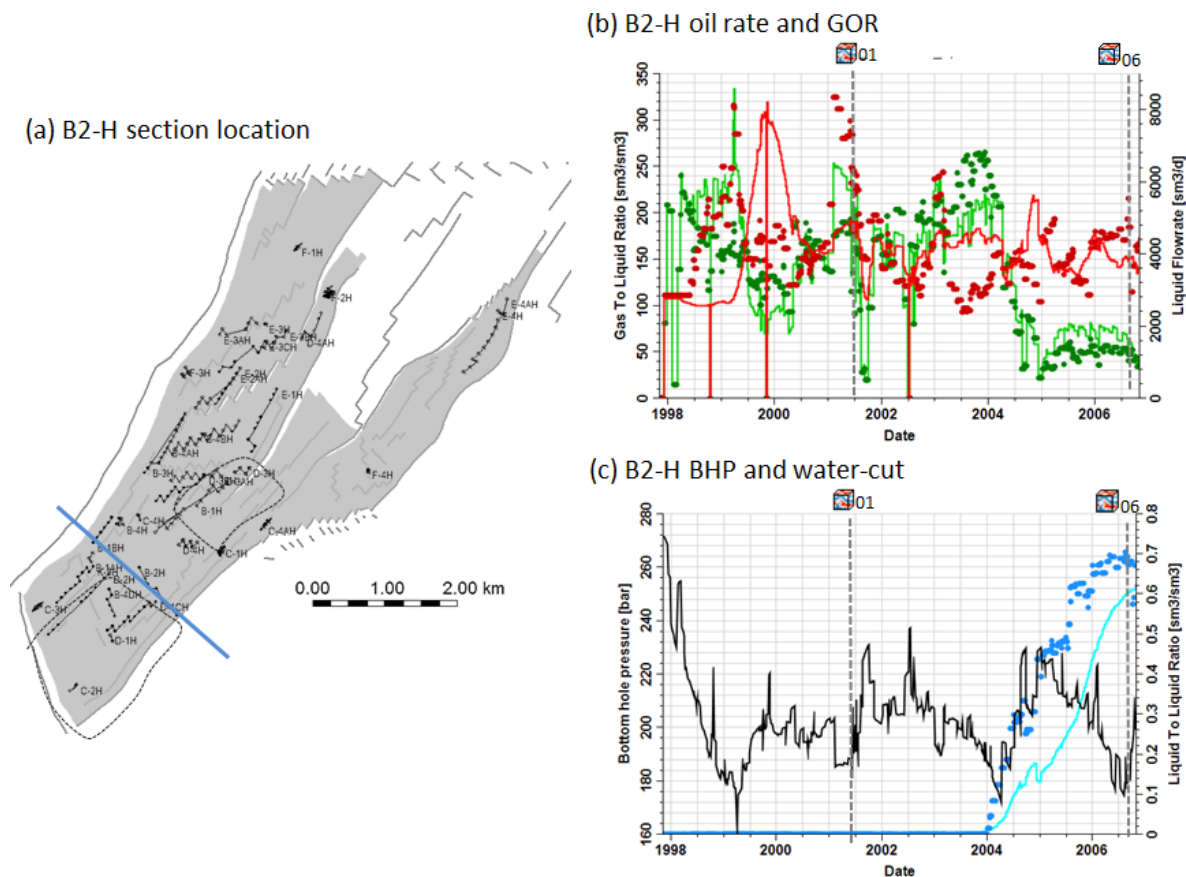


Figure 6.44: (a) Well and analysed vertical seismic section locations; (b) gas-oil ratio (red) and oil production rate (green); and (c) BHP (black) and water-cut (blue) for B2-H. Circles are the historical and solid lines are the simulated rates.

The interpreted OWC in this area is not very clear on the observed seismic (Figure 6.45a), however it is confirmed by well data that water reached this well in the beginning of 2004. Historical data from this well shows water production being underestimated by the simulator since this time. Figure 6.45b shows the water does reach B-2H well, but in a slightly less amount than it should to produce the hardening anomaly on sim2seis (around 20% increase near the oil-water contact). The connectivity of the faults across this line can also be reviewed in order to assess why less water is reaching this area. The interpretation in this area can be classified as medium confidence.

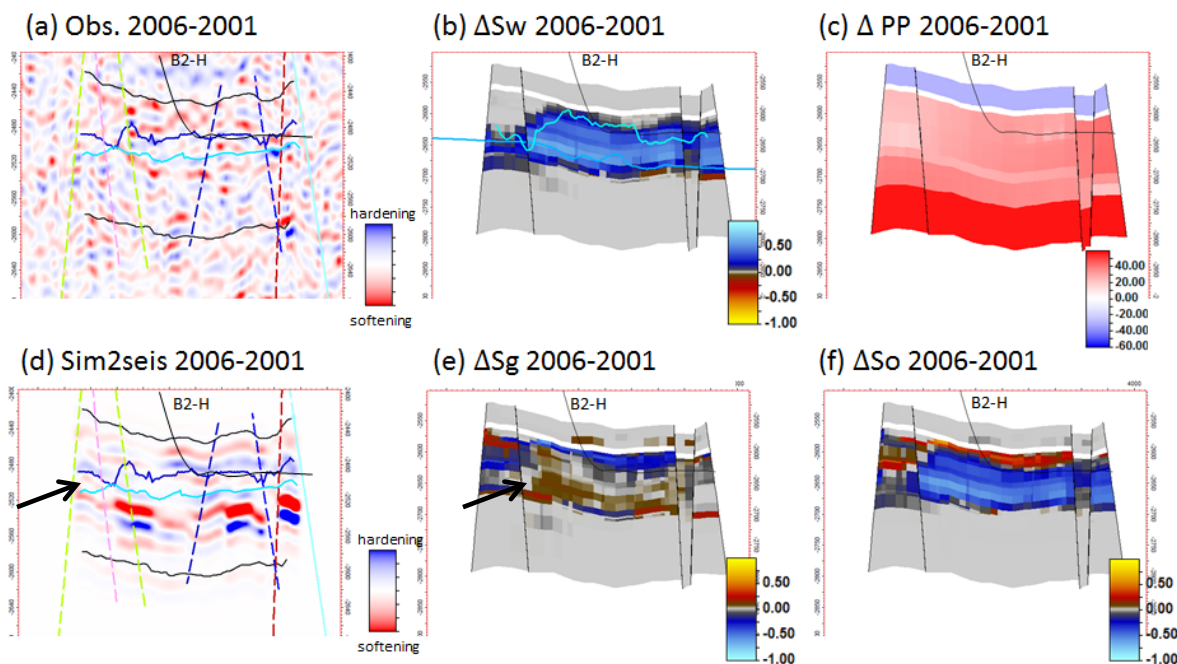


Figure 6.45: Observed seismic (a), Sim2seis (b), water saturation (c), gas saturation (d), pore pressure (bar) (e) and oil saturation (f) 2006-2001 differences. The blue lines in (a), (b) and (c) represent the interpreted OWC movement between 2001 and 2006 near B2-H.

Well C3-H

C3-H is a water and gas injector well perforated in the water leg southwest of segment-C in May 1999 to support injection from C1-H and C-2H. Figure 6.46a shows the location of the well and the analysis area.

Previous interpretation from Osdal (2004) on inverted data showed that the injected gas caused a decrease in impedance close to C-3H that could be seen moving north along the main fault. In the amplitude domain, however, this decrease in impedance can only be seen in 2004 and 2006-2001 differences (black arrow from Figure 6.47a). In the time-shift domain, the effect is also more obvious when comparing 2004 and 2006 against 2001 (Figure 6.48a to c). This effect roughly matches with sim2seis result (black arrow from Figure 6.47d) and no updates are suggested.

Osdal (2004) also discusses there was an increase in impedance due to water flooding in the C-2H area, as indicated by the blue lines in Figure 6.47a and d. The hardening effect is weak throughout the section both in the observed data and sim2seis, except for the area very close to both wells. This anomaly interpretation was classified as low confidence and therefore no updates are suggested.

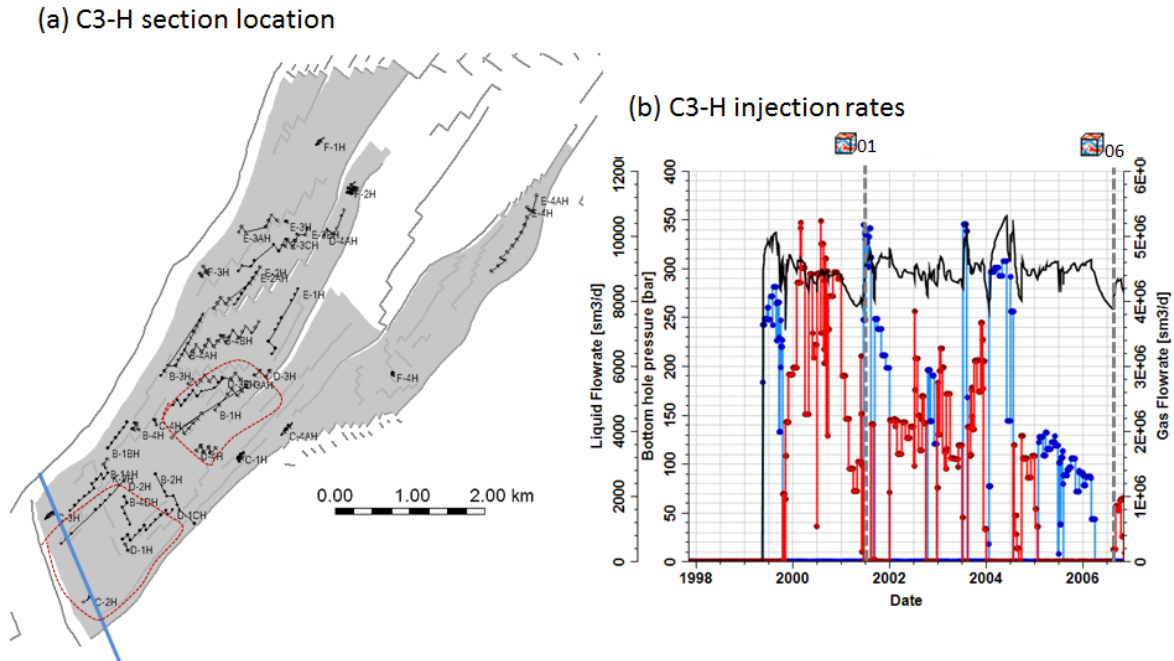


Figure 6.46: (a) Well and analysed vertical seismic section locations; and (b) gas (red) and water (blue) injection rates and simulated BHP (black line) for C3-H. Circles are the historical and solid lines are the simulated rates.

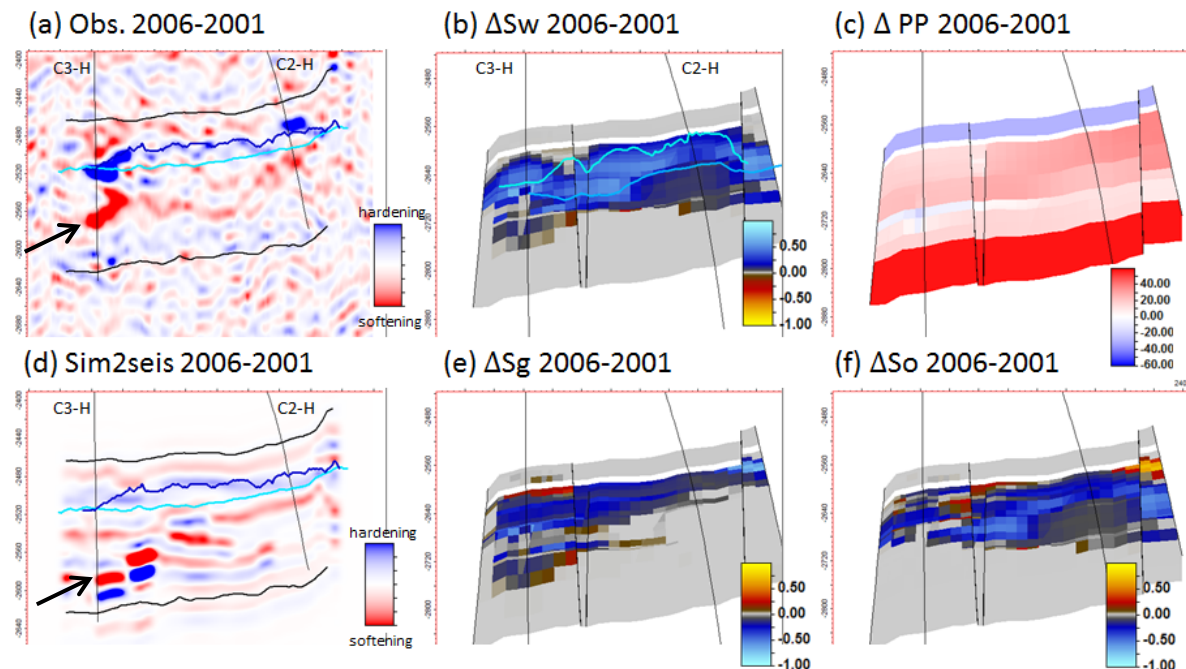


Figure 6.47: Observed seismic (a), Sim2seis (b), water saturation (c), gas saturation (d), pore pressure (bar) (e) and oil saturation (f) 2006-2001 differences. The blue lines in (a), (b) and (c) represent the interpreted OWC movement between 2001 and 2006 near C3-H and C2-H.

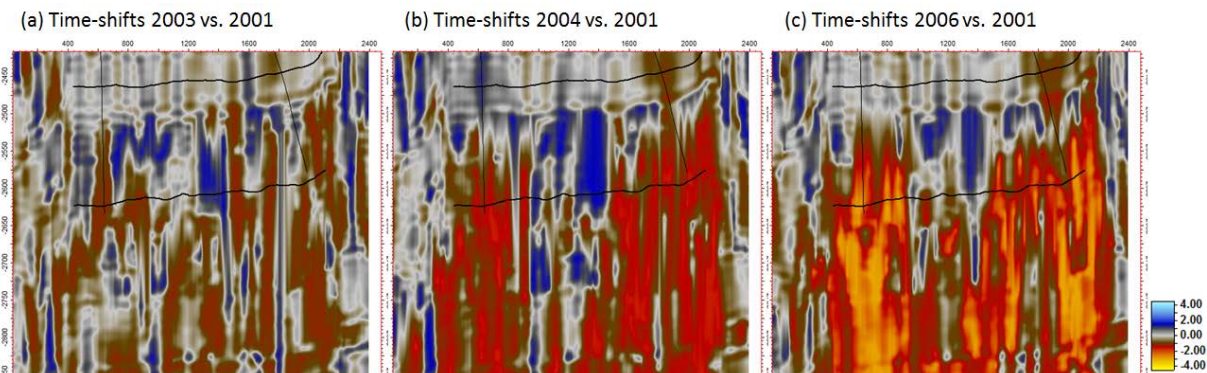


Figure 6.48: Time-shifts between 2001 and 2003 (a), 2004 (b) and 2006 (c). Negative values represent timing delay from baseline to monitor near C3-H and C2-H.

6.3.3. D-Segment

Wells D3-AH and D3-BY1HT2

D3-AH was perforated in Ile 2 and Tofte 3 Formation and open in mid-2000 and shut in June 2005. In October 2005 several side-tracks from D3-AH were attempted, but only D3-BY1HT2 was successful. This side-track started production February 2006. Figure 6.49 shows the location of both wells.

Observed seismic data in this area is noisy and no clear amplitude differences are visible in this section (Figure 6.51a). The time-shifts, however, indicate the reservoir below these wells has softened (delay in timing, indicated in Figure 6.52) due to pore pressure and gas saturation increase from the nearby water injector well, especially between 2001 and 2006, where the delays are up to 4ms. Advance in time-shifts are also visible within the area where the OWC has risen up, up to 1.5ms from 2001 and 2004 and 2006. Sim2seis (Figure 6.51b) amplitude differences do not match with the observed, but it does match with the time-shift measurements. The OWC interpretation does not follow a consistent amplitude difference, but it follows the time-shifts and is nearly consistent with well data (Figure 6.50b and d). The interpretation in this area is therefore classified as medium confidence and no simulation model updates are suggested based on the seismic analysis. However, it is advised that there is a mismatch between the water production rates from the simulation and history data for both wells, indicating the simulation model should be improved in the area.

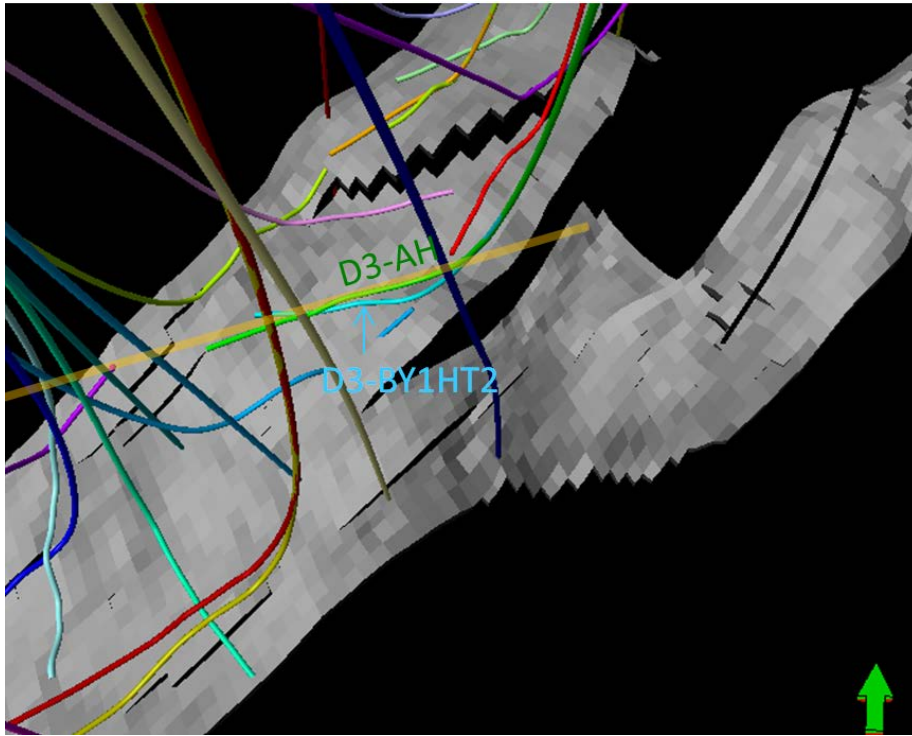
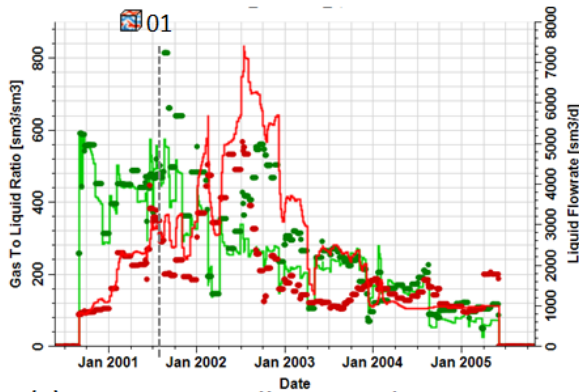
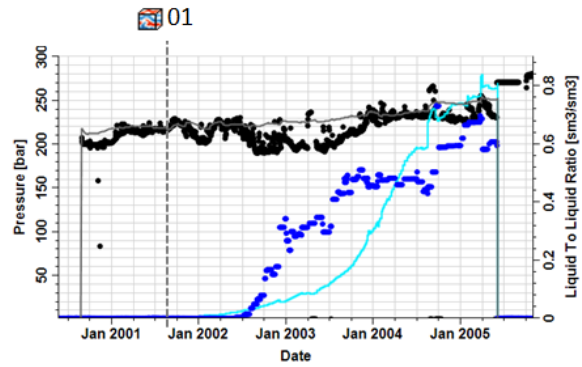


Figure 6.49: 3D view of D3-AH and D3-BY1HT2 wells and analysed vertical seismic section across them.

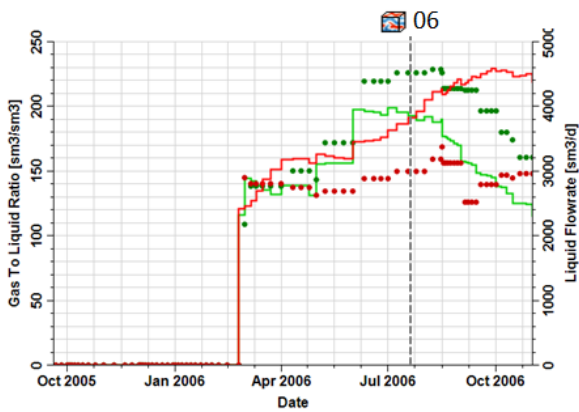
(a) D3-AH oil rate and GOR



(b) D3-AH BHP and water-cut



(c) D3-BY1HT2 oil rate and GOR



(d) D3-BY1HT2 BHP and water-cut

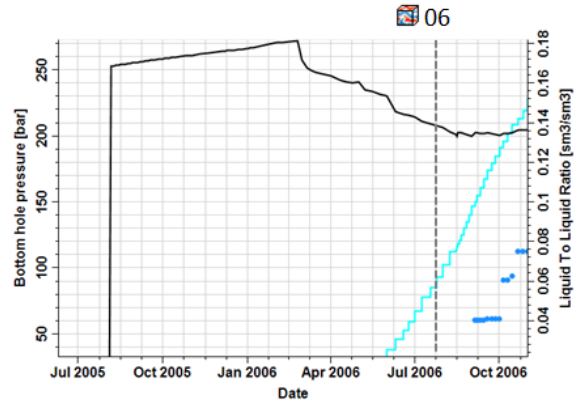


Figure 6.50: (a) and (c) gas-oil ratio (red) and oil production rate (green); (b) and (d) BHP (black) and water-cut (blue) for D3-AH and D3-BY1HT2 wells. Circles are the historical and solid lines are the simulated rates.

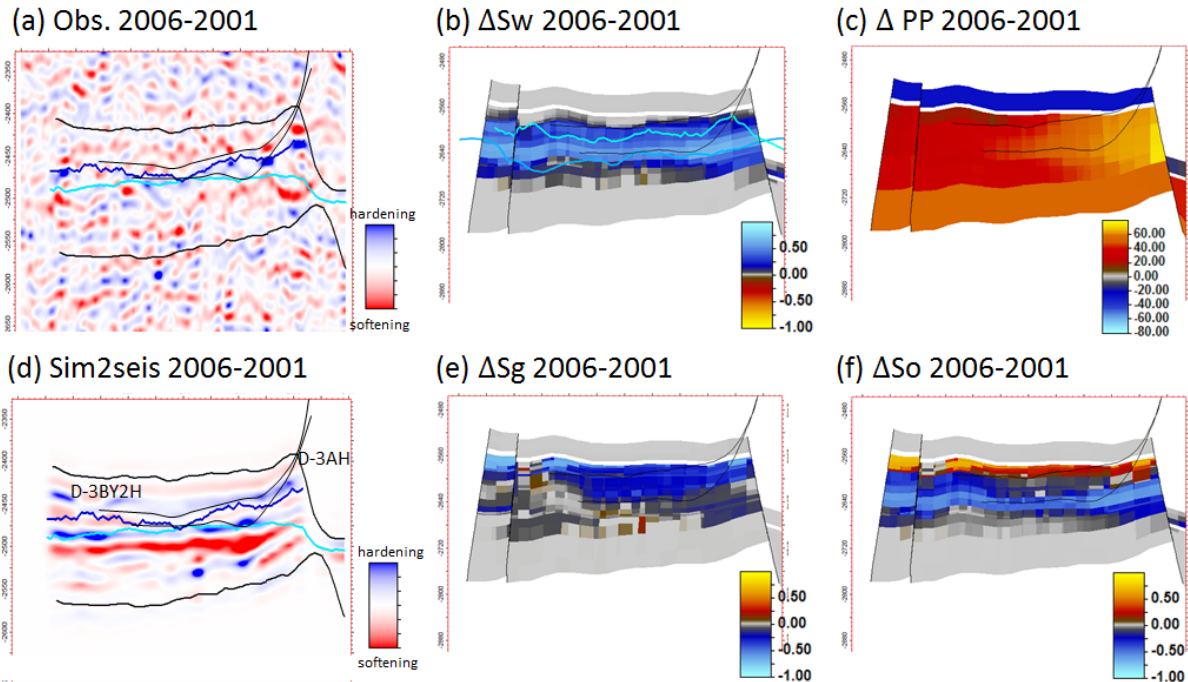


Figure 6.51: Observed seismic (a), Sim2seis (b), water saturation (c), gas saturation (d), pore pressure (bar) (e) and oil saturation (f) 2006-2001 differences. The blue lines in (a), (b) and (c) represent the interpreted OWC movement between 2001 and 2006.

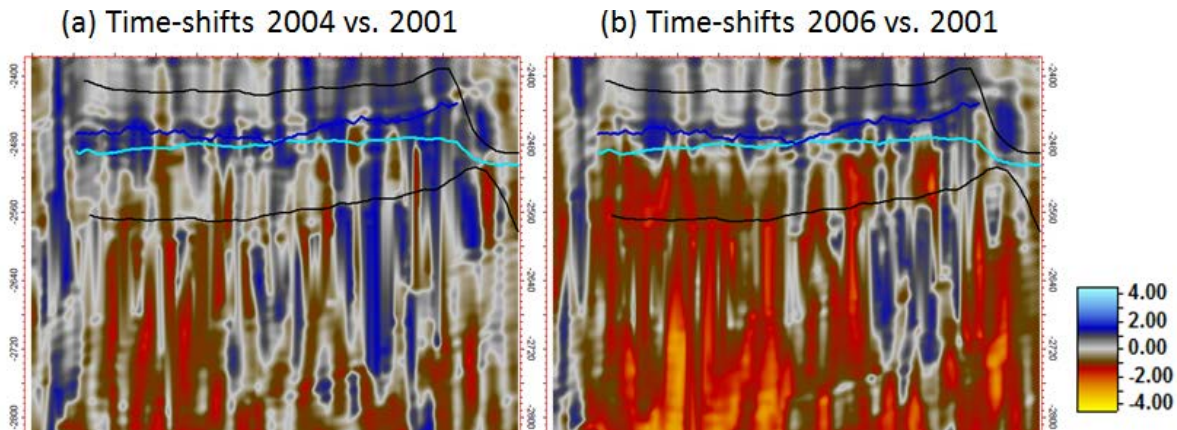


Figure 6.52: (a) Time-shifts between 2001 and 2004 and (b) Time-shifts between 2001 and 2006 near D3-AH and D3-BY1HT2 wells

Wells F2-H and D4-AHT2

Well F2-H was open in the water leg (approximately 31.5m below the OWC) north of D-segment to inject water (Statoil, 1999). Injection from this well started in October 1999. D4-AHT2 was a side-track from the producer D4-H, perforated in Not 2.2 and Not 2.3 Formations in June 2003. Figure 6.53 shows the location of both wells.

Although considerably noisy, the 4D seismic in this area presents a number of important features to understand this part of the field.

The red graph from Figure 6.54b shows that more gas went out of solution in the simulator than in observed history data in the period between mid-2004 and 2006. This agrees with observed seismic, as Figure 6.55a shows the gas effect (red anomaly) in the top reservoir not as strong and continuous as sim2seis (Figure 6.55d). However, as the extension of this anomaly in the observed seismic is uncertain on this vertical section view, further investigation was done on the RMS differences from the top reservoir maps, which are presented in the following Section 6.3.4.

The blue anomaly below the strong red event in sim2seis was interpreted as a sidelobe; however this effect seems to blend with water saturation increase on the left, which was therefore assumed to be a match with observed seismic of medium quality. The OWC movement is laterally contained both in the simulator (Figure 6.55b) and in the observed seismic. With a good confidence level on this interpretation due to consistency between well data, amplitudes and time-shift measures, and fair matches between observed seismic and simulator, no changes on simulation model for these interpretations are suggested. On the other hand, the water reaching the well (indicated by the blue arrow in Figure 6.55b), seems to be underestimated by the simulator, as indicated by the production graphs in Figure 6.54c. However, no observed seismic anomaly related to water in this layer is seen.

The red anomaly in the observed seismic near well F-2H, interpreted as caused by pore pressure increase from the water injector, is incompatible with sim2seis, where no changes are visible. The pore pressure seems to be underestimated in the simulator in this area, showing an increase between 30 and 40 bar (Figure 6.55c). As this anomaly is consistent for all seismic monitors and confirmed by time-shift measures and well activity, the interpretation was classified as high confidence, and updates are suggested in order to mimic the observed 4D seismic in this area.

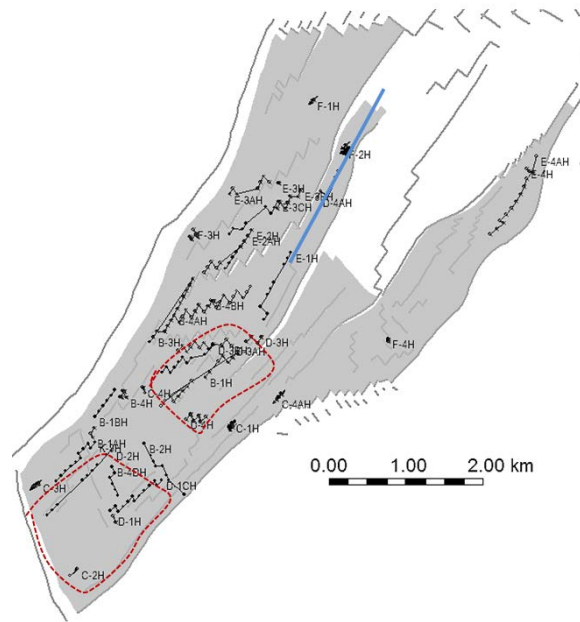


Figure 6.53: (a) Well and analysed vertical seismic section location.

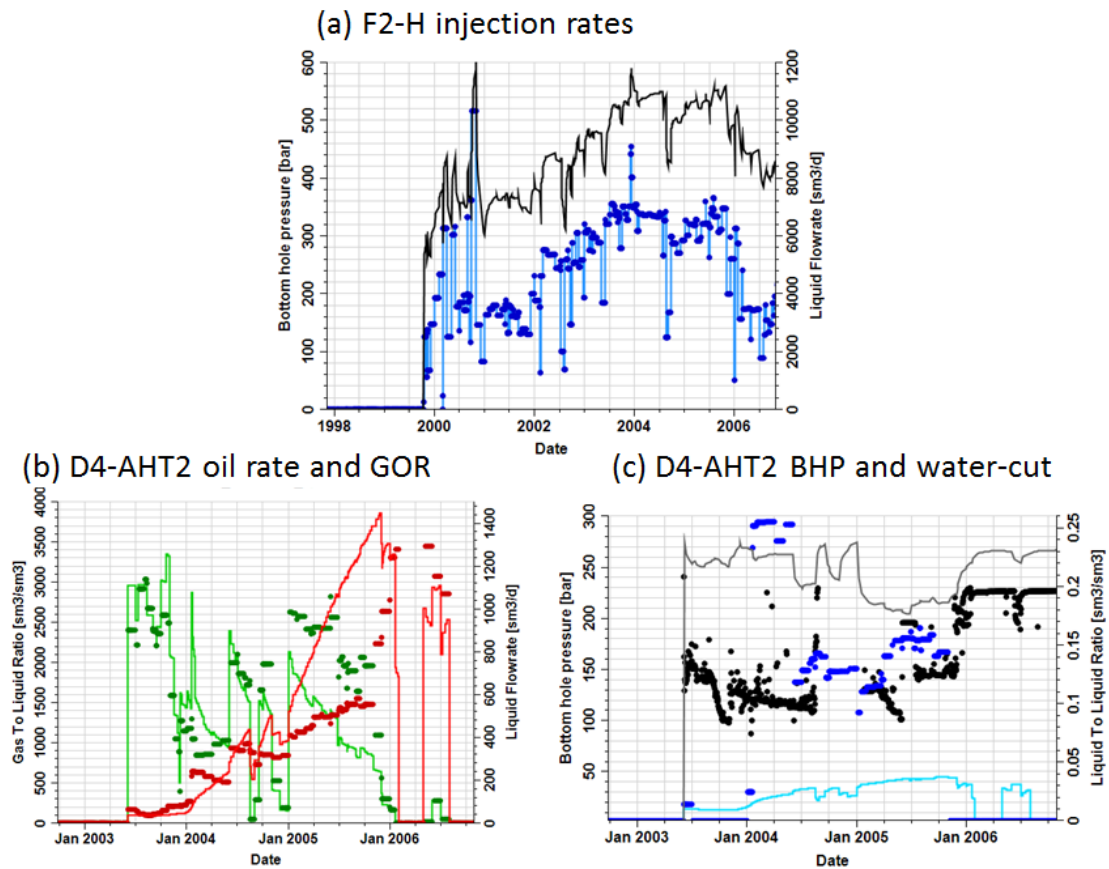


Figure 6.54: (a) Simulated BHP (black) and water injection rate (blue) for F-2H; (b) gas-oil ratio (red) and oil production rate (green); and (c) BHP (black) and water-cut (blue) for D4-AHT2. Circles are the historical and solid lines are the simulated rates.

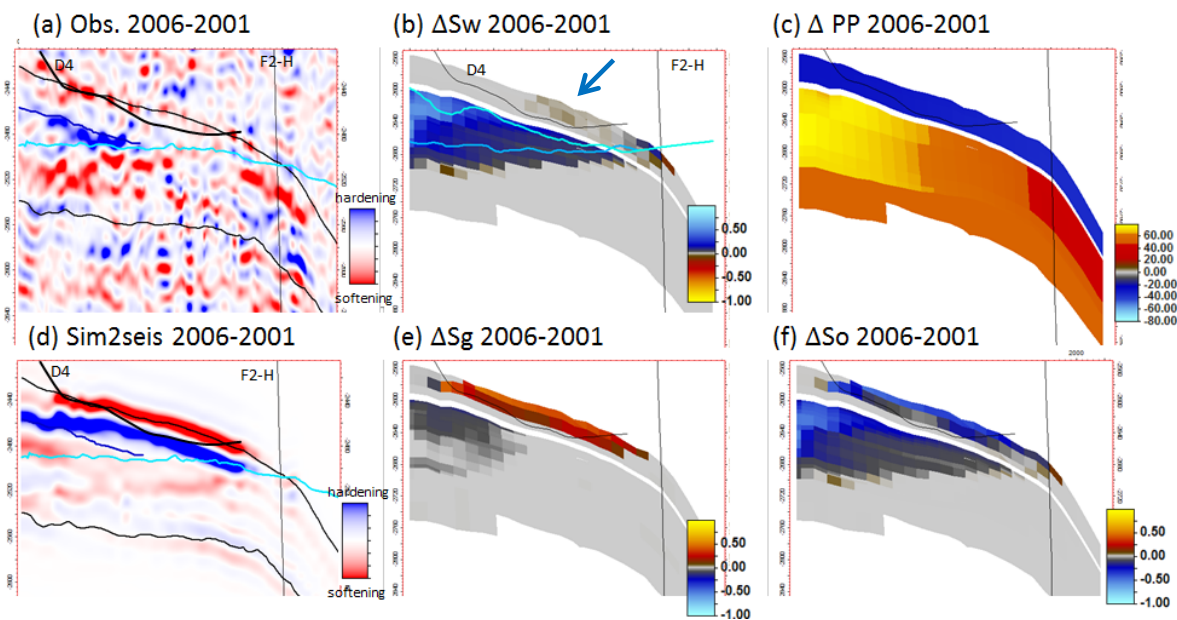


Figure 6.55: Observed seismic (a), sim2seis (b), water saturation (c), gas saturation (d), pore pressure (bar) (e) and oil saturation (f) 2006-2001 differences. The blue lines in (a), (b) and (c) represent the interpreted OWC movement between 2001 and 2006.

6.3.4. E-Segment

Well E3-CHT2

The well E-3CHT2 was open in May 2005 aiming to produce oil in the Ile Formation. Figure 6.56a shows the location of the well. Production data from this well showed that the water breakthrough occurred two months later (Figure 6.56d). Observed seismic difference between 2006 and 2004 (Figure 6.57a) shows a continuous and consistent hardening (blue) effect interpreted as related to the OWC rise in the section across this well. Sim2seis difference (Figure 6.57d) shows the same blue anomaly, however as result of an abrupt depletion of 69 bar and 52 bar in the well's completion cells from the simulation model (Figure 6.57c). The water saturation increase (Figure 6.57b) is a secondary cause of this sim2seis anomaly, exactly at the well completion location (which makes the well history data and simulation match as shown in Figure 6.56d) and not as continuous across the section, as it was overlaid by the depletion effect.

The delayed time-shifts measured in this section (Figure 6.58) also show the pore pressure increase effect related to the neighbour F-3H water injector well, and it roughly follows the horizontal shape from the hardening anomaly. For this case, we have classified the comparison as a "false match". It is recommended to review the water saturation

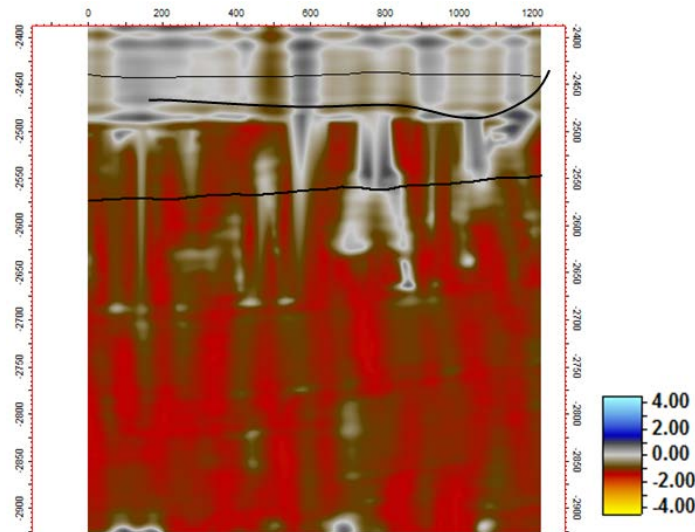


Figure 6.58: Time-shifts for 2004 vs. 2006 comparison near well E3-CHT2.

Wells F1-H and F3-H

Both water injector wells F1-H and F3-H are located in the water leg in E-segment (Figure 6.59a). F1-H started injecting water in September 1999 and F3-H started one year later.

Several mismatches are observed between observed and sim2seis (Figure 6.60a and d):

- The blue anomaly near F3-H (Figure 6.60a) was interpreted as the OWC movement from 2001 and to 2006, which is classified as high confidence level, as it is a strong and consistent amplitude difference confirmed by well activity (water injection). This anomaly is very weak in sim2seis (Figure 6.60d), since very little water is reaching this area in the simulator (Figure 6.60b). For that reason, it is suggested to review the water saturations from simulator in this area.
- The red anomaly in the observed seismic near well F-1H, interpreted as caused by pore pressure increase from the water injector, is unmatched with sim2seis, where no changes are visible. Similarly to F2-H well, the pore pressure seems to be underestimated in the simulator in this area, showing an increase in pore pressure below 20 bar (Figure 6.60c). As this anomaly is consistent for all seismic monitors and confirmed by time-shift measures and well activity, the

interpretation was classified as high confidence, and updates are suggested in order to mimic the observed 4D seismic in this area.

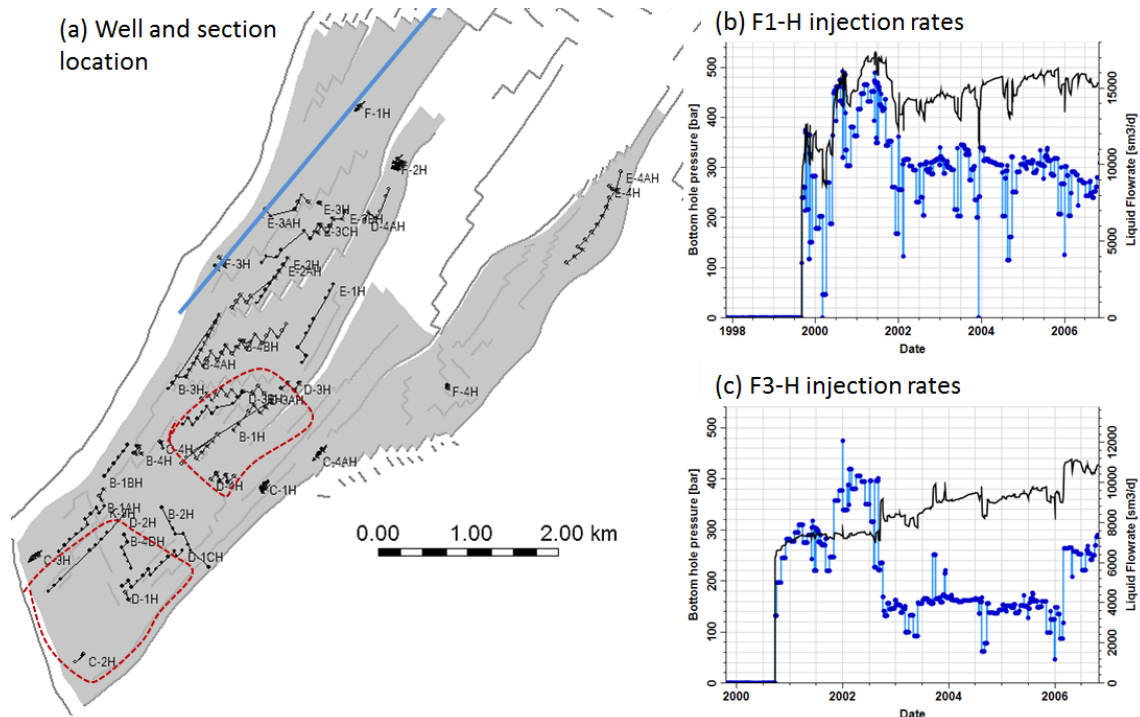


Figure 6.59: (a) Location of the wells and interpreted seismic section (blue line); (b) water injection rate (blue) and BHP (black) for F-1H; and (c) water injection rate (blue) and BHP (black) for F-3H. The solid lines are the simulation results and the circles are the historical data for the well.

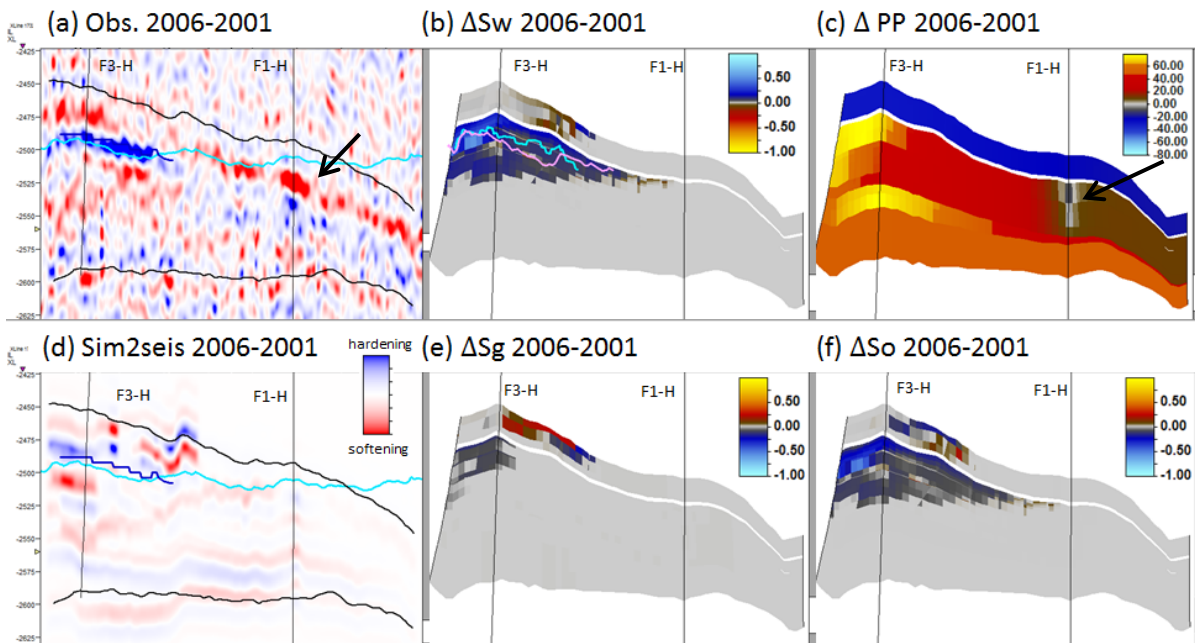


Figure 6.60: Observed seismic (a), water saturation (b), pore pressure (bar) (c), sim2seis (d), gas saturation (e) and oil saturation (f) 2006-2001 differences. The blue lines in (a), (b) and (c) represent the interpreted OWC movement between 2001 and 2006.

Wells B3-H, E-2H and E2-AH

This is a complex area, where several wells are producing close to each other at the same time. There are two major faults in the area, one along D and E-segments limit and another along E-segment (Figure 6.61a and b). B3-H well was open in July 1999 and completed in Ile 2 and Tofte 3 Formations. E-2H well produced between November 1999 and July 2005 in Ile 3 and 2 Formations. Then, this well was side-tracked to E-2AH in August 2005. Other wells in this area are E-3H, plugged in 2000 (before first available seismic); E3-AHT2, which produced horizontally along Not 2 Formation between December 2000 and January 2005; B4-BH, a horizontal well in Ile 2 Formation that produced between 2001 until reaching a high water production in 2003; and E3-CHT2, discussed in the previous section.

Most of these wells have produced deeper in the reservoir; however, the analysis in this area was done in the top reservoir. This is because the OWC movement and pressure effect from both water injectors F1-H and F3-H in the production zone and underburden are known to be confidently interpreted, as discussed in previous items.

The softening (red anomaly) from Figure 6.62a to c was interpreted as related to gas saturation increase. The hypothesis of this anomaly being a pore pressure increase effect was discarded, as the previous analysis showed the pressure response in this area occurs deeper in the section, and not at the top. Petrophysical logs from neighbour well F3-H also indicated presence of gas at the top, which also agreed with the bright 3D seismic verified in the maps from Section 6.1. The anomaly is mismatched with sim2seis to the east of fault 10 (yellow polygon) for all survey comparisons (Figure 6.62d to f). This is because the simulator had already a high gas saturation in this area before production started, and no changes in gas saturation from simulation occurred (Figure 6.62g to i). As the observed anomaly is consistent, it is suggested to look into the simulation model and understand why it does not present the same changes. The differences in the simulation also seem to be very compartmentalised across fault 10, as opposed to the observed 4D signal. A review on its connectivity is suggested.

The stronger red anomaly across D-segment was discussed in the previous section with D4-AHT2 well. In the map RMS view, it is less evident than in the vertical section that the softening effect from the top in sim2seis is stronger than observed between 2004

and 2006. However, this analysis does confirm the reservoir is compartmentalised between E and D-segments, and is a good match with sim2seis.

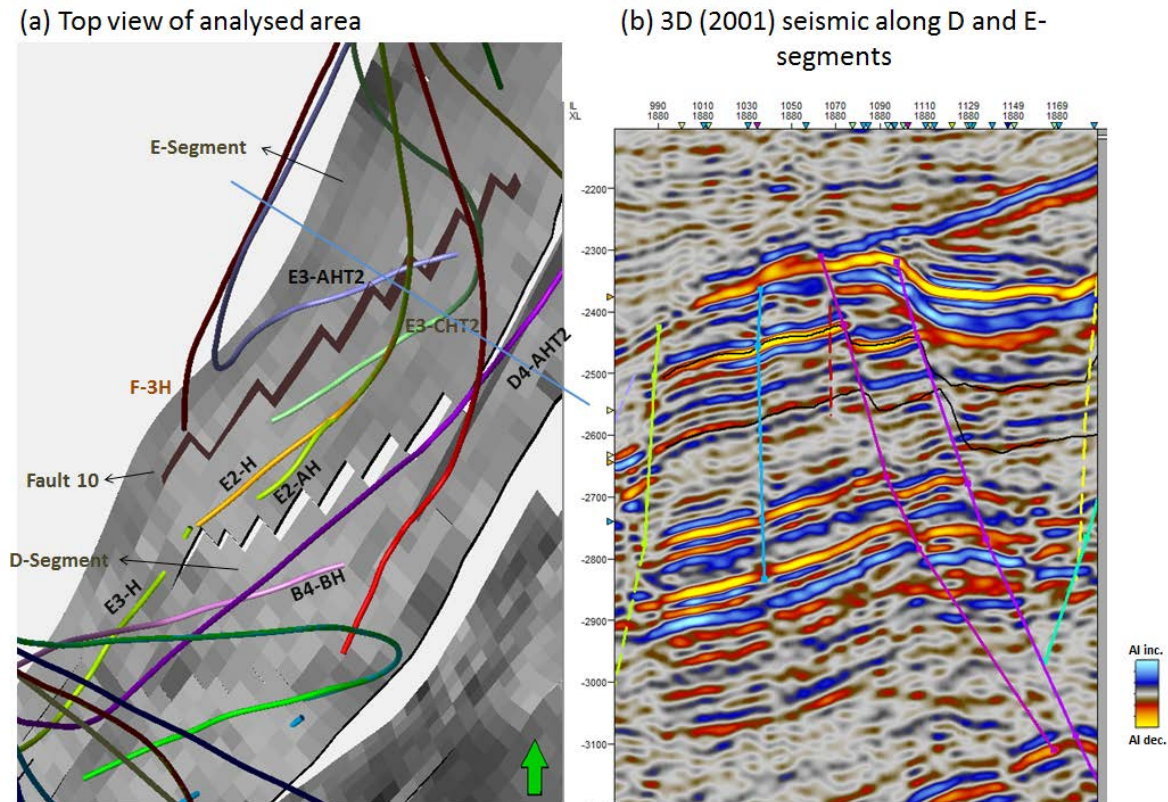


Figure 6.61: (a) Map view of well completion trajectories between segments D and E and (b) 3D seismic across D and E-segments (blue line in (a)) and the major fault in blue between them.

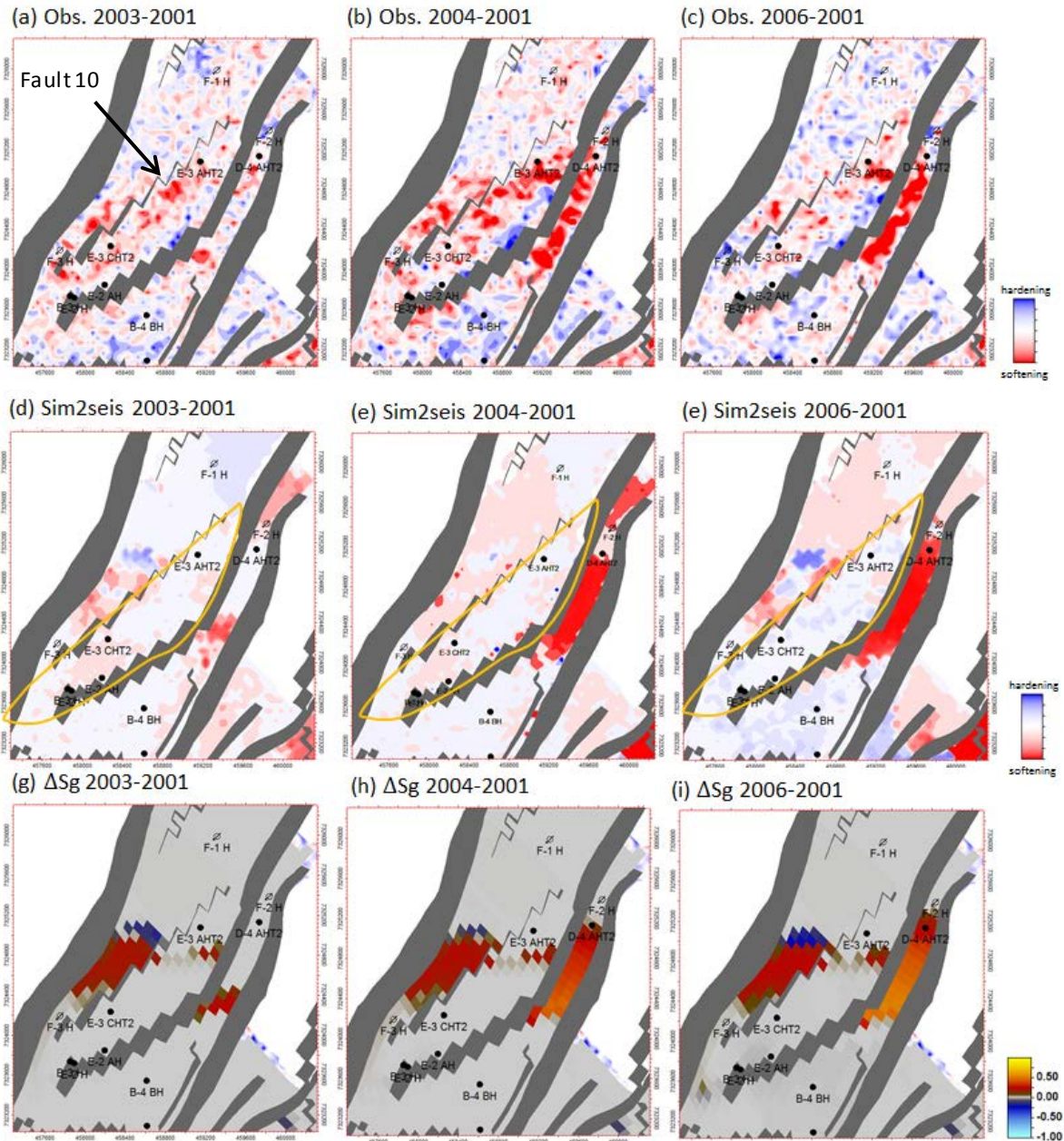


Figure 6.62: (a to c) Observed RMS amplitude differences from top reservoir to 15ms below; (d to f) sim2seis RMS amplitude differences; and (g to i) gas saturation differences for 2003, 2004 and 2006 minus 2001 comparisons, extracted from a 15ms window below top reservoir.

6.4. Field analysis

Following the methodology presented for all the areas, the result is a final map on the reliability of the seismic interpretation. Figure 6.63 shows the location of all the interpretations and their rank: green for high, yellow for medium and red for low

confidence, for each pair of survey. The areas delimited by the blue dashed lines are the areas where no 4D signal was detected, or were obscured by background noise.

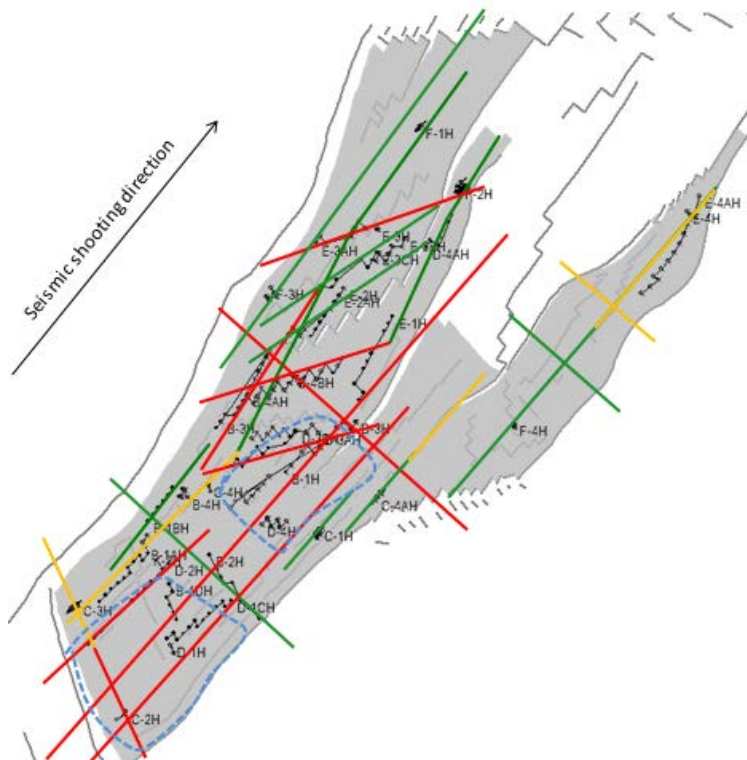


Figure 6.63: Location of the interpreted seismic sections throughout the field. The lines in green present high seismic interpretation confidence, yellow are medium confidence and red, low confidence. No clear 4D signal was detected in the dashed areas.

Based on the full analysis, one seismic interpretation confidence map for each survey comparison was created (Figure 6.64a to c). The low confidence areas for all the three cases, in general, agree with the poor repeatability data (NRMS values above 0.3, roughly delimited by the polygons in Figure 6.64a to f), especially near the undershoot area in the southwest part of the field discussed in section 6.2. Regardless, the workflow has provided significant interpretation insights within these polygons, where up to medium or even high interpretation confidence levels were achieved, such as the two examples indicated by the black arrows from Figure 6.64a to f in the northeast of G and D-segments. These examples indicate that even with a poor repeatability it is still possible to observe 4D signals depending on the production activity and sensitivity of the reservoir rocks to these activities.

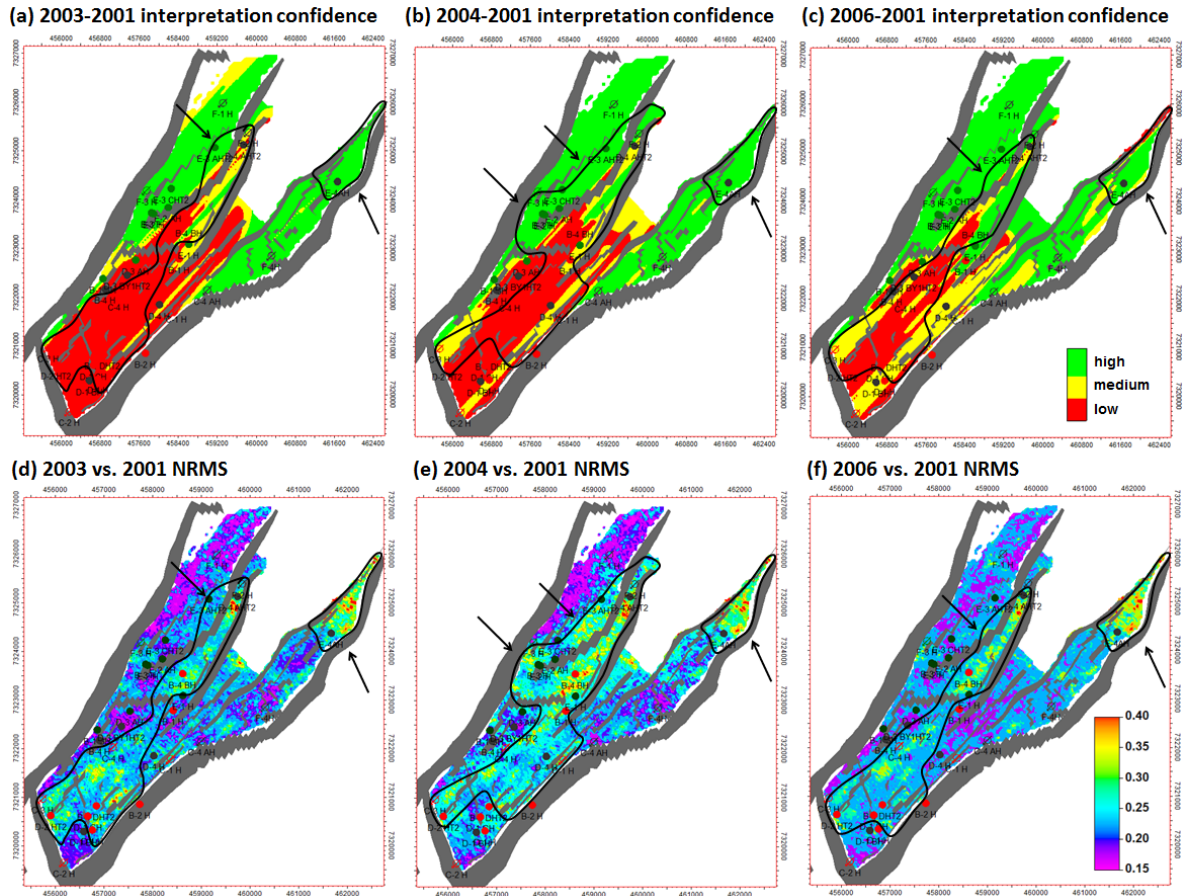


Figure 6.64: Interpretation confidence maps for each survey comparison: (a) 2003, (b) 2004 and (c) 2006 versus 2001. The black polygons represent the high NRMS areas defined in Figures (d), (e) and (f). The black arrows show examples where seismic confidence is medium to high in spite of a poorer repeatability.

The same analysis was done for the separate OWC interpretations provided with the benchmark package (Figure 6.65a and b). This rank was based on the continuity of the 4D signals observed on seismic amplitudes, consistency with well production data and petrophysical logs.

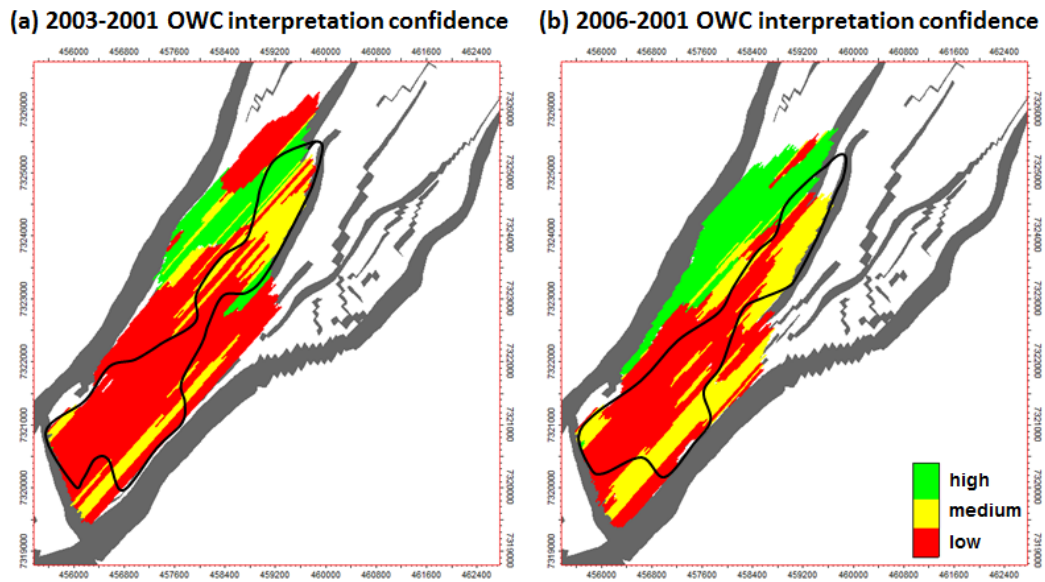


Figure 6.65: OWC Interpretation confidence maps for each survey comparison: (a) 2003 and (b) 2006 versus 2001. The black polygons represent the high NRMS areas.

7. CONCLUSIONS

This work describes a methodology that provides a systematic and integrated 4D seismic semi-quantitative interpretation to identify areas of the data we are confident enough to be incorporated in data assimilation technique to future improvements in reservoir simulation models. This work demonstrated that integration between geophysics, geology and engineering disciplines is required in order to properly interpret 4D data and presented an alternative procedure to perform this task.

We presented an application of the workflow for the Norne field, where we observe uncertainties related to the noise content and repeatability issues on the observed seismic data, which might prevent us from drawing confident recommendations. It was shown that:

- A good match between observed seismic and sim2seis is not always an indication that no updates are needed (as seen on the “false match” example).
- A bad match may not indicate that the model should be modified (in case the confidence in the seismic is low).
- There is a risk when automatically implementing updates to the simulation model using observed seismic and sim2seis comparison techniques, as we have seen this information can introduce ambiguous or dubious information to the process. The confidence level flagging proposed in this work addresses this potential pitfall.

It is important to note that the dataset used was acquired and processed more than a decade ago. Modern acquisition techniques and processing algorithms are very likely to provide more reliable data. Vintage data can always be re-processed with these modern techniques but never be re-acquired. Therefore, the presence of uncertainties in 4D seismic interpretation, especially from vintage data, is very common. The main contribution of this work is the assessment of these uncertainties prior to using their information. Another important contribution of this work is that it provides a general overview of the potential applications of the 4D seismic data provided in the benchmark to history matching studies.

7.1. Suggestions for future work

This work was carried out in the amplitude and time-shift domains. It is suggested that other domains (such as impedances) can provide additional information to this study. However, it is important to stress that we raised several interpretation uncertainties, and their knowledge should be incorporated into more quantitative studies. Inversion techniques can also provide more quantitative information, such as saturation estimates, that can also be compared with the simulated data. Including the angle stacks can also improve our understanding on decoupling 4D effects.

Another suggestion is to apply the suggested updates to the simulation model and verify the synthetic response, ideally iteratively, until the response matches with the high confidence level observed seismic, closing the loop of this methodology. The present analysis can also be repeated using a model that has been history-matched using well data only, to compare and evaluate the value of 4D seismic on history matching this field.

8. REFERENCES

ALVAREZ, Erick; MACBETH, Colin; BRAIN, Jonathan. Quantifying remaining oil saturation using time-lapse seismic amplitude changes at fluid contacts. **Petroleum Geoscience**. v. 22, n. 4, p.1-13, 1 nov. 2016. Geological Society of London.

ALLO, Fabien et al. Reducing turn-around time for time-lapse feasibility studies. In: **13th International Congress of the Brazilian Geophysical Society & EXPOGEF, Rio de Janeiro, Brazil, 26–29 August 2013**. Society of Exploration Geophysicists and Brazilian Geophysical Society, 2013. p. 1013-1018.

AMINI, Hamed. **A pragmatic approach to simulator-to-seismic modelling for 4D seismic interpretation**. 2014. PhD Thesis. Heriot-Watt University.

AMUNDSEN, Lasse; LANDRØ, Martin. 4D Seismic – Status and Future Challenges, Part I. In: **GeoExpro**, pp. 66–68, 2007.

ASCHJEM, Gunnar. **Mapping Reservoir Changes Using 4D Seismic on the Norne G-segment, Norwegian Sea**. 2013. Master's Thesis. Norwegian University of Science and Technology.

BACON, Michael; SIMM, Robert; REDSHAW, Terence. **3-D seismic interpretation**. Cambridge University Press, 2007.

BERRYMAN, James G.; MILTON, Graeme W. Exact results for generalized Gassmann's equations in composite porous media with two constituents. **Geophysics**, [s.l.], v. 56, n. 12, p.1950-1960, dez. 1991. Society of Exploration Geophysicists.

BERRYMAN, James G.; WANG, Herbert F. Elastic wave propagation and attenuation in a double-porosity dual-permeability medium. **International Journal of Rock Mechanics and Mining Sciences**, v. 37, n. 1, p. 63-78, 2000.

BOUTTE, Dalton. Through the continuous life cycle of reservoir, geophysics makes its mark. **The Leading Edge**, [s.l.], v. 26, n. 11, p.1376-1379, nov. 2007. Society of Exploration Geophysicists.

BULAND, Arild et al. Bayesian time-lapse inversion. **Geophysics**, [s.l.], v. 71, n. 3, p.43-48, may 2006. Society of Exploration Geophysicists.

BRICENO, A.; MACBETH, C.; MANGRIOTIS, M. D. Towards an Effective Petroelastic Model for Simulator to Seismic Studies. In: **78th EAGE Conference and Exhibition 2016**. 2016.

BRITO, Daniel Ullmann et al. Incorporation of 4D seismic in the re-construction and history matching of Marlim Sul deep water field flow simulation model. In: **SPE EUROPEC/EAGE Annual Conference and Exhibition**. Society of Petroleum Engineers, 2011.

BROWN, Robert J. S.; KORRINGA, Jan. ON THE DEPENDENCE OF THE ELASTIC PROPERTIES OF A POROUS ROCK ON THE COMPRESSIBILITY OF THE PORE FLUID. **Geophysics**, [s.l.], v. 40, n. 4, p.608-616, ago. 1975. Society of Exploration Geophysicists.

BYERLEY, Grant et al. 4D seismic monitoring applied to SAGD operations at Surmont, Alberta, Canada. In: **SEG Technical Program Expanded Abstracts 2009**. Society of Exploration Geophysicists, 2009. p. 3959-3963.

BYERLEY, Grant; SINGER, Lyndsay; ROSE, Phil. Resaturated pay: A new infill target type identified through the application and continuous improvement of 4D seismic at the Forties Field. **The Leading Edge**, [s.l.], v. 35, n. 10, p.831-838, out. 2016. Society of Exploration Geophysicists.

CALVERT, M. A. et al. Halfdan 4D workflow and results leading to increased recovery. **The Leading Edge**, [s.l.], v. 35, n. 10, p.840-848, out. 2016. Society of Exploration Geophysicists.

CGG. Hampson-Russell **Time-lapse guide**, 2009.

CHENG, Nan; OSDAL, Bård. Updating the Norne Reservoir Model Using 4D Seismic Data. In: **IO Workshop, Center for Integrated Operations in the Petroleum Industry at NTNU, Trondheim, Norway**. 2008.

CHU, D. et al. Effectively Handling Different Types of Data in Facility Areas for Improved 4D Imaging. In: **77th EAGE Conference and Exhibition 2015**. 2015.

CORREIA, Gil G.; SCHIOZER, Denis J. Reservoir characterization using electrofacies analysis in the sandstone reservoir of the Norne Field (offshore Norway). **Petroleum Geoscience**, v. 22, n. 2, p. 165-176, 2016.

DADASHPOUR, Mohsen et al. Porosity and permeability estimation by integration of production and time-lapse near and far offset seismic data. **Journal Of Geophysics And Engineering**, [s.l.], v. 6, n. 4, p.325-344, 8 set. 2009. IOP Publishing.

DROTTNING, Asmund; BRANSTON, M.; LECOMTE, I. Value of illumination-consistent modelling in time-lapse seismic analysis. **First break**, v. 27, n. 10, 2009.

EIKEN, Ola. et al. Seismic monitoring of the Heidrun, Norne and Midgard fields using steerable streamers. In: **65th EAGE Conference & Exhibition**. 2003.

EIKEN, Ola et al. D. A Proven Method for Acquiring Highly Repeatable Towed Streamer Seismic Data. In: **Insights and Methods for 4D Reservoir Monitoring and Characterization**. Society of Exploration Geophysicists and European Association of Geoscientists and Engineers, 2005. p. 209-216.

FAHIMUDDIN, Abul. **4D seismic history matching using the ensemble Kalman filter (EnKF): possibilities and challenges**. 2010. PhD Thesis. The University of Bergen.

FALEIDE, Jan Inge et al. Structure and evolution of the continental margin off Norway and the Barents Sea. **Episodes**, v. 31, n. 1, p. 82-91, 2008.

FAWKE, Anna. Correspondence, 2008. (in: Verlo & Hetland, 2008)

GASSMANN, Fritz. Elastic waves through a packing of spheres. **Geophysics**, [s.l.], v. 16, n. 4, p.673-685, oct. 1951. Society of Exploration Geophysicists.

GRUDE, Sissel; OSDAL, Bård; LANDRØ, Martin. Sea-bed diffractions and their impact on 4D seismic data. **Geophysical Prospecting**, v. 61, n. s1, p. 199-214, 2013.

HAN, De-hua; BATZLE, Michael. Constrained and simplified Gassmann's equations. In: **SEG Technical Program Expanded Abstracts 2002**. Society of Exploration Geophysicists, 2002. p. 1837-1841.

HERRON, Donald A. **First steps in seismic interpretation**. Society of Exploration Geophysicists, 2011.

HILL, David et al. Full-field 4d image-modelling to optimize a closed-loop seismic reservoir monitoring work-flow. In: **International Conference and Exhibition, Barcelona, Spain, 3-6 April 2016**. Society of Exploration Geophysicists and American Association of Petroleum Geologists, 2016. p. 326-326.

HUANG, Yi et al. Enhanced dynamic interpretation from correlating well activity to frequently acquired 4D seismic signatures. **The Leading Edge**, [s.l.], v. 30, n. 9, p.1042-1050, sep. 2011. Society of Exploration Geophysicists.

HUANG, Yi et al. Proving the value of 4D seismic data in the late-life field—Case study of the Norne main field. **First Break**, v. 31, n. 9, p. 57-67, 2013.

HUBANS, C. 4D Noise Understanding to Validate 4D Anomalies. In: **78th EAGE Conference and Exhibition 2016**. 2016.

JOURDAN, J. A.; LEFEUVRE, Frédéric; DUBUCQ, Dominique. Integration of 4D seismic into the dynamic model: Girassol, deep offshore Angola. **First break**, v. 24, n. 4, p. 51-58, 2006.

JOHNSTON, David H. **Practical applications of time-lapse seismic data**. Society of Exploration Geophysicists, 2013.

KLOOSTERMAN, H. J. et al. Successful application of time-lapse seismic data in Shell Expro's Gannet Fields, Central North Sea, UKCS. **Petroleum Geoscience**, [s.l.], v. 9, n. 1, p.25-34, 1 jan. 2003. Geological Society of London.

KRAGH, Ed; CHRISTIE, Phil. Seismic repeatability, normalized rms, and predictability. **The Leading Edge**, [s.l.], v. 21, n. 7, p.640-647, jul. 2002. Society of Exploration Geophysicists.

LECOMTE, Isabelle; GJØYSTDAL, Håvar; DROTTNING, Åsmund. Simulated Prestack Local Imaging: a robust and efficient interpretation tool to control illumination, resolution, and time-lapse properties of reservoirs. In: **SEG Technical Program Expanded Abstracts 2003**. Society of Exploration Geophysicists, 2003. p. 1525-1528.

LECOMTE, Isabelle et al. Efficient and flexible seismic modeling of reservoirs: A hybrid approach. **The Leading Edge**, v. 23, n. 5, p. 432-437, 2004.

LECOMTE, Isabelle. Resolution and illumination analyses in PSDM: A ray-based approach. **The Leading Edge**, v. 27, n. 5, p. 650-663, 2008.

LECOMTE, Isabelle et al. Ray-based seismic modeling of geologic models: Understanding and analyzing seismic images efficiently. **Interpretation**, v. 3, n. 4, p. SAC71-SAC89, 2015.

LUMLEY, David et al. Seismic monitoring of CO₂ geo-sequestration: realistic capabilities and limitations. In: **SEG Technical Program Expanded Abstracts 2008**. Society of Exploration Geophysicists, 2008. p. 2841-2845.

LUMLEY, David. 4D seismic monitoring of CO₂ sequestration. **The Leading Edge**, v. 29, n. 2, p. 150-155, 2010.

LYGREN, M. et al. History matching using 4D seismic and pressure data on the Norne field. In: **67th EAGE Conference & Exhibition**. 2005.

O'CONNELL, Richard J. A viscoelastic model of anelasticity of fluid saturated porous rocks. In: JOHNSON, D. L.; SEN, P. N. (Ed.). **AIP Conference Proceedings**. AIP, 1984. p. 166-175.

OLIVEIRA, Rildo Marcio et al. Marlim field: Incorporating 4D seismic in the geological model and application in reservoir management decisions. In: **Latin American & Caribbean Petroleum Engineering Conference**. Society of Petroleum Engineers, 2007.

MACBETH, Colin. A classification for the pressure-sensitivity properties of a sandstone rock frame. **Geophysics**, v. 69, n. 2, p. 497-510, 2004.

NPD – Norwegian Petroleum directorate. Facts 2008 - The Norwegian petroleum sector, 2008.

NPD – Norwegian Petroleum directorate. Fact map, 2016. Available at: http://gis.npd.no/factmaps/html_20/. Accessed in Oct. 2016.

OSDAL, Bård; ALSOS, Trine. Seismic Modelling of Eclipse Simulations and Comparison with Real 4D Data at the Norne Field. In: **64th EAGE Conference & Exhibition**. 2002.

OSDAL, Bård et al. Mapping the fluid front and pressure buildup using 4D data on Norne Field. **The Leading Edge**, v. 25, n. 9, p. 1134-1141, 2006.

OSDAL, Bård et al. Using Onboard Time Lapse Processing for Quality Control of Time Lapse Acquisition on the Norne Fields. In: **70th EAGE Conference and Exhibition incorporating SPE EUROPEC 2008**. 2008.

OSDAL, Bård; ALSOS, Trine. Norne 4D and Reservoir Management—The keys to success. In: **72nd EAGE Conference and Exhibition incorporating SPE EUROPEC 2010**. 2010.

OSDAL, Bård et al. Estimation of changes in water column velocities and thicknesses from time lapse seismic data. **Geophysical Prospecting**, [s.l.], v. 59, n. 2, p.295-309, 27 set. 2010. Wiley-Blackwell.

OSDAL, Bård; LANDRØ, Martin. Estimation of changes in water column velocities and thicknesses from time lapse seismic data. **Geophysical Prospecting**, v. 59, n. 2, p. 295-309, 2011.

EL OUAIR, Youness et al. Integrated reservoir management approach: From time-lapse acquisition to reservoir model update at the Norne Field. In: **International Petroleum Technology Conference**. International Petroleum Technology Conference, 2005.

RIBEIRO, Christophe et al. Time-lapse simulator-to-seismic study—Forties field, North Sea. In: **SEG Technical Program Expanded Abstracts 2007**. Society of Exploration Geophysicists, 2007. p. 2944-2948.

RICKETT, J. E.; LUMLEY, D. E.. Cross-equalization data processing for time-lapse seismic reservoir monitoring: A case study from the Gulf of Mexico. **Geophysics**, [s.l.], v. 66, n. 4, p.1015-1025, jul. 2001. Society of Exploration Geophysicists.

ROGGERO, Frederic et al. Matching of Production History and 4D Seismic Data--Application to the Girassol Field, Offshore Angola. In: **SPE Annual Technical Conference and Exhibition**. Society of Petroleum Engineers, 2007.

ROSE, Philip et al. Forties infill drilling eight years on; continued success through the application of thorough development geoscience driven by 4D seismic. In: **Offshore Europe**. Society of Petroleum Engineers, 2011.

RWECHUNGURA, Richard Wilfred et al. The Norne Field Case-A Unique Comparative Case Study. In: **SPE Intelligent Energy Conference and Exhibition**. Society of Petroleum Engineers, 2010.

SANTOS, J. M. C. et al. 4D Seismic Interpretation of the Norne Field-A Semi-quantitative Approach. In: **78th EAGE Conference and Exhibition 2016**. 2016.

SARKAR, Sudipta; GOUVEIA, Wences P.; JOHNSTON, David H.. On the inversion of time-lapse seismic data. **Seg Technical Program Expanded Abstracts 2003**, [s.l.], 1489–1492, jan. 2003. Society of Exploration Geophysicists.

SIMM, Rob; BACON, Michael. **Seismic Amplitude: An interpreter's handbook**. Cambridge University Press, 2014.

STAMMEIJER, J. G. F.; HATCHELL, P. J. Standards in 4D feasibility and interpretation. **The Leading Edge**, v. 33, n. 2, p. 134-140, 2014.

STAPLES, Rob et al. 4D seismic for oil-rim monitoring. **Geophysical Prospecting**, v. 53, n. 2, p. 243-251, 2005.

STATOIL. **Plan for Development and Operation**, Reservoir Geology, Support Documentation, 1994.

STATOIL. **Norne Well 6608/10-F2-H Geological and Petrophysical Report**, Support Documentation, 1999.

STATOIL. **PL128-Norne Field Reservoir Management Plan**, Support Documentation, 2001.

STATOIL. **Annual reservoir development plan/Norne field**, Support Documentation, 2004.

STATOIL. **Norne Well 6608/10-B-1AH/AHT2 & B-1 BH Geological and Petrophysical Report**, Support Documentation, 2005.

STATOIL. **Long life at Norne, 2015**. Available at:
<http://www.statoil.com/en/NewsAndMedia/News/2015/Pages/Norne9Jan2015.aspx>.
Accessed in 2015.

STOVAS, Alexey; ARNTSEN, Børge. Vertical propagation of low-frequency waves in finely layered media. **Geophysics**, [s.l.], v. 71, n. 3, p.87-94, may 2006. Society of Exploration Geophysicists.

SUMAN, Amit. **Joint Inversion of production and time-lapse seismic data: Application to Norne Field**. 2013. PhD Thesis. Stanford University.

TRANI, Mario et al. Estimation of changes in saturation and pressure from 4D seismic AVO and time-shift analysis. **Geophysics**, [s.l.], v. 76, n. 2, p.1-17, mar. 2011. Society of Exploration Geophysicists.

VERLO, Signe Berg; HETLAND, Mari. **Development of a field case with real production and 4D data from the Norne Field as a benchmark case for future reservoir simulation model testing**. Master's thesis. 2008. Norwegian University of Science and Technology.

WESTERNGECO. **Data processing report for Statoil block 6608/10 (Norne): ST0113, ST0103, ST0305, ST0409, ST0603 - 2006 4D processing**. 2007.

WHITE, R. E.; SIMM, Rob. Tutorial: Good practice in well ties. **First Break**, v. 21, n. 10, 2003.

YAN, Tianjiao. **History Matching of Production and 4D Seismic Data:-Application to the Norne Field**. 2014. Master's thesis. Norwegian University of Science and Technology.

YIN, Zhen et al. Evaluation of inter-well connectivity using well fluctuations and 4D seismic data. **Journal of Petroleum Science and Engineering**, v. 145, p. 533-547, 2016.